PD
539.7
G 326
V.6, No.3

POWER REACTOR TECHNOLOGY

A Quarterly Technical Progress Review

Prepared for DIVISION OF TECHNICAL INFORMATION, USAEC, by
W. H. ZINN and J. R. DIETRICH, GENERAL NUCLEAR ENGINEERING CORPORATION

ILLINOIS STATE LIBRARY
AUG 13 1963

June 1963

● VOLUME 6

● NUMBER 3

TECHNICAL PROGRESS REVIEWS

To meet the needs of industry for concise summaries of current atomic developments, the Atomic Energy Commission is publishing this series, Technical Progress Reviews. Issued quarterly, each of the reviews digests and evaluates the latest findings in a specific area of nuclear technology and science.

The four journals published in this series are:

Nuclear Safety, Wm. B. Cottrell, W. H. Jordan, and associates, Oak Ridge National Laboratory

Power Reactor Technology, W. H. Zinn and J. R. Dietrich, General Nuclear Engineering Corporation

Reactor Materials, R. W. Dayton, E. M. Simons, and associates, Battelle Memorial Institute

Reactor Fuel Processing, Stephen Lawroski and associates, Chemical Engineering Division, Argonne National Laboratory

Each journal may be purchased ($2.00 per year for subscription and individual issues $0.55) from the Superintendent of Documents, U. S. Government Printing Office, Washington 25, D. C. See back cover for remittance instructions and foreign postage requirements.

The views expressed in this publication do not necessarily represent those of the United States Atomic Energy Commission, its divisions or offices, or of any Commission advisory committee or contractor.

Availability of Reports Cited in This Review

Unclassified AEC reports are available for inspection at AEC depository libraries and are sold by the Office of Technical Services, Department of Commerce, Washington 25, D. C. Some of the reports cited are not available owing to their preliminary nature; however, the information contained in them will eventually be made available in formal progress or topical reports.

Unclassified reports issued by other Government agencies or private organizations should be requested from the originator.

Unclassified British and Canadian reports may be inspected at AEC depository libraries. British reports are sold by the British Information Service, 45 Rockefeller Plaza, New York, N. Y.; Canadian reports (AECL series) are sold by the Scientific Document Distribution Office, Atomic Energy of Canada, Ltd., Chalk River, Ontario, Canada.

Classified U. S. and foreign reports identified in this journal as Classified may be purchased by properly cleared Access Permit Holders from the Division of Technical Information Extension, U. S. Atomic Energy Commission, P. O. Box 1001, Oak Ridge, Tenn. Such reports may be inspected at classified AEC depository libraries.

POWER REACTOR TECHNOLOGY

A REVIEW OF RECENT DEVELOPMENTS

Prepared for DIVISION OF TECHNICAL INFORMATION, USAEC,
by W. H. ZINN and J. R. DIETRICH,
GENERAL NUCLEAR ENGINEERING CORPORATION

● JUNE 1963

● VOLUME 6

● NUMBER 3

Foreword

This quarterly review of reactor development has been prepared at the request of the Division of Technical Information of the U. S. Atomic Energy Commission. Its purpose is to assist interested organizations in the task of keeping abreast of new results in reactor technology for civilian application.

Power Reactor Technology contains reviews of selected recently published reports that are judged noteworthy, in the fields of power-reactor research and development, power-reactor applications, design practice, and operating experience. It is not meant to be a comprehensive abstract of all material published during the quarter, nor is it meant to be a treatise on any part of the subject. However, related articles are often treated together to yield reviews having some breadth of scope, and from time to time background material is added to place recent developments in perspective.

The intention is to cover the various areas of reactor development from the general viewpoint of the reactor designer rather than from the more detailed points of view of specialists in the individual areas. To whatever extent the coverage of *Power Reactor Technology* may occasionally overlap the fields of the other Technical Progress Reviews, the overlaps will be motivated by this objective of viewing current progress through the eyes of the reactor designer.

A degree of critical appraisal and some interpretation of results are often necessary to define the significance of reported work. Any such appraisals or interpretations represent only the opinions of the reviewers and the editor of *Power Reactor Technology*, who are General Nuclear Engineering Corporation personnel. Readers are urged to consult the original references in order to obtain all the background of the work reported and to obtain the interpretation of the results given by the original authors.

W. H. ZINN, President
J. R. DIETRICH, Vice-President and Editor
General Nuclear Engineering Corporation

PD
539.7
G 326
V.6, No 3

Contents

Foreword

I ECONOMICS AND APPLICATIONS: POWER PLANTS IN NUCLEAR DEFENSE 1

II FLUID AND THERMAL TECHNOLOGY 4
Conduction 4
Hydrodynamics of Two-Phase Flow . . . 5
Burnout in Two-Phase Flow 10
References 10

III MATERIALS 12
Uranium Oxide 12
Absorber Materials 15
Zirconium Alloys 16
Stainless Steel 17
Graphite 18
References 18

IV CONTAINMENT, RADIATION CONTROL, AND SITING 20
Iodine Removal 20
Proposed Ravenswood Containment 21
Pressure Suppression 27
References 27

V DESIGN PRACTICE 28
Consolidated Edison Nuclear Steam Generating Station 28
Review of Nuclear Vessel Problems . . . 40
Recent ASME Boiler Code Nuclear Cases 41
PM-1 Core Design 43
References 46

VI OPERATING EXPERIENCE 49
Shippingport Atomic Power Station 49
Yankee Core Evaluation Program 55
References 56

VII GAS-COOLED REACTORS 57
ANP Terminal Reports 57
Army Reactor Systems Program 57
Advanced Reactor Studies 60
Progress Reports 64
References 64

VIII PRESSURIZED-WATER REACTORS: PROPOSED SECOND CORE FOR INDIAN POINT 66
Fuel Elements 66
Fuel Assemblies 66
Control Rods 68
Reference 68

IX ORGANIC-COOLED AND -MODERATED REACTORS 70
Coolant Treatment 70
Stability of Organic Materials 70
References 72

X SUPERCRITICAL WATER REACTORS 73

XI PHYSICS 79
Resonance Absorption 79
Critical and Exponential Experiments . . . 80
Shielding 83
References 87

Issued quarterly by the U. S. Atomic Energy Commission. Use of funds for printing this publication approved by the Director of the Bureau of the Budget on November 1, 1960.

Section

I

Power Reactor Technology

Economics and Applications: Power Plants in Nuclear Defense

Brookhaven National Laboratory and Oak Ridge National Laboratory, with the assistance of Sargent & Lundy and Burns and Roe, Inc., have compared the nuclear defense capabilities of 300-Mw(e) nuclear and coal-fired generating stations.[1] The comparison includes a study of the feasibility of plant protection from nuclear attack and an evaluation of the economics of the protected plants. Since power-generating costs vary in different sections of the United States, comparisons were performed for three geographical areas: the Southeast, the Midwest, and southern New England.

Early in the study[1] it was estimated that, on an economic basis, nuclear power plants of less than 300-Mw(e) output could not compete with coal-fired plants of a like rating. The plant size for the study was chosen as this minimum competitive value. In order to limit the study effort, one specific type of nuclear plant was selected: for the final comparisons, the nuclear plant utilized a pressurized-water reactor.

To determine the nuclear plant selection, four reactor types were considered. These reactors powered 300-Mw(e) generating stations, and they were placed on the same basis by use of the normalized information on the specific types reported in Refs. 2 and 3. The four reactor types, which were chosen to cover a range of containment possibilities as well as a range of reactor characteristics, were as follows:

1. The pressurized-water reactor (PWR), typical of a relatively high-power-density reactor cooled by high-pressure liquid and having a secondary containment shell

2. The fast-breeder reactor, typical of a low-pressure liquid-cooled reactor with a secondary containment shell

3. The sodium graphite reactor, typical of a low-pressure liquid-cooled reactor without a secondary containment shell

4. The gas-cooled reactor, typical of a natural-uranium plant without secondary vapor containment

Reference 1 contains a discussion of the pressure, thermal, and radiation effects of nuclear weapons and concludes that, for both nuclear and coal-fired power stations, the pressure effects are the ones most likely to result in the cessation of plant operation. Consideration of the inherent blast resistance and the economic attractiveness of the different nuclear plants led to the selection of the PWR as the type best suited to nuclear defense applications. The conclusions reached regarding it would probably be equally applicable to a boiling-water plant.

Three approaches were considered for providing the blast protection necessary in the event of a nuclear attack: (1) location of the plants at sufficiently great distances from prime target areas, (2) "hardening" of the plants by suitable protective structures, and (3) construction underground or in cavities in mountains. Of these, the third was judged[1] excessively expensive and was quickly discarded. The alternative of hardening the plants was favorable, relatively, to the nuclear plant. It was estimated that the usual reactor containment structures would provide protection for internal components when subjected to overpressures up to 10 psi, the level produced by the assumed blast at the assumed plant location, and consequently additional hardening, for the nuclear plant, would be needed only for those parts outside the containment building. However, the most favorable approach, on an absolute basis, was found to be the relatively remote siting of unhardened plants. In this

case also, the nuclear plant benefited, since its normal overall construction was estimated to be capable of withstanding overpressures up to 3 psi, the pressure that would occur at a distance of 15 miles from ground zero with the assumed blast (20 Mt). It was concluded that a 300-Mw(e) nuclear plant would probably require a location at least 15 miles from the nearest population center to satisfy safeguard requirements in any case and that the degree of protection provided by this amount of separation therefore did not involve any penalty for the nuclear plant beyond its normal costs. The coal-fired plant, on the other hand, required a location about 30 miles from ground zero in order to withstand the blast overpressure (about 1 psi). The estimated construction costs for the two plant types, with the three different protection measures, were as follows:

	Nuclear plant	Coal-fired plant
Unhardened (remote) plant	$60,050,000	$50,500,000
Hardened aboveground plant	62,824,000	65,572,000
Hardened underground plant	79,583,000	67,000,000

Up to this point in the comparison of the nuclear defense capabilities of nuclear and coal-fired power plants, it is seen that, since special construction is not employed to protect the plants, the basic economic relations between the two types have not changed. The total power-generating cost for the nuclear plant is about 7.4 mills/kw-hr; the comparable cost for a coal-fired plant is estimated[1] to be less in the Midwest and Southeast and about the same in southern New England.

The overall role of power plants in national defense would consist in surviving an attack and retaining the capability of continued power production. The main advantage of the nuclear plant lies in its ability to produce power without a continuous large-tonnage fuel supply. If the coal-fired plants are to produce power for any substantial period after a nuclear attack, the fuel transportation problem must be alleviated. Reference 1 contains an economic evaluation of three approaches to the problem, all of which leave something to be desired from the point of view of defense. These approaches are (1) stockpiling of a one- to five-year supply of coal, (2) pipeline pumping of coal slurry, and (3) mine-mouth plant siting. The actual studies of the fueling concepts were performed by Sargent & Lundy and were reported in Report SL-1925, "Fueling of Thermal-Electric Plants To Meet Civil Defense Requirements." This report is included as an appendix in Ref. 1.

To stockpile a one- to five-year supply of coal would require additional storage area and handling equipment, and the stockpiled coal and its handling equipment would be subject to contamination by radioactive fallout following a nuclear attack. A fueling system using pipeline pumping of a coal-water slurry from a mine mouth or other source to the power plant has the disadvantage of a relatively high vulnerability to blast damage because of the widely dispersed nature of the system components. Mine-mouth plant siting is a concept in which the coal mine itself functions as the stockpile of emergency fuel. Power is generated at the mine mouth and is fed by long-distance high-voltage transmission lines to the load center. The transmission lines are vulnerable to blast damage, but they are judged to be rather easily repaired.

The results of the analyses of total power-generating costs for unhardened nuclear and

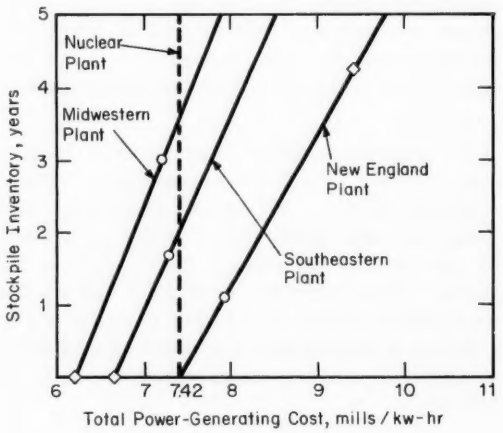

	Mine-Mouth Plants ◇	Coal-Slurry Plants ○
Midwestern Area	6.24	7.28
Southeastern Area	6.48	7.18
New England Area	9.48	7.98

Fig. I-1 Comparison of power-generating costs for nuclear and coal-fired plants with various coal-stockpile inventories.[1]

coal-fired plants are summarized by Fig. I-1. The figure shows that, in New England, the nuclear power plants have an economic advantage over the coal-fired plants, regardless of the method of providing fuel for the latter. In the Southeast and the Midwest, coal-fired plants with fuel stockpiles up to about two and three and one-half years' supply of coal, respectively, are cheaper than nuclear plants: both mine-mouth plants and coal-slurry plants are cheaper than nuclear plants in these areas. Thus the conclusions of the comparison are that remotely sited, unhardened plants of the following types furnish the most economic electric power to the specified areas:

Southeast	Mine-mouth plant
Midwest	Mine-mouth plant
New England	Nuclear plant

In a study of this type it is difficult to develop quantitative conclusions of lasting validity, when changes are occurring rather rapidly in the technology, containment approaches, and siting principles for nuclear plants. It is interesting, however, to observe that nuclear plants apparently do enjoy some advantages with respect to surviving nuclear attacks, even when this is not a specific design objective. It is also interesting to note that the underground location of nuclear plants, which is the approach most often suggested for decreasing their vulnerability still further, appeared to be so unattractive economically.

References

1. Brookhaven National Laboratory and Oak Ridge National Laboratory, A Comparison of the Nuclear Defense Capabilities of Nuclear and Coal-Fired Power Plants, USAEC Report BNL-6080, May 1962.
2. Sargent & Lundy, Power Cost Normalization Studies, Civilian Power Reactor Program—1959, USAEC Report SL-1674, Sept. 1, 1959.
3. Civilian Power Reactor Program. Part I, Summary of Technical and Economic Status as of 1959, USAEC Report TID-8516, 1960.

Section

II

Power Reactor Technology

Fluid and Thermal Technology

Conduction

The thermal conductivity of UO_2 is discussed in Sec. III of this issue of *Power Reactor Technology*. Reference 1 treats another conductance phenomenon important in the determination of internal temperatures of oxide fuel elements: the thermal conductance of UO_2-metal interfaces. The study was both analytical and experimental, with the experimental determinations of the interfacial conductance between UO_2 and stainless steel being made in essentially an axial heat-flow apparatus. Heat flow was from an electric resistance heater through a molybdenum rod, and through a stainless-steel disk, a UO_2 disk, and another stainless-steel disk in series. Guard rings around this assembly minimized radial heat conduction. The samples could be axially loaded so that interface contact pressures from 91 to 570 psi could be attained. The effects of three different filling gases and vacuum were investigated. Interface temperatures ranged up to 770°F with heat fluxes up to 7.3×10^4 Btu/(hr)(sq ft). A range of surface roughness corresponding to arithmetical mean heights from 11×10^{-6} to 1417×10^{-6} cm was covered. The samples were prepared by first lapping the contact surfaces to optical flatness and then roughening them to the desired degree.

In the theoretical treatment[1] the contributions of the solid conductance and fluid conductance are examined separately. Experimentally the contribution of the solid-to-solid contacts was determined by runs *in vacuo*, and the contribution of the fluid to the transport of heat across the interface was obtained by the difference between the results with the filling gas and without the filling gas. The solid conductance was found to be independent, within the accuracy of the experiments, of heat flux and interface temperature. There was also no significant change with contact pressure over the range used. The analytical and experimental results for solid conductance are described as in approximate agreement. The gas conductance was found to vary as expected with the filling gas and to be independent of the gas pressure (except, of course, under high-vacuum conditions). The theoretical values of the gas conductance, which were based on simple geometrical models of the roughness and which allowed for accommodation effects in collisions between the gas molecules and the surfaces, were compared with the results of the experiments reported and with other published data. In nearly all cases the agreement was within a factor of 2.

The differences between these results and those of Ref. 2 [see *Power Reactor Technology*, 4(2): 40-43], which were derived from measurements on operating UO_2 fuel elements, are striking. The results of Ref. 2 indicated little effect of the filling gas and an important effect of contact pressure. Reference 1 discusses these differences. Much of the disagreement may result from the difference between a carefully controlled experimental configuration and a configuration which, although carefully constructed, attempts to approximate the conditions in a practical fuel element. Although the discrepancies emphasize the difficulty of applying theoretical techniques to the practical case, they do not by any means detract from the usefulness of the "idealized" approach, which not only gives insight into the basic phenomena but contributes to an understanding of the processes operating in the "practical" case by the very discrepancies that it reveals.

An interesting conduction problem is discussed in Ref. 3. The basic problem is that of determining the surface temperature of a tube

in which heat is generated electrically. Quite often the surface temperature on one side of the tube wall is determined by placing a thermocouple on the other side of the wall and adding the calculated temperature drop through the wall. The reference discusses the use of an analog computer in determining the temperature drop of a wall for which temperature-variable electrical and thermal conductivities are assumed. The particular physical situation, although not of direct interest to the reactor designer, is one frequently encountered by workers in the field of experimental heat transfer. The appropriate equations are developed and circuit diagrams are presented for use in coding the analog computer.

A related discussion in Ref. 4 is aimed directly at the problem of burnout of a water-cooled fuel element and its simulation by electrically heated tubes. In particular, Ref. 4 is an examination of the question of how well the electrically heated tube reproduces the actual thermal behavior of the fuel rod during a transient when the heat-transfer surface is suddenly insulated by steam blanketing. The transient equations are formulated for the reactor fuel rod and for the electrically heated simulation. An equivalent slab is substituted for the cylindrical geometry of the systems to aid in mathematical manipulations, and the temperature-independent physical properties of UO_2 and cladding are assumed. Since the electrically heated cladding may be backed up by a structural material in the experimental setup, this effect is also included. The results are shown in Fig. II-1, where the transient response of a fuel rod is compared to that of an electrically heated test section backed with alumina or asbestos-phenolic. It can be seen that the time variation of the surface temperature rise varies for the three systems, and this rise depends upon the backup material in the electrically heated case. Whether this varying rate of temperature increase with onset of burnout would result in different burnout heat fluxes is, of course, not established by these data. Reference 4 recommends that this question be made the subject of an experimental study.

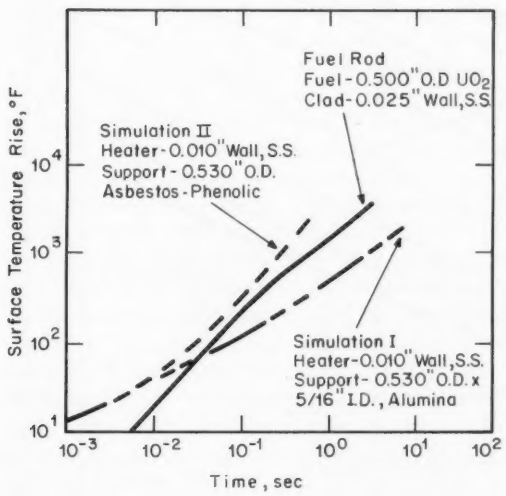

Fig. II-1 Surface temperature rise vs. time for a UO_2 fuel rod and two electrical simulation geometries in the event of sudden and total insulation of the heat-transfer surface[4] at a heat flux of 500,000 Btu/(hr)(sq ft).

Hydrodynamics of Two-Phase Flow

Critical flow in two-phase single-component systems is treated in Ref. 5. The study is a combined analytical and experimental one. The analysis proceeds by assuming annular flow in a pipe and examining momentum and continuity equations. When the dynamics of two-phase flow with slip is considered, the appropriate definition for the specific volume of the two-phase mixture is not immediately apparent. By analogy to the equation of motion for single-phase flow, a new definition for the specific volume of the two-phase system is developed:[5]

$$v = \frac{x^2 v_g}{\alpha_g} + \frac{(1-x)^2 v_l}{1-\alpha_g} \qquad (1)$$

where v = specific volume of two-phase mixture, cu ft/lb
$v_{g,l}$ = specific volume of saturated vapor and liquid, cu ft/lb = $1/\alpha_{g,l}$
x = quality, lb/lb
α_g = void fraction of the vapor phase, cu ft/cu ft

This equation can be contrasted to the equation for homogeneous flow

$$v = v_l (1-x) + v_g x \qquad (2)$$

which is obviously inappropriate when there is slip, and to the commonly used expression for slip flow

$$v = \frac{1}{\rho_l(1 - \alpha_g) + \rho_g \alpha_g} \qquad (3)$$

Values of v calculated by Eq. 1 lie between the values calculated by Eqs. 2 and 3.

Critical flow is defined as the condition existing when the flow rate no longer increases with increasing pressure difference, and in addition, the reference[5] adopts a second definition which states that critical flow exists when the pressure gradient along the pipe has an absolute, finite, maximum possible value for a given flow rate and quality. The sum of the acceleration and friction pressure-drop terms was maximized to fulfill the latter definition by treating the slip ratio, k, as an extra degree of freedom in the two-phase flow system. Thus this view of the critical-flow phenomenon has made possible the evaluation of the slip ratio at the critical-flow condition on purely theoretical grounds. The results are shown in Fig. II-2, which is a plot of the critical mass flow rate, G_{crit}, as a function of pressure and quality.

Fauske[5] points out that his analysis for two-phase critical flow does not lead to the sonic-velocity limitation, although it does approach that limit as quality is increased toward 1.0 and the single-phase condition is approached (Fig. II-3). He states that, in this respect, the two-phase case does differ inherently and significantly from the single-phase case, and he cites experimental evidence that pressure disturbances can, indeed, be propagated upstream in two-phase critical-flow systems.

The reference shows impressive agreement between theory and experimental results, both those of Fauske[5] and of others.

The measurement of flow of a two-phase material by means of orifices is discussed in Ref. 6. The report deals with experimental results obtained using steam-water, air-water, gas-distillate, and gas-water mixtures. The

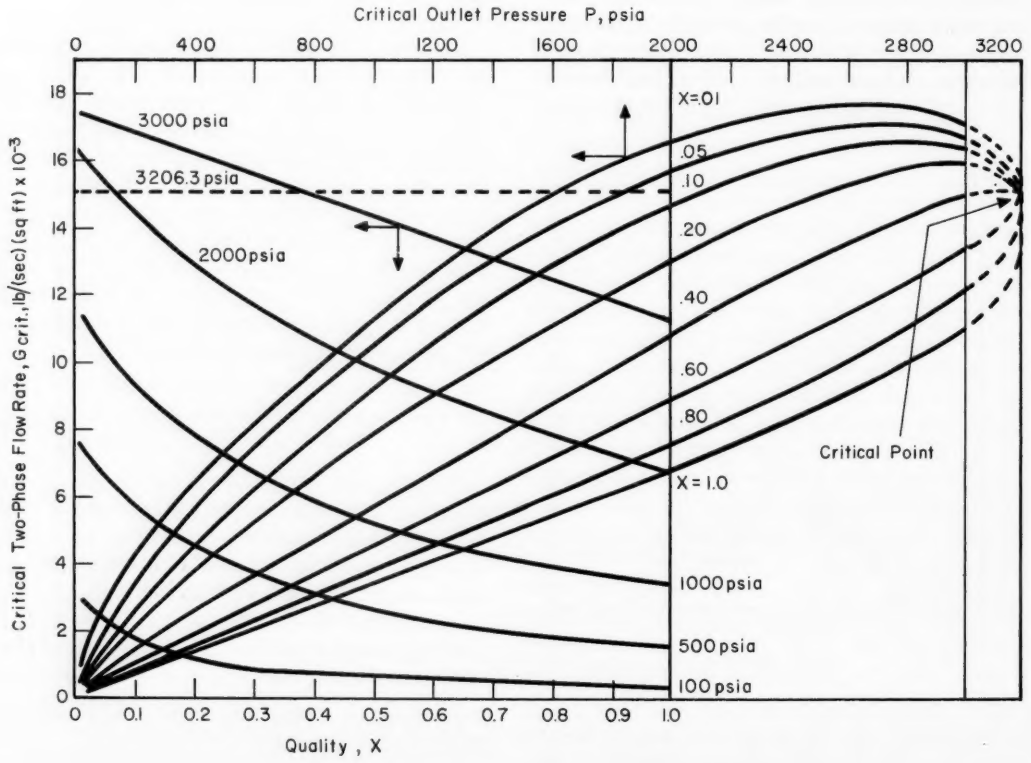

Fig. II-2 Theoretical predictions of critical flow rates.[5]

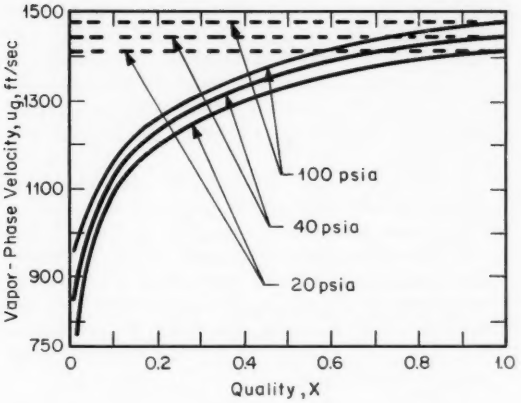

Fig. II-3 Theoretical prediction of the vapor-phase velocity compared with the velocity of sound.[5] ——, two-phase mixture. – – –, saturated steam.

flow rates were measured by means of sharp-edged concentric orifices manufactured and installed in accordance with requirements of the American Gas Association[7] and the American Society of Mechanical Engineers.[8] Details of the orifice arrangements are given, and an empirical calibration equation, which is stated to be accurate to 1.5%, is given also.

The pressure drop through an orifice is used in Ref. 9 as the basis for a device to control automatically the exit quality from a boiling channel. The objective is to control the exit qualities for individual fuel assemblies in a forced-circulation boiling reactor. If no effort is made to control local flow rates in such a reactor, the exit quality of the higher power assemblies will be higher than that of the lower power assemblies, both because of the higher rate of steam generation and because of the increase in pressure drop for a given mass flow rate with steam-void fraction. Inasmuch as the burnout heat flux usually decreases as quality increases, the higher power assemblies in such a situation find their burnout ratio decreased for two reasons: (1) their higher heat flux and (2) their higher exit quality. Ordinarily in boiling-reactor design this effect is allowed for to the extent possible by fixed devices for the control of flow distribution. The fuel assemblies expected to operate at higher powers are provided with relatively higher flow rates by orificing the lower power assemblies or by other means. The aim of the automatic control device is to provide exit quality control which will be maintained despite changes of power distribution during the life of the core.

The schematic of the device is shown in Fig. II-4, and the theory of operation is quoted here.[9]

> The device operates as follows:
>
> 1. The venturi at the inlet gives a signal which is a measure of the mass flow rate of the liquid entering the channel, the density being known from the inlet conditions.
> 2. The venturi at the exit gives a signal which is a measure of the mass flow rate and the density at the channel exit.
> 3. The two signals are subtracted across an opposing set of bellows in the comparator . . .
> 4. Any changes in either venturi signal which upsets the null force balance on the three-way spool valve in the comparator will move the (three-way spool) valve. This will cause water to flow in or out of the bellows which moves the flow control valve. The high pressure water used to actuate the bellows comes from the channel just upstream of the inlet venturi.

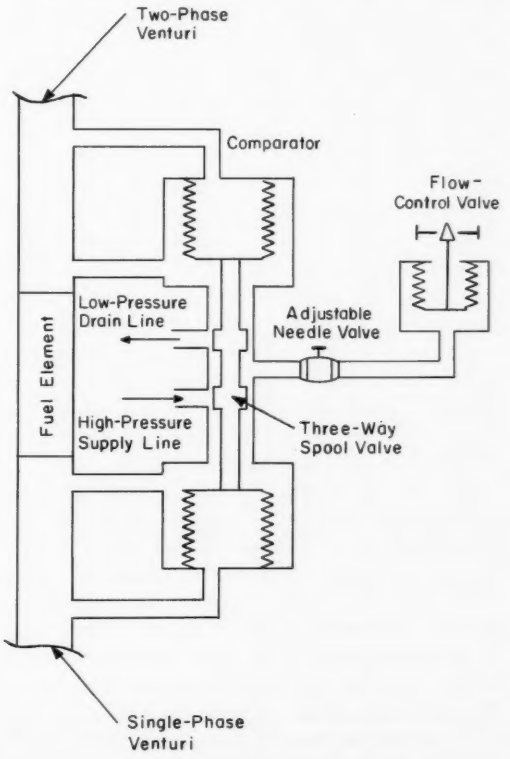

Fig. II-4 Control system schematic.[9]

5. The flow control valve opens or closes directly with the bellows motion. This increases or decreases the liquid flow rate in the channel and will correspondingly lower or raise the exit quality.

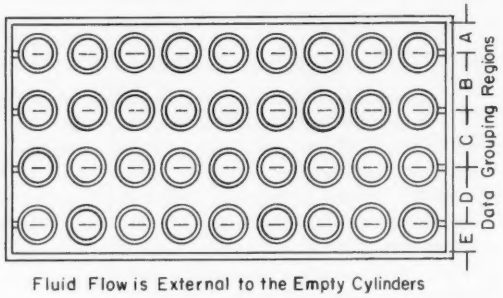

Fig. II-5 Schematic diagram of air-water test section.[10]

The proof-of-principle device was tested on air-water mixtures at low pressure and room temperature. The device held the discharge quality to within 3% of the design value for changes of up to 30% in the simulated power. The operating characteristics were such that an increase in the simulated power led to a slight decrease in quality, rather than the increase in quality which would have been expected with a fixed orifice and forced circulation. The particular scheme illustrated in Fig. II-4 is not fail-safe, although a design is illustrated which would not shut off flow to the channel if the various bellows failed or the transmission lines broke. One safety problem yet remaining appears to be the problem of the comparator becoming stuck in a position that would lead to the closing of the flow-control valve. The recommended design solution[9] is to design a comparator that does not stick. The design of a device to fit a BWR fuel element is proposed as part of a future program.

The measurement of void fractions in parallel-rod arrays is the subject of the experimental data reported in Ref. 10. The particular geometry studied is shown in cross section as Fig. II-5. Gamma-attenuation techniques, employing a Tm^{170} source, were used to determine the voids. The device was calibrated against an aluminum-Lucite mockup. The data grouping regions are shown in Fig. II-5, and some results are shown in Fig. II-6. The conclusions of the study are quoted[10] as follows:

1. The gamma attenuation method can be used for measuring void fractions in a parallel rod array so long as a fine traversing technique is employed.
2. Accuracies of within about 5% absolute void fraction can be expected although this will depend upon many factors not varied in the present experiments.
3. Measured void fractions in air-water flow among parallel rods agree fairly well with similar results for rectangular channels and round tubes.
4. The distribution of density in the air-water flow indicates a tendency for the gas to collect between pins in the square pitch array. (However, the distribution in a boiling flow would be expected to be significantly different from that observed in the present experiment.)

References 11 and 12 both apply to specific reactor designs but contain information of general use. Reference 11 reports on tests designed to study the parallel-flow vibration of a prototype element of the Consumers Power Company reactor (Big Rock Point, Mich.), whereas Ref. 12 is concerned with the effect of water surface waves in boiling-water reactors, with emphasis on the Vallecitos Boiling-Water Reactor (VBWR).

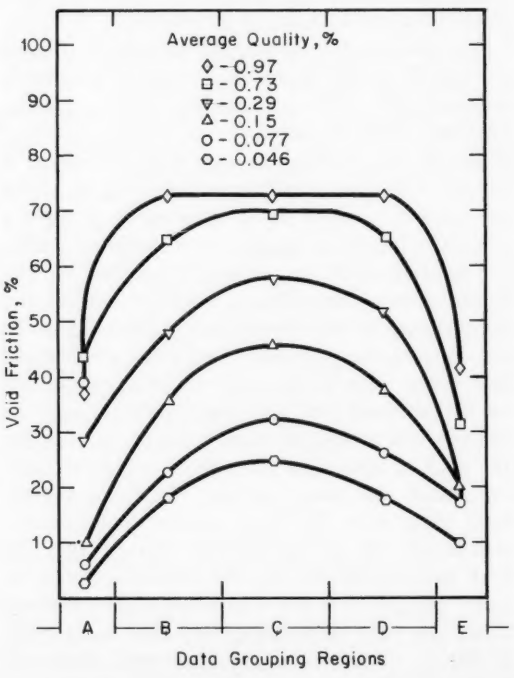

Fig. II-6 Regionwise void distribution.[10] The superficial liquid velocity is 3.2 ft/sec.

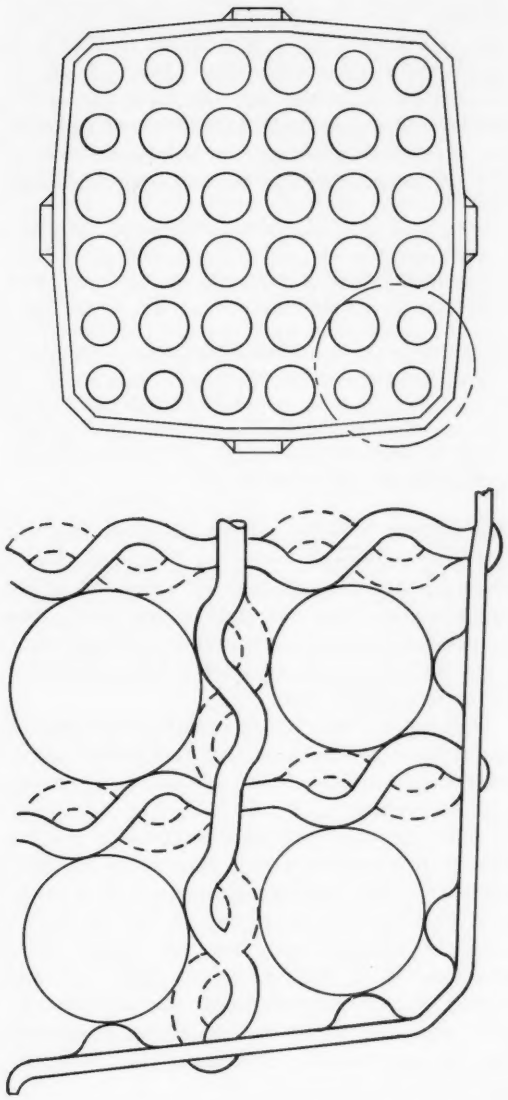

Fig. II-7 Intermediate spacer of Consumers Power Company reactor multirod element.[11]

A cross section of the Consumers fuel bundle is shown in Fig. II-7; other data on the fuel bundle are given in Table II-1. The spacers are not fastened to the fuel-rod cladding, and they have between 0.002 and 0.013 in. of clearance (cold).* The three rods at each of the four corners differ from the remaining rods in the bundle since they are used as the structural frame of the assembly. They are bolted to each end, and their dimensions are smaller. The fuel-rod tubing has a 0.302-in. inside diameter and an 0.018-in. wall thickness. Tests were also performed on a single rod to examine the applicability of theoretical work on vibration of rods, and the author concludes that "...multirod vibration may be estimated from single rod measurements or analysis."

*It is not clear from the reference just how the three intermediate spacers are held in position with respect to each other.

Table II-1 SPECIFICATIONS OF CONSUMERS STRAIGHT-THROUGH FUEL RODS[11]

Cladding length, in.	73.3
Cladding inside diameter, in.	0.351/0.348
Cladding wall thickness, in.	0.020/0.018
Cladding material	304 stainless steel
Form of fuel	Sintered pellets
Type of fuel	Uranium dioxide
Diameter of fuel pellets, in.	0.346 to 0.343
Length of fuel pellets, in.	0.50
Number of intermediate spacers	3

The work described in Ref. 12 was done as part of the VBWR Stability Experiment and is concerned with causes of steady-state flux noise; in particular, it examines the premise that water waves in the VBWR contribute to the noise. The VBWR exhibits random oscillations in neutron flux, fuel-channel flow rate, and recirculation-loop flow rate which lie in the frequency range from about 0.4 to 1.0 cps. Experiments were performed in a 3-ft-diameter air-water reactor model at atmospheric pressure and temperature. In general, the wave frequencies were comparable to the noise observed in the VBWR, and extrapolations of the air-water test results to the reactor are shown in Table II-2. Peak-to-peak amplitudes of 8 ft are not possible in the VBWR because the waves would hit the head of the reactor pressure vessel. Howard and Hamilton[12] suggest that under these conditions water would be expected to

Table II-2 RESULTS OF EXTRAPOLATING AIR-WATER WAVE TESTS TO THE VBWR[12]

Power, Mw(t)	Flow, gal/min	Total peak-to-peak wave amplitudes, ft
15	4,000	0.5
15	20,000	4
40	20,000	8

enter the steam outlet line, and they observe that the VBWR steam does have a high moisture content. In the experiments the suppression of waves by wave baffles of various designs was investigated. These baffles appeared to be quite effective, and, if they were incorporated in the VBWR, the peak-to-peak amplitudes apparently might be reduced to less than 0.5 ft for the case of 40 Mw(t) at 20,000 gal/min. The authors' recommendations[12] are as follows:

> 1. The validity of the wave theory be tested in a boiling water reactor having free surface steam separation. The test would consist of measuring the reactor flux noise behavior both with and without a wave baffle.
>
> 2. Precautions against water surface waves be incorporated in future boiling water reactor designs. These take different forms depending on type of steam separation . . .

Burnout in Two-Phase Flow

Reference 13 is an analytical study of the prediction of critical heat flux in forced convection. The method used is that of superposition and is very similar to that used by Gambill[14] [*Power Reactor Technology*, 6(1):18]. The principle of the superposition method is to divide the problem into subproblems. Solutions to the subproblems are derived and added algebraically to obtain a descriptive equation for the whole process. The approach used in Ref. 13 is described by the following quotation:

> In the case of subcooled flow, the critical heat flux under non-flow or pool boiling conditions is first specified. To this heat transfer rate are next added the heat conducted from the surface by the subcooled non-flowing fluid and the heat convected from it by the subcooled flowing fluid. Similarly, in the case of net vapor generation, heat convected from the surface is first added to the pool boiling critical heat flux and an equivalent mass transfer rate is next subtracted from it to account for the presence of vapor in the stream.

The various subcorrelations are given, and the final correlation is tested by comparison with experimental data. In general, about 85% of the experimental data correlate within ±30%. The correlation for forced-convection boiling contains an adjustable constant determined from the experimental data.

Included in Ref. 15 are results of an attempt to increase the burnout heat flux by the use of roughened surfaces. The particular geometry studied is shown in Fig. II-8, and it is of interest to note that the roughened surface is not the heat-transfer surface but, rather, the opposite surface in the annular geometry. At a mass flow of 1.12×10^6 lb/(hr)(sq ft), the improvement in burnout heat flux was about +22%, whereas, at a mass flow of 1.68×10^6 lb/(hr)(sq ft), the improvement was about +50%. The reference states that the effects of washer spacing and annular clearance will be investigated.

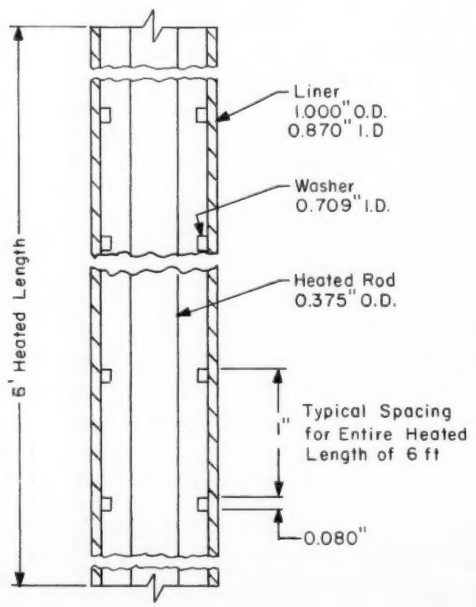

Fig. II-8 Single rod test section with rough liner.[15]

References

1. A. C. Rapier, T. M. Jones, and J. E. McIntosh, The Thermal Conductance of Uranium Dioxide/Stainless Steel Interfaces, British Report TRG-332 (W), June 26, 1962.
2. I. Cohen, B. Lustman, and J. D. Eichenberg, Measurement of the Thermal Conductivity of Metal-Clad Uranium Oxide Rods During Irradiation, USAEC Report WAPD-228, Bettis Atomic Power Laboratory, August 1960.
3. D. G. Harden and L. T. Bryant, Analog Computation of Temperature Distribution in Solids with Electrical Heat-Generation and Temperature-

Dependent Properties, USAEC Report ANL-6645, Argonne National Laboratory, November 1962.

4. B. Matzner, Basic Experimental Studies on Boiling Fluid Flow and Heat Transfer at Elevated Pressures, Monthly Progress Report, USAEC Report TID-15169, Columbia University, Engineering Research Laboratories, Mar. 30, 1962.
5. H. K. Fauske, Contribution to the Theory of Two-Phase, One-Component Critical Flow, USAEC Report ANL-6633, Argonne National Laboratory, October 1962.
6. J. W. Murdock, Two-Phase Flow Measurement with Orifices, *J. Basic Eng.*, 84(4): 419 (December 1962).
7. American Gas Association, Orifice Metering of Natural Gas, Gas Measurement Committee Report No. 3, April 1955.
8. American Society of Mechanical Engineers, Test Code Supplement on Instruments and Apparatus, Part 5, Chap. 4, Flow Measurement, PTC 19.5:4—1959.
9. R. L. Mela, R. Moissis, D. A. Gall, E. F. Doyle, and N. A. Radovcich, Final Report, Automatic Flow Balancing Device for Boiling Water Reactors, USAEC Report NYO-10475, Dynatech Corporation, Dec. 17, 1962.
10. R. A. Condon and N. C. Sher, Measurement of Void Fractions in Parallel Rod Arrays, *Nucl. Sci. Eng.*, 14(4): 427 (December 1962).
11. E. P. Quinn, Vibration of Fuel Rods in Parallel Flow, USAEC Report GEAP-4059, General Electric Company, Atomic Power Equipment Department, July 1962.
12. C. L. Howard and R. G. Hamilton, Water Surface Waves in Boiling Water Reactors, USAEC Report GEAP-4061, General Electric Company, Atomic Power Equipment Department, Aug. 31, 1962.
13. S. Levy, Prediction of the Critical Heat Flux in Forced Convection Flow, USAEC Report GEAP-3961, General Electric Company, Atomic Power Equipment Department, June 20, 1962.
14. W. R. Gambill, Generalized Prediction of Burnout Heat Fluxes for Flowing, Subcooled, Wetting Liquids, Paper AIChE No. 17 presented at Fifth National Heat Transfer Conference and Exhibit, Houston, Texas, Aug. 5-8, 1962.
15. J. A. Hodde (Ed.), Fuel Cycle Program, A Boiling Water Reactor Research and Development Program, Quarterly Report No. 5, July 1961-September 1961, USAEC Report GEAP-3835, General Electric Company, Atomic Power Equipment Department, Oct. 10, 1961.

Section

III

Power Reactor Technology

Materials

Uranium Oxide

Previous issues of *Power Reactor Technology* have reviewed a considerable amount of information pertaining to the thermal conductivity of UO_2. The consensus of the reviews has been that many variables, such as density, temperature, irradiation, and departures from the stoichiometric composition, can influence the thermal conductivity. Moreover, observations of irradiated UO_2 specimens and their performance records have suggested that the effective thermal conductivity of UO_2 operating at "in-service" temperatures (from about 400°C to melting) is greater than that indicated by extrapolation of the comparatively low-temperature (<1500°C) laboratory experiments. These observations have led to predictions of higher values for the thermal conductivity of UO_2 at the temperatures of interest than have heretofore been used in fuel-element designs.

The predictions are based mainly upon comparisons with the high-temperature heat-transfer mechanisms existing in materials that have properties of thermal translucence similar to that of UO_2. They suggest that the normal conductive mode of heat transport should be reinforced by a substantial radiative heat-transfer component. The radiative component has been thought to be associated with recrystallization.

The difficulties associated with the measurement of thermal conductivity at elevated temperatures have precluded a straightforward experimental test of the existence of such a crystal-associated heat-transfer effect at the temperatures of interest. However, measurements of the thermal conductivity of single-crystal UO_2, pressed-and-sintered UO_2, and packed-powder UO_2 have been made at low temperatures (1200°C).[1] Comparisons of the thermal conductivities of these materials, at various temperatures, are shown in Fig. III-1. The data do, at least, show a beneficial effect of converting from a polycrystalline to a single-crystal composition.

In a discussion of the results of the work, the reference attributes the low thermal conductivity of the packed-powder specimen to interfacial effects associated with the compacted particles. The exact nature of these effects has not been determined. The decreased conductivity of specimen A, after thermal cracking, is ascribed to the thermal-barrier effect of the crack. The reference calls attention to the fact that the widely used thermal-conductivity curves advanced by Kingery and other earlier investigators are in good agreement with those of specimen A over the range of temperatures considered.

A converse opinion for the apparent improvement in thermal conductivity with temperature is contained in Ref. 2. These investigators suggest that the improvement is associated with the composition of the UO_2 rather than the freedom from grain boundaries. The reference states that when single-crystal UO_2 was oxidized to remove the metallic uranium which had been observed metallographically, the thermal conductivity of the resulting stoichiometric oxide was less than that of the as-received hypostoichiometric material; moreover, by reducing polycrystalline sinters to hypostoichiometric composition, thermal conductivities approaching those of single-crystal material were obtained. The reference suggests that the improvement in thermal conductivity with temperature results from "...the inclusion of a large electronic conduction component at elevated temperatures when the excess uranium dissolves to form hypostoichiometric uranium dioxide." Reference 2 also suggests that this effect, if true, could have important implications

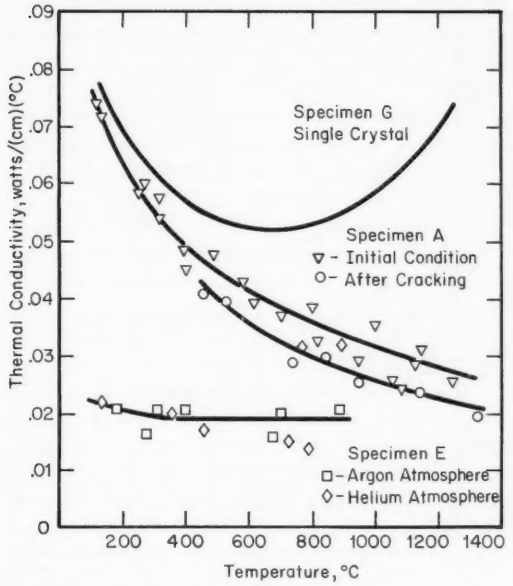

Specimen A - Disk

Nonirradiated UO_2
Die Pressed, Sintered

Length	2.256 cm
Diameter	7.513 cm
Weight	1055 g
Density	10.59 g/cm³ (96.5% TD)

Specimen E - Disk

Nonirradiated UO_2
Vibrationally Compacted Particles of Fused UO_2 Contained in Stainless-Steel Cup (0.029-in. Wall Thickness)

Length	2.502 cm
Diameter	8.738 cm
Weight	1428 g
Density	9.52 g/cm³ (86.8% TD)

Fig. III-1 Thermal conductivity[1] of UO_2.

for the direct conversion from nuclear to electrical energy.

In the work of Ref. 1, irradiation damage was found to affect thermal conductivity adversely, but the effects decreased with temperature. At low temperatures (< 500°C) the conductivity was reduced by about 10 to 20%; at temperatures of 1000°C and above little if any reduction was noted. This temperature effect is thought to be a thermal-annealing effect, which has been otherwise demonstrated by comparing the thermal conductivities of samples, irradiated at temperatures below 100°C, before and after postirradiation heating in the range of 100 to 1000°C. These experiments indicate that the UO_2 recovers from the effects of radiation damage at specific temperatures. As shown in Figs. III-2 to III-4, the temperatures or inflection points at which recovery occurs are 150 to 200°C and 350 to 400°C. A third inflection point may exist at about 800°C, but the data are not definitive on this point. It does appear, however, that the recovery of thermal conductivity is essentially complete at about 1000°C, and it is therefore expected that, in fuel elements operating at 1000°C or above, the effect of irradiation damage on thermal conductivity may be neglected at least for the present design range of fuel exposure (10,000 to 15,000 Mwd/ton).

Postirradiation examinations of a rather large number of fuel specimens have provided clues as to the thermal behavior of UO_2 during irradiation and have served as bases for explanations of the postirradiation structure exhibited by UO_2 fuels in general. Experimental data of this type, and their interpretation, were reviewed in *Power Reactor Technology*, 6(2): 28-42. Recently additional information has become available[3,4] which appears to give further substantiation of the theoretical interpretation and which probably played an important part in its derivation.

The postirradiation examination of a long-exposure (20,000 to 23,500 Mwd/ton) UO_2 fuel rod disclosed a marked dissimilarity in the appearance of two cross sections taken through the same fuel rod at points only $\frac{5}{8}$ in. apart axially. Photomicrographs of these two cross

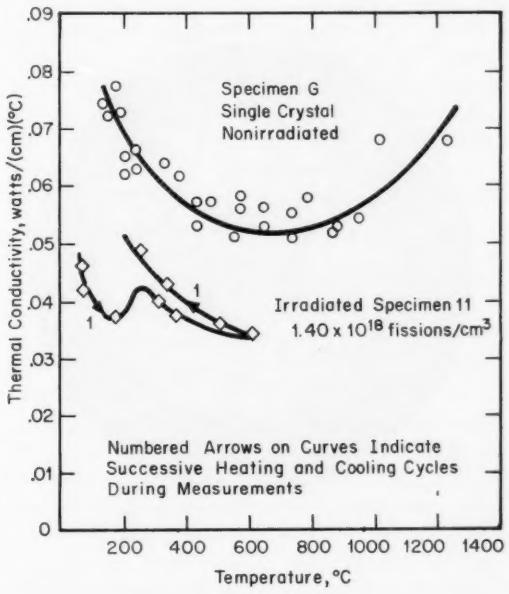

Fig. III-2 Thermal conductivity[1] of UO_2. (Single crystal, irradiated sintered cylinder, specimen 11; maximum UO_2 temperature during irradiation, < 100°C.)

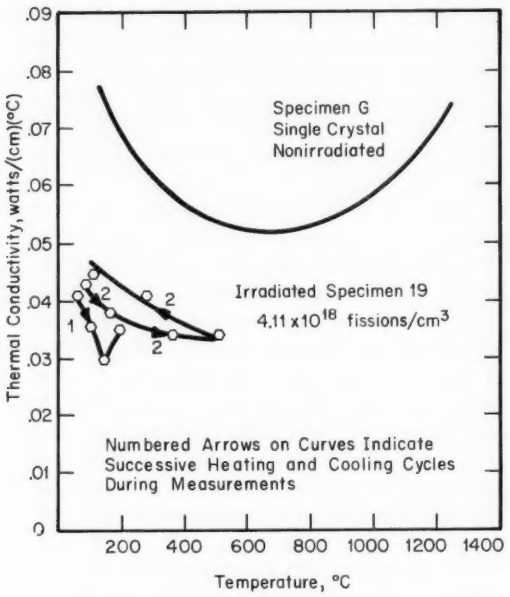

Fig. III-3 Thermal conductivity[1] of UO_2. (Irradiated sintered cylinder, specimen 19; maximum UO_2 temperature during irradiation, < 100°C.)

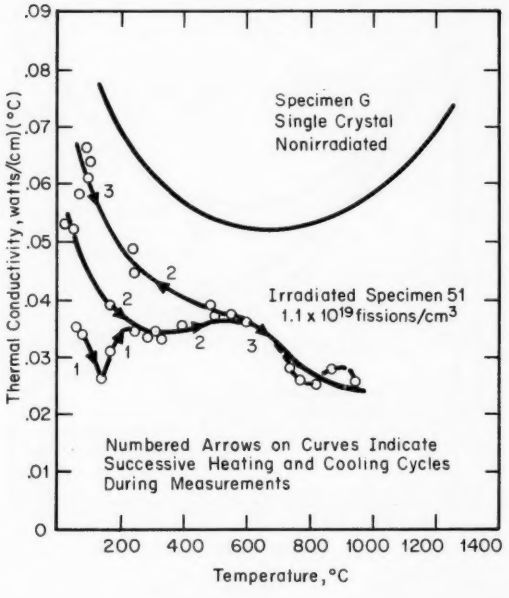

Fig. III-4 Thermal conductivity[1] of UO_2. (Irradiated sintered cylinder, specimen 51; maximum UO_2 temperature during irradiation, < 100°C.)

(a) (b)

Fig. III-5 Photomosaics of UO_2 irradiated to ~20,000 Mwd/ton of uranium. These two cross sections were ~$^5/_8$ in. apart in the fuel capsule.[3]

sections are shown in parts *a* and *b* of Fig. III-5. The cross section in part *b* is typical of the structure to be expected and clearly shows the effect of long-term temperature refinement in both the grain-growth region and that solidified portion which is considered to have been molten early in life. However, the cross section in part *a* of Fig. III-5 exhibits only the typical early-life grain-growth structure. Neither an early-life molten zone nor any refinement of the grain-growth region is evident. On the basis of only the visible evidence and the proximity of the two fuel segments, the observer is led to the conclusion either that the same operating conditions can produce radically different structures in UO_2 fuel or that the operating conditions (presumably the linear power density) for the two segments of fuel were different. Extensive examination of the fuel material between and about the cross sections shown in Fig. III-5 has yielded evidence in support of the latter contention.[3]

It was known that the cross section in part *a* of Fig. III-5 was located above that of part *b* in the vertically oriented, operating fuel rod. As a result of the postirradiation examination of various cross sections through the fuel between those in parts *a* and *b* of Fig. III-5, it was learned that the cross section in part *a* was taken through the top of a centrally located, cylindrically shaped void. This void, manifested as the large central hole shown in part *a*, is thought to have been formed by the flow of molten UO_2 from fuel in the region of part *a* into existing voids and cracks in the UO_2 which was located immediately below that in part *a* and which included the region of part *b*. As a consequence the fuel content of part *a* was reduced, whereas that of part *b* was increased, and an attendant proportional change in the power generated by the fuel in these cross sections occurred. The temperature of the fuel in part *a* was consequently reduced with respect to that of part *b* for the remainder of the irradiation period. This temperature reduction terminated the grain-growth and refinement process and left the typical short-term grain-growth structure observed in part *a*.

Absorber Materials

In-pile work on the properties of the rare-earth oxides has been reported by Atomics International (AI)[5] and General Electric Company (GEAP).[6] The AI work on the Hallam reactor program was concerned with the behavior of 90% Gd_2O_3 material and a 45% Gd_2O_3–45% Sm_2O_3 (balance inert) mixture. The specimens for irradiation were prepared by vibratory compaction (67 to 71% of theoretical density) and irradiated in the Hanford KW reactor to an exposure (calculated) of 5×10^{20} nvt. Maximum temperatures in the oxides were plotted as 1400°F (1200°F average) for two of the test capsules and 1100°F (950°F average) for the third. The major point developed was that the apparent thermal conductivities of the oxides did not change during the exposure. The comparatively loosely packed oxide evidently suffered no visible damage, and the oxide containers remained undistorted.

The objective of the GEAP program[6] was to investigate the more interesting rare earths; it was not directed toward a specific control-rod design. Europium, dysprosium, erbium, samarium, and gadolinium were investigated as sesquioxides and as borates. The borates were prepared by heating mixtures of the rare-earth oxides and boron, boron oxide, or tetraboric acid in air. The process was satisfactory with all three forms of boron. The consolidation of the powdered borates into sound, mechanically strong bodies either by pressing and sintering or by hot pressing was not successful. The hot-pressed material at densities in the 95 to 98% range was still poorly bonded. Although it is necessary to add TiO_2 to Eu_2O_3 and Dy_2O_3 to reduce their tendency to hydrate in room air, the lanthanon borates are stable, even in 500°C steam.

Compatibility studies of these oxides and the two borates were made by mixing them, in powder form, with powdered metals and heating in vacuum. Results for 12 metals are given.[6] Molybdenum and tungsten were inert to all the test materials, whereas type 304 stainless steel was inert to Dy_2O_3 and Sm_2O_3 but reacted with Eu_2O_3 at 1200°C.

Irradiations were carried out in the General Electric Testing Reactor to integrated thermal-neutron fluxes of between 0.4 and 2.4×10^{21} nvt, as determined by analysis of aluminum–0.01% cobalt monitor wire. Maximum operating temperatures were 320°C and below. Specimen densities before irradiation had ranged from 42 to 97% of theoretical. Serious cracking occurred in only a few of the 21 specimens irradiated, and dimensional changes, except for one Dy_2O_3

specimen, were at most ±2 mils for 0.38-in.-diameter pellets. Metallographic and X-ray studies were made on some of the irradiated materials. No conclusions were drawn as to which of the oxides or borates would be better for a given purpose, but the data presented will permit some comparisons.

The previously reviewed [*Power Reactor Technology*, 6(2): 49] investigation of the hafnium control rods used in the operation of the Shippingport reactor has continued with the examination[7] of one of the original corner-position rods. This rod has been exposed for 13,700 effective full-power hours and has reached an integrated fast (> 0.625 ev) neutron exposure of 1.03×10^{22}, roughly three times that of the rod previously examined. Of major concern were the effects of irradiation on the mechanical properties of hafnium and the hafnium-Zircaloy weld and on the corrosion behavior of the metal and the weld. Strength increases after irradiation showed an apparent saturation effect at 5.64×10^{21} nvt, but this was followed by a second increase in strength at 10×10^{21} nvt. Elongation showed no great change after two seed lives as compared with that after one seed life. Both strength characteristics and corrosion behavior could be affected by the buildup of tantalum as a transmutation product, but in neither case was the presence of this effect clearly established. The corrosion behavior and mechanical properties were quite acceptable after two seed lives, and considerably longer potential lives were indicated.

Zirconium Alloys

Further information on the mechanical properties of Zircaloy-2 is provided by recent Hanford reports on creep properties[8] and on impact and notch-bend testing.[9] The creep program was undertaken to determine properties for the pressure-tube design to be employed in the Plutonium Recycle Test Reactor and the New Production Reactor. Data, all for unirradiated material, are given for several stress levels at 550, 650, and 750°F for 10,000-hr test periods. Testing was done in vacuum. The Zircaloy-2 was tested in the annealed or 15% cold-worked condition. Some experiments were carried out by cycling the temperature while the specimens remained under constant load. In addition to the detailed information given on several curves plotting creep rate vs. strain, it was concluded that design criteria for Zircaloy could be set by requiring a total creep-strain limit of 1% at 550 and 650°F. The use of 15% cold-worked Zircaloy is recommended since its behavior is regular and predictable as compared to the annealed form of the alloy in which strain-age-hardening effects cause unpredictable behavior. Temperature cycling between room temperature and 550°F increased creep rates by a factor of 5.

The Hanford notch-bend work[9] had as one objective the investigation of the method as a possible substitute for the Charpy impact test. The notch-bend apparatus, a modified stiffness tester, requires little space and is therefore suited for hot-cell work. The use of this method for irradiated samples would also reduce greatly the amount of material that would have to be irradiated. Although the fracture angle of a bent notched specimen would seem to be a measure of, or at least related to, those properties determined by the conventional impact test, no such correlation was found on the unirradiated material tested. However, considerable work was done on the relations between impact strength and orientation in rolled Zircaloy plate. Notched specimens taken from a rolled sheet in the longitudinal-horizontal position had higher strengths at room temperature than did transverse-vertical specimens, but at 300°C this relation was reversed. The importance of directionality or orientation on the properties of specimens taken from Zircaloy sheet or tube should be emphasized. It was found, for example, that notch-bend specimens with the notch in the transverse-horizontal direction, a direction corresponding to a longitudinal scratch on a tube, showed brittle fractures to temperatures as high as 400°C.

Values are given for a large number of impact and bend tests at several temperatures from room temperature to 300°C. As might be expected, both cold working and the addition of hydrogen to Zircaloy lower the impact strength and raise the transition temperature. Experimental difficulties in adding hydrogen to cold-worked material prevented measurement of the combined effect.

Results of a $2\frac{1}{2}$-year program on the unirradiated thermal-stress-fatigue behavior of Zircaloy have been reported by American-Standard.[10] The ability of a fuel-element cladding to resist the effects of alternate heating

and cooling, particularly when such thermal cycling results in plastic deformation, is obviously important. The study of this special case of fatigue behavior presents experimental difficulties. The apparatus used employed a thin-walled tube specimen with heavy ends so designed that they could be fixed to rigid supports. The tube was heated by direct electrical conduction and was cooled by passing gas through the tube. Specimens were machined from both reactor-grade zirconium and cold-worked and annealed Zircaloy-2. The measurement of strains with a load cell made it possible to plot hysteresis loops for repeated plastic-strain cycles. Since a large number of data are presented, a typical value would be difficult to select, but the failure of cold-worked Zircaloy-2 in 800 cycles when cycled from room temperature to 300°C appears to be representative. In failure, circumferential ridges formed and cracked. For comparison, more conventional strain-cycling tests were carried out on similar axially loaded specimens. One of several conclusions was that thermal-fatigue life decreases with increasing ΔT and mean temperature. No endurance-limit phenomena were found. Zircaloy-2 had a greater thermal-stress-fatigue life than zirconium. If other conditions were equal, strain-cycle-fatigue life was approximately four times greater than thermal-stress-fatigue life.

Recently published information relating to zirconium corrosion leans heavily toward theoretical studies of corrosion mechanisms and the problems of alloy development. The proceedings of the symposium on zirconium alloy development held at Pleasanton, Calif., in November 1962 have been reported.[11] Some 22 papers are included from authors representing France, West Germany, Norway, Canada, and Great Britain, as well as the United States. Subject matter concerns the development of the Zircaloys, the physical metallurgy and phase-diagram relations of various alloys, texture studies, corrosion mechanisms, and the development of alloys resistant to corrosion in high-temperature (750 to 900°F) steam.

The high-temperature-steam problem is discussed in a Harwell paper.[12] Zircaloy-2 and van Arkel zirconium were exposed to steam and oxygen atmospheres. Corrosion in these media is described as a balancing of the thickening of the protective oxide layer and the degradation of this layer by cracking and the development of porosity. The addition of boric acid to the steam greatly reduced the corrosion of pure zirconium by eliminating the formation of "pustules" of oxide through which the metal was rapidly attacked. The diffusion rate of oxygen through the protective coating should be rate controlling, and a value for the diffusion coefficient of oxygen in zirconia has been determined by Douglass.[13] In this determination, use was made of the fact that the black protective oxide, as usually found on autoclaved Zircaloy, is anion deficient. When the oxide becomes stoichiometric ZrO_2, the color changes to white and the oxide is usually nonprotective. These color changes made it possible to measure interface migration. The activation energy found, 33.4 kcal/mole for $ZrO_{1.994}$, was in agreement with the parabolic law behavior of zirconium corrosion in oxygen. Work at Hanford has also been reported[14] on the study of corrosion mechanisms and posttransition behavior in steam and oxygen. Before transition, cubic law behavior was found, and for this behavior activation energies of 51 kcal/mole were determined for zirconium and Zircaloy-2 in oxygen.

Stainless Steel

Because the swaging of compacted-powder type fuel elements subjects the cladding to considerable working, some question exists as to the effects of the working on the mechanical properties. Cladding from both swaged and tandem-rolled compacted elements was investigated at General Electric[15] in comparison with as-received material. The type 304 stainless-steel cladding (the carbon content of 0.023% would indicate an actual 304L composition) which had received cold work equivalent to 36% reduction in area was removed from 0.4-in.-OD 0.015-in.-wall fuel elements produced by both processes. All the material was unirradiated. The specimens were 1.2 in. long and were made by flattening the tube. Tests were carried out at room temperature and at 650°F on specimens representing both the longitudinal and transverse directions. At 650°F the yield strength in the transverse direction was 39,000 psi with 37% elongation for the as-received material, 82,000 psi with 10% elongation for the swaged cladding, and 101,000 psi with 8% elongation for the rolled cladding. In the longitudinal direction the elongation for the swaged cladding dropped to only 4.1% at 650°F, a level

that might seem dangerously low for material intended to be subjected to the high radiation levels expected for fuel-element cladding. Possible annealing treatments were not discussed. Metallographic examination showed the maximum penetration of UO_2 particles into the cladding to be 0.004 in., or 26.5% of the wall thickness. The steel, which from the photomicrographs appeared to be more than normally dirty, had a tendency to form long oxide stringers up to 12 mils in length in the worked material. X-ray diffraction work showed considerable preferential orientation from the reduction operations.

A report[16] from MSA Research Corporation presents considerable information on creep, stress-rupture, and fatigue for type 316 stainless steel and a 2¼% chromium–1% molybdenum steel at 1100 and 1200°F in sodium and purified helium. Trends show no important difference in the stress-rupture behavior of type 316 in air and sodium but a slightly shorter life for the chromium-molybdenum alloy in sodium as compared with air. Both alloys showed higher creep rates in sodium and longer fatigue lives in helium or sodium than in air.

Graphite

A requirement for a low-permeability form of graphite has resulted in the development at Harwell[17] of a technique for producing shaped pyrolytic graphite in which cotton wool is formed about a tube, baked, and then impregnated at 800°C in a methane atmosphere, with subsequent "graphitization" at 2700°C. The work has been carried out on a laboratory scale, and the product has been found to have a permeability in the 10^{-10} cm^2/sec range. The method appears to have promise as a convenient way of forming shapes of interest in nuclear technology.

Harwell has provided translations of two important French papers[18,19] on the reaction of oxygen with graphite, and Ryan at Hanford reports[20] further work on the influence of impurities on localized oxidation. Lewis[21] also discusses the effects of catalytic impurities in graphite, as well as the larger subject of graphite reactivity as it affects reactor safety.

A paper from Risley[22] discusses the problem of thermal expansion in graphite. Transcrystalline cleavage cracks, visible in electron photomicrographs, make possible the accommodation of thermal expansion. The expansion behavior of polycrystalline graphite is also related to the degree of orientation, which controls the contribution of *c*-axis expansion to the expansion in a given direction.

Reynolds and Thrower[23,24] have provided theoretical analyses of the defect behavior in graphite as studied by transmission electron microscopy. Both irradiated and unirradiated graphites were studied. Los Alamos[25] has furnished a survey of available information of the molded pitch-impregnated graphite that is designated H4LM; this graphite is frequently considered for reactor use. A more general bibliography[26] on graphite has been compiled from references in *Nuclear Science Abstracts* for the period 1948 to mid-1961.

References

1. J. L. Daniel, J. Matolich, Jr., and H. W. Deem, Thermal Conductivity of UO_2, USAEC Report HW-69945, Hanford Atomic Products Operation, September 1962.
2. J. E. May, M. J. F. Notley, R. L. Stoute, and J. A. L. Robertson, Observations on the Thermal Conductivity of Uranium Dioxide, *Trans. Am. Nucl. Soc.*, 5(2): 473 (November 1962).
3. S. Goldsmith and P. F. Ashbrook (Eds.), Research and Development Programs Executed for the Division of Reactor Development January, February, March, 1962, Quarterly Progress Report, USAEC Report HW-73915, Hanford Atomic Products Operation, Aug. 1, 1962.
4. D. R. DeHalis, Hanford Atomic Products Operation to C. K. Soppet, General Nuclear Engineering Corporation, personal communication, February 1963.
5. T. E. Redding, Irradiation Test of Gadolinium and Samarium Oxides for the HNPF Control Rod Program, USAEC Report NAA-SR-6514, Atomics International, Nov. 30, 1962.
6. E. W. Hoyt, W. V. Cummings, D. L. Zimmerman, and H. E. Perrine, Rare Earth Oxides and Rare Earth Borates—Corrosion, Compatibility, and Radiation Effects, USAEC Report GEAP-3909, Vallecitos Atomic Laboratory, Apr. 17, 1962.
7. G. J. Salvaggio, F. A. Nichols, and J. P. Bacca, Jr., Properties of a Hafnium Control Rod After Exposure During Two Seed Lives in PWR Core 1, USAEC Report WAPD-TM-337, Bettis Atomic Power Laboratory, November 1962.
8. P. J. Pankaskie, Creep Properties of Zircaloy-2 for Design Application, USAEC Report HW-76267, Hanford Atomic Products Operation, Oct. 10, 1962.
9. R. L. Call, Impact Testing and Slow Notch-Bend

Testing of Zircaloy-2, USAEC Report HW-74339, Hanford Atomic Products Operation, July 17, 1962.

10. K. E. Horton and R. S. Stewart, Thermal-Stress-Fatigue Behavior of Zirconium and Zirconium Alloys, USAEC Report ATL-A-127, Advanced Technology Laboratories Division of American-Standard, Oct. 31, 1961.
11. H. H. Klepfer (Comp.), Proceedings of the USAEC Symposium on Zirconium Alloy Development, Castlewood, Pleasanton, California, Nov. 12-14, 1962, USAEC Report GEAP-4089, Vols. I and II, Vallecitos Atomic Laboratory, Nov. 30, 1962.
12. J. N. Wanklyn, C. F. Britton, D. R. Silvester, and N. J. M. Wilkins, The Corrosion of Zirconium and Its Alloys in High Temperature Steam. Part III. The Influence of the Environment on Oxidation, British Report AERE-R-4130, August 1962.
13. D. L. Douglass, Corrosion Mechanism of Zirconium and Its Alloys—Diffusion of Oxygen in Zirconium Dioxide, USAEC Report GEAP-3999, Vallecitos Atomic Laboratory, July 27, 1962.
14. R. W. Westerman, High Temperature Oxidation of Zirconium and Zircaloy-2 in Oxygen and Water Vapor, USAEC Report HW-73511, Hanford Atomic Products Operation, April 1962.
15. W. V. Cummings, D. R. Lewis, and R. E. Blood, Examination of 304 Stainless Steel Cladding from Cold-Swaged and Rolled Fuel Rods, USAEC Report GEAP-3997, Vallecitos Atomic Laboratory, July 1962.
16. MSA Research Corporation, Effect of 1200°F Sodium on Austenitic and Ferritic Steels. Physical Properties of Materials, USAEC Report MSAR-62-126, Oct. 19, 1962.
17. K. W. Carley-Macauly and M. Mackenzie, Special Ceramics Symposium, 1962—Pyrolytics Session. The Development of New Types of Pyrolytic Carbon, British Report AERE-R-3949, June 1962.
18. X. Duval, Reaction Kinetics of Different Types of Carbon. General Introduction. Reactions of Graphite with Oxygen, British Report AERE-TRANS-886, January 1962.
19. E. Bauer (Ed.), Study of the Initial Phase of Oxidation of Nuclear Graphite in Air at Temperatures Between 420°C and 650°C (I and II), British Report AERE-TRANS-887, January 1962.
20. B. A. Ryan, Localized Oxidation in Nuclear Graphites, USAEC Report HW-73859(Rev.), Hanford Atomic Products Operation, Aug. 14, 1962.
21. J. B. Lewis, The Thermal Reactivity of Nuclear Grade Graphites to Oxygen, British Report AERE-R-3997, March 1962.
22. A. L. Sutton and V. C. Howard, The Role of Porosity in the Accommodation of Thermal Expansion in Graphite, British Report TRG-171(C), Apr. 4, 1962.
23. W. N. Reynolds and P. A. Thrower, Irradiation Damage in Graphite, British Report AERE-R-3979, March 1962.
24. P. A. Thrower and W. N. Reynolds, Microstructural Changes in Neutron-Irradiated Graphite, British Report AERE-R-4007, March 1962.
25. R. G. Merryman, P. Wagner, and D. P. MacMillan, H4LM Graphite, USAEC Report LAMS-2725, Los Alamos Scientific Laboratory, July 5, 1962.
26. T. F. Davis (Comp.), Graphite, A Selected Bibliography, USAEC Report TID-3314, February 1962.

Section

IV

Power Reactor Technology

Containment, Radiation Control, and Siting

Iodine Removal

A review in *Power Reactor Technology*, 5(4): 29-33, covered several papers that dealt with the behavior of iodine in reactor buildings after the accidental release of fission products and with the methods of partially removing such iodine from the building atmosphere in order to minimize the amount that might be dispersed through building leaks. One method of reducing the fission-product concentration is the circulation of the containment-building air through a filter and adsorption unit. This approach was shown by experiment to be most effective when a carbon bed was used as the adsorption unit.

A recent report[1] describes the adsorption of iodine vapor on small-scale carbon filters and presents a design for a full-size carbon filter. The filters are used in combination with an upstream particulate filter and, although designed specifically for use in reactor installations where ventilating air is intentionally exhausted after an accident, they should be suitable for use in any application that requires the removal of iodine vapor from similar atmospheres. During tests the filters consistently exhibited iodine adsorption efficiencies of 99.99% or better when exposed to conditions ranging from prefiltered mixtures of steam, air, and entrained liquid-water particles to superheated steam at temperatures of about 130°C.

The full-size activated-carbon filter described in Ref. 1 has a face area of about 14.6 sq ft and a bed thickness of 1 in.; it passes 1000 cfm of air at a pressure drop of about 0.7 in. H_2O. An isometric drawing of the unit is given in Fig. IV-1.

The bed material is new, activated carbon from coconut shell which has a mesh distribution of 10 to 14 and a minimum hardness of 95% as determined by a standard military specification. New carbon is specified because of the uncertainties in controlling the properties of regenerated carbon. A narrow gradation of small-size particles was selected because of the difficulties encountered in obtaining a uniformly packed filter when a greater size gradation was used. A hard carbon is specified in order to reduce the formation (by erosion) and subsequent release of carbon dust that might carry with it appreciable amounts of adsorbed iodine.

The filters are installed in a vertical rack but with the pleats in a horizontal plane. Commercial filters are commonly installed with the pleats in a vertical plane, but the vertical orientation gives a greater height for settling of carbon within each pleat and was therefore rejected for this application. Baffles of nonperforated metal are specified on all edges of the pleated sections to eliminate significant bypassing of the flow at carbon-metal interfaces. No internal spacers are used to maintain the thickness of the bed. Instead, external spacers are provided so that no carbon-metal interfaces are added to the assembly.

A minimum charge of 54 lb of carbon, equivalent to a minimum packing density of 35 lb/cu ft, is specified for each filter. After the filter is packed, all fines and dust are blown from the unit with filtered compressed air.

Destructive and nondestructive tests of the full-size carbon filters, as well as particulate filters for removal of at least 99% of 0.3-μ particles, are to be covered in subsequent Savannah River reports.

Reference 2 describes an experimental program to determine the effectiveness of metallic copper in removing iodine vapor from air. After the program had begun, other work (reviewed in the *Power Reactor Technology* article

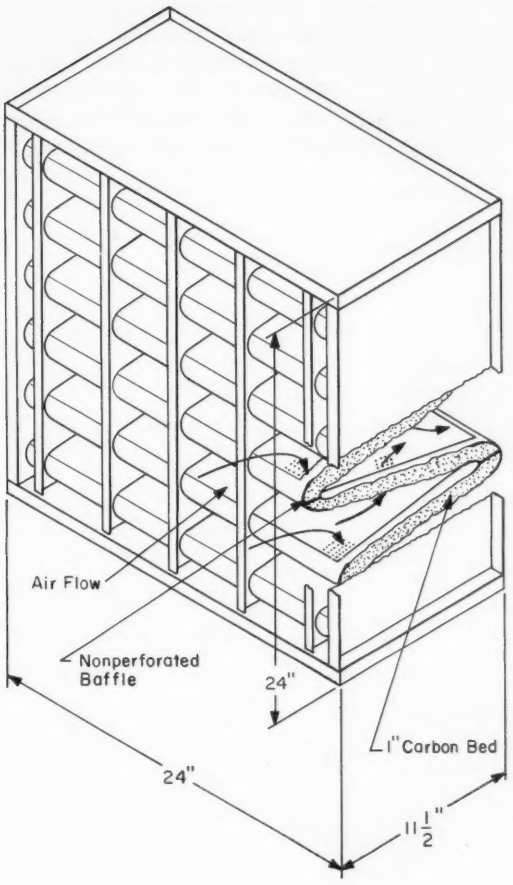

Fig. IV-1 Isometric view of carbon filter.[1]

mentioned above) showed that carbon was clearly superior to copper as an adsorber of iodine. The copper work was continued, however, because it was felt that the mass-transfer results had an intrinsic value of their own.

Proposed Ravenswood Containment

The Ravenswood nuclear steam generating unit has been proposed by the Consolidated Edison Company of New York, Inc., for construction on a site located on the East River adjacent to New York City. Since this site would represent a significant departure from the current practice of locating nuclear plants away from heavily populated areas, the containment concept associated with it is of particular interest. The material reviewed here is taken from the preliminary hazards summary report.[3] The major characteristics of the Ravenswood plant design, which was prepared by the Westinghouse Electric Corporation and Stone & Webster Engineering Corporation, are summarized in Table IV-1. The plant is to have an electrical output of 1054 Mw by means of a single pressurized-water reactor and an oil-fired superheater. The reactor can also be used to generate up to 2 million lb of 400-psia saturated steam per hour, for a steam-

Table IV-1 PRINCIPAL PARAMETERS OF THE PROPOSED RAVENSWOOD NUCLEAR STEAM GENERATING UNIT

Reactor plant	
Total heat output, Mw(t)	2030
Total heat output, Btu/hr	6930×10^6
Primary coolant system	
Number of coolant loops	5
Nominal operating pressure, psia	2035
System coolant volume, cu ft	11,930
Total coolant flow rate, lb/hr	118×10^6
Temperature of coolant into reactor vessel, °F	543
Temperature of coolant out of reactor vessel, °F	588
Reactor core	
Weight of uranium dioxide, kg	103,000
Full-power lifetime, first cycle, hr	13,700
Reactor vessel	
Overall length of vessel, ft-in.	46-6½
Weight of vessel closure head, lb	184,000
Weight of vessel shell, lb	1,070,000
Steam generators	
Number of units	5
Overall length, ft-in.	52-6
Dry weight, lb	430,000
Distribution-system steam reboilers	
Type	Submerged tube
Number	5
Dimensions per unit	
Diameter, ft-in.	10-4
Length, ft	58
Superheater plant	
Number of superheaters	2
Total steam flow, lb/hr	8,800,000
Final steam temperature, °F	1000
Dimensions per furnace	
Width at tubes, ft	45
Depth at tubes, ft	30
Volume, cu ft	132,500
Turbine-generator plant	
Turbine speed, rpm	1800
Steam pressure at throttle, psig	560
Steam temperature at throttle, °F	1000
Turbine rating at 2.0 in. Hg and 0% makeup, Mw	1054
Generator rating, Mva	1276

distribution system, by means of reboilers. The arrangement of the reactor within the containment building is shown in Fig. IV-2, and a schematic diagram of the containment system is shown in Fig. IV-3. Figure IV-4 illustrates the corner detail of the containment building.

The proposed containment structure is a multilayer, reinforced concrete and steel "igloo," designed structurally to meet the requirements of ACI-318 of the American Concrete Institute. The outer layer is normal-density reinforced concrete with a thickness of

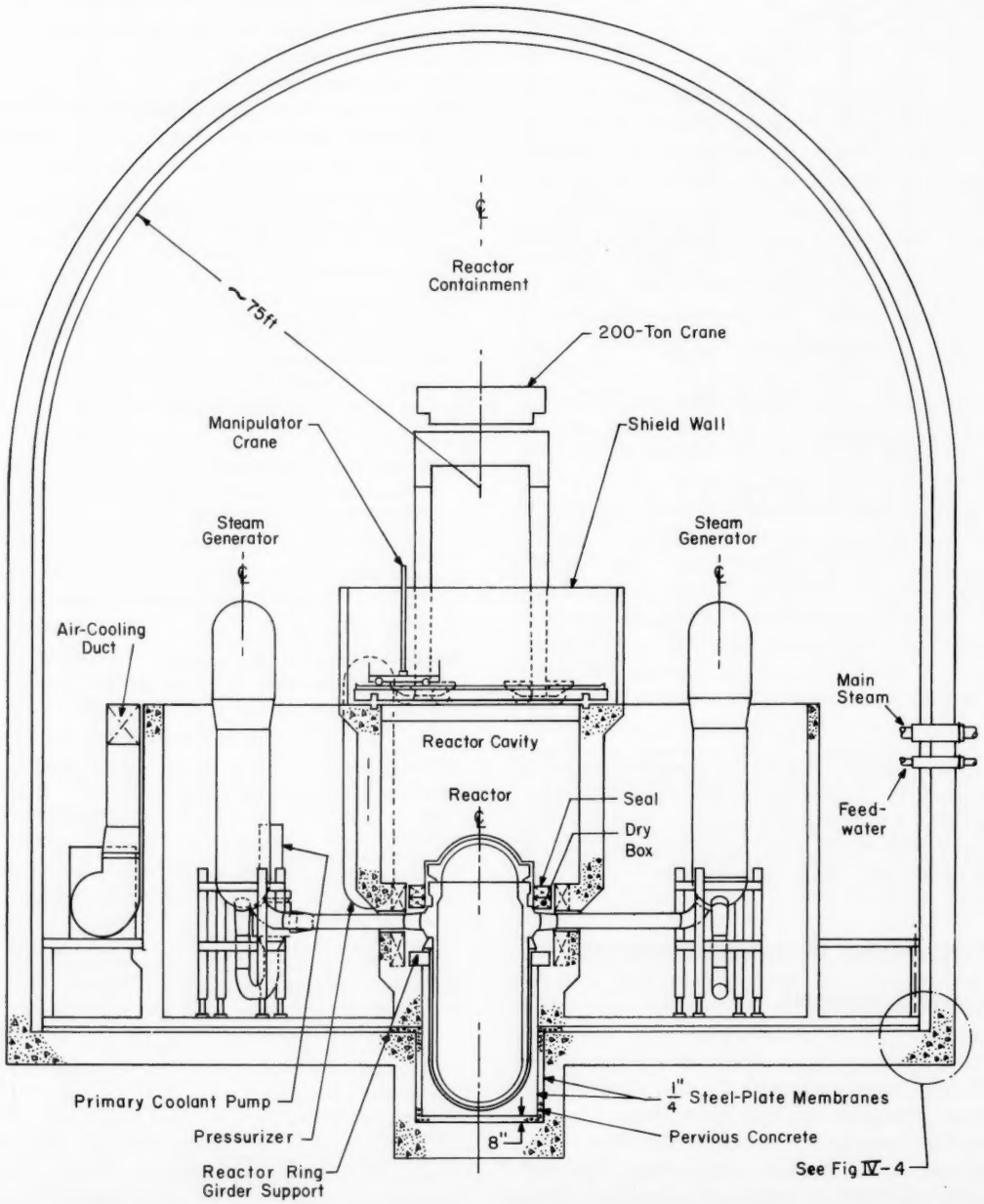

Fig. IV-2 Cross section of proposed Ravenswood containment building.[3]

5 ft 6 in. This outer layer serves as protection against external missiles and as a secondary shield. Apparently the building cannot be occupied during reactor operation. Immediately adjacent to this concrete structure on its inner surface is a welded vessel made of $\frac{1}{4}$-in. steel plate, the "outer membrane." Another steel vessel, also fabricated of $\frac{1}{4}$-in. steel plate, is located within the outer membrane and is separated from it by a distance of 2 ft. Between the two membranes is the "negative pressure zone" that is filled with pervious concrete in the sidewall and dome portions of the containment building. The pervious concrete layer serves to transmit the internal design pressure loading from the inner membrane to the outer membrane and the outer reinforced-concrete shell and allows flow of those gases or liquids which may exist within the negative pressure zone. The negative pressure zone extends under the floor of the containment building to surround the reactor cavity completely. The bottom construction involves a layer of cement blocks between the inner and outer membranes. The outer membrane rests on the concrete foundation pad, and the inner membrane supports the concrete floor of the containment building. The floor membranes connect with their respective sidewall membranes and thus surround the reactor and associated equipment with a complete negative pressure envelope from which leakage gases can be collected and pumped back into the inner containment volume. The internal design pressure for the complete structure is 40 psig, and the design limit on the leakage is 0.1% of the containment volume per 24 hr at 15 psig.

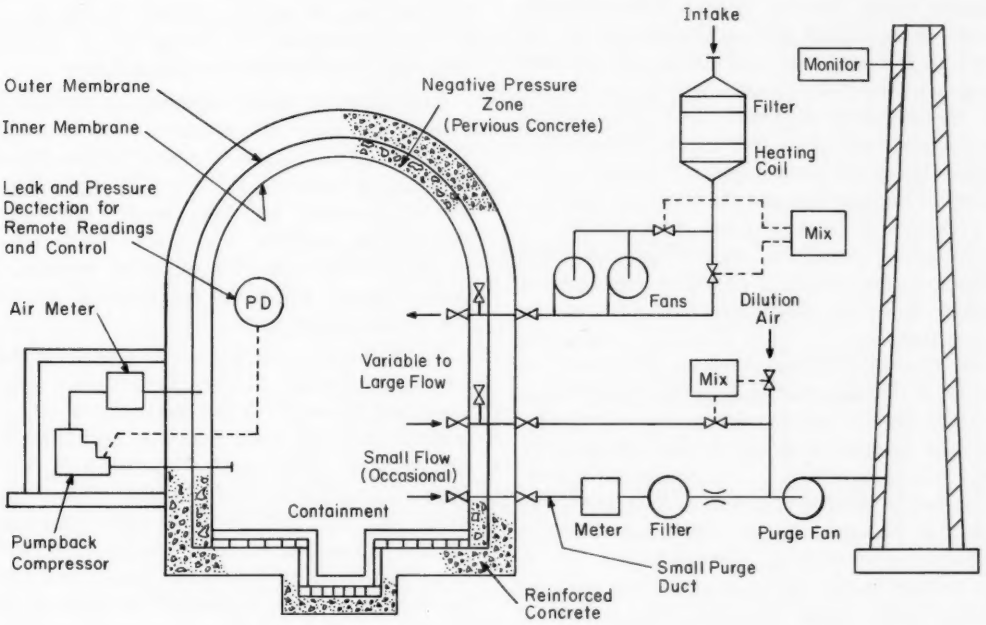

Fig. IV-3 Schematic of the proposed Ravenswood reactor containment structure showing purge and leak-detection systems.[3]

The five proposed containment auxiliary systems are the pumpback system, the leak-detection system, the air-recirculation system, the purge system, and the spray system. The pumpback system is shown in Fig. IV-3. Its purpose is to maintain the negative pressure (−10 in. Hg gauge) in the negative pressure zone by pumping any leakage back into the inner containment volume. There are three pumpback compressors, each rated at 8 cfm and capable of maintaining the desired vacuum against a 50-psig backpressure. The essential components of the leak-detection system are the two sets of air meters and the pressure-measurement device shown within the contain-

ment building. The total leakage into the negative pressure zone is measured by the air meter located in the pumpback compressor circuit. Any air buildup within the containment building, as a result of leakage through the outer membrane, is normally relieved periodically through the small purge duct to the stack. This reduces the building pressure to a standard value that is slightly above atmospheric. In principle the measurement, by the meter in the purge duct, of the air volume thus released determines the amount of air leaking into the negative pressure zone through the outer membrane. The difference between the purge release and the pumpback determines the amount of leakage through the inner membrane. In practice the calculations must allow for variations in pressure, temperature, and humidity, and for losses of air to the containment building from the pneumatic control systems located therein.

The air-recirculation system, not shown on Fig. IV-3, dissipates the heat released within the containment building during normal operation. The system consists of four 90,000-cfm fans, cooling and heating coils, and ductwork, all located within the containment building. The system is designed to keep the temperature in the containment building between 50 and 120°F. Also located in the building are five recirculating absolute-filter units to reduce the content of particulates in the containment air. Two units are shielded and three units are unshielded. One shielded unit is used prior to normal personnel entry whereas the remainder may be used following an accident.

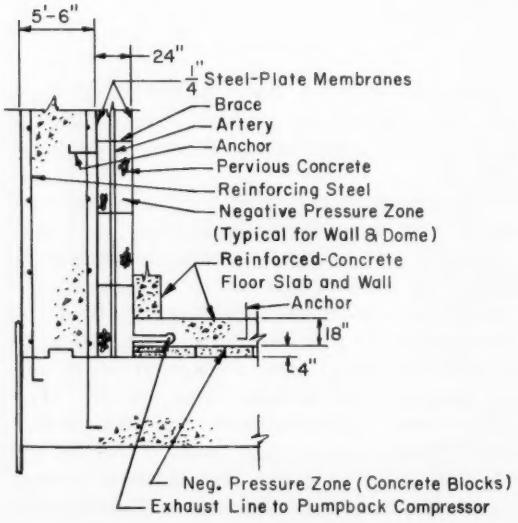

Fig. IV-4 Corner detail of the proposed Ravenswood containment building.[3]

The purge system, indicated in Fig. IV-3, is designed to remove radioactive gases from the containment building prior to routine entry of the building. A capacity of two air changes per hour is provided. The purge air is delivered near the air-recirculation fan intakes.

The building spray system is designed to reduce the internal pressure after an accident involving the release of water vapor. Two recirculation pumps take water from a sump in the containment building, pass it through the decay-heat coolers, and discharge it through spray nozzles into the building volume. The water drains back into the sump to complete the recirculation cycle.

Pervious, or porous, concrete is prepared by mixing processes similar to those for regular concrete but under rigid quality control. It is stated[3] that the control of the aggregate to a single size classification, between $\frac{3}{8}$ in. and $\frac{3}{4}$ in., assures the porous quality. The permeability is such that 12 to 20 cfm of air can be passed through a square foot of area with a pressure drop of 0.2 in. of water per foot of pervious concrete thickness. A typical composition per cubic yard of pervious concrete is as follows:

Type II Portland cement, lb	447
Coarse aggregate (crushed gravel or stone), lb	2446
Water per sack of cement, gal	3.73

The containment building is erected by utilizing the steel membranes as forms for the pouring of the pervious concrete, and this structure is built up in layers about 3 ft deep, as permitted by the strength of the forming structures. When the structure is completed, it is to be filled with a low-pressure air-freon mixture and sniffed for leaks so as to establish the integrity of the structure. The structure is then to serve as a partial form for the pouring of the thick outer layer of normal reinforced concrete.

A number of penetrations are necessary through the containment building for the passage of steam pipes, electrical wiring, and air ducts. Part *a* of Fig. IV-5 illustrates the pipe penetration technique, and part *b* of Fig. IV-5 illustrates

an electrical penetration for 4160- and 600-volt circuits. The air-duct penetrations are fitted with two tight-fitting butterfly valves. When the butterfly valves are closed, a pipe connection ties the duct space between the valves to the pumpback system to monitor for leakage. There are two large penetrations in the building, one for personnel access and one for equipment.

containment building, which is normally above ambient atmospheric pressure, just prior to readying the containment building for access. The duct is equipped with tight-fitting valves and an iodine filter.

Reference 3 discusses the containment approach in terms of the "worst conceivable accident." This accident involves the flashing

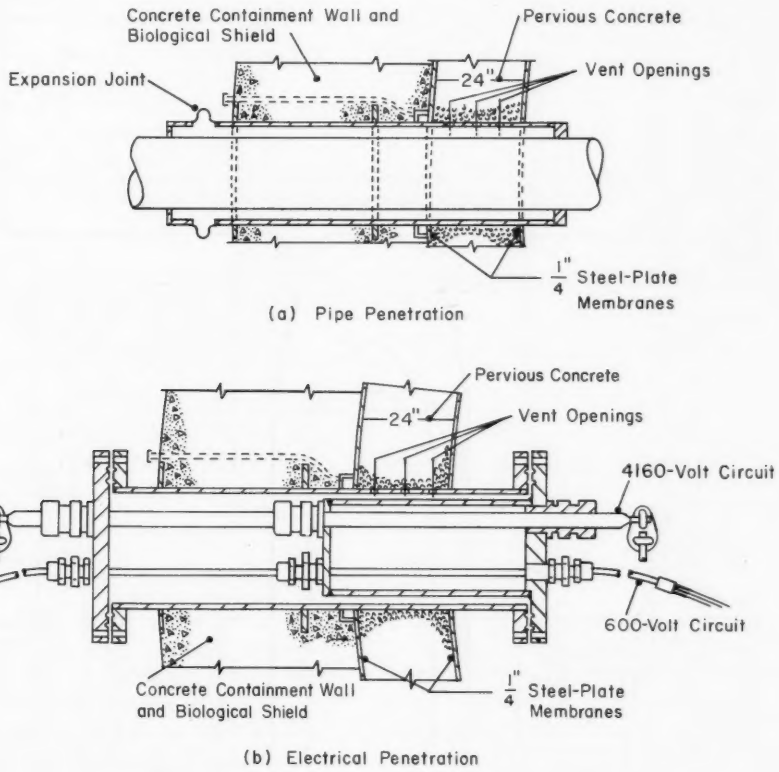

Fig. IV-5 Containment-building penetrations[3] for the proposed Ravenswood plant.

The equipment hatch is a single air lock with two gasketed doors, and during reactor operation the space between the doors is vented to the negative pressure zone. The personnel access passage contains three interlocked gasketed doors in series, and during reactor operation the inner air lock is vented to the negative pressure zone. The remaining penetration of significance is the small purge duct that connects the containment building to the stack by means of the purge fan (Fig. IV-3). This small duct system provides for the measurement of the air flow rate to the stack, but it also serves the purpose of relieving the pressure within the

of the entire contents of the primary coolant system into the containment building and the subsequent melting of the entire core and dispersion of fission products within the building. During this accident the internal building pressure increases to 40 psig, but it is rapidly reduced by the building spray to about atmospheric, and the fission products, except the noble gases, are expected to deposit on surfaces or to be removed by the air filters in the building. During this time period the pumpback compressor will presumably be operating, and, if there are substantial leaks in the outer membrane, the amount of inleakage must be com-

pensated for by a corresponding withdrawal of contaminated air from within the building. This is not released to the stack, unless it can be diluted to below the maximum permissible concentrations for continuous exposure in unrestricted areas, but is pumped to containers for safe disposal in a remote area. The design leak rate is 0.1% of the contained volume (about 2.58×10^6 cu ft) per 24 hr at 15 psig. If it is assumed that half of this leaks through the outer membrane and half leaks through the inner membrane, the contaminated-air disposal rate is $(2.58 \times 10^6)(0.001)/(2)(24)(60)$, or about 1 cfm.

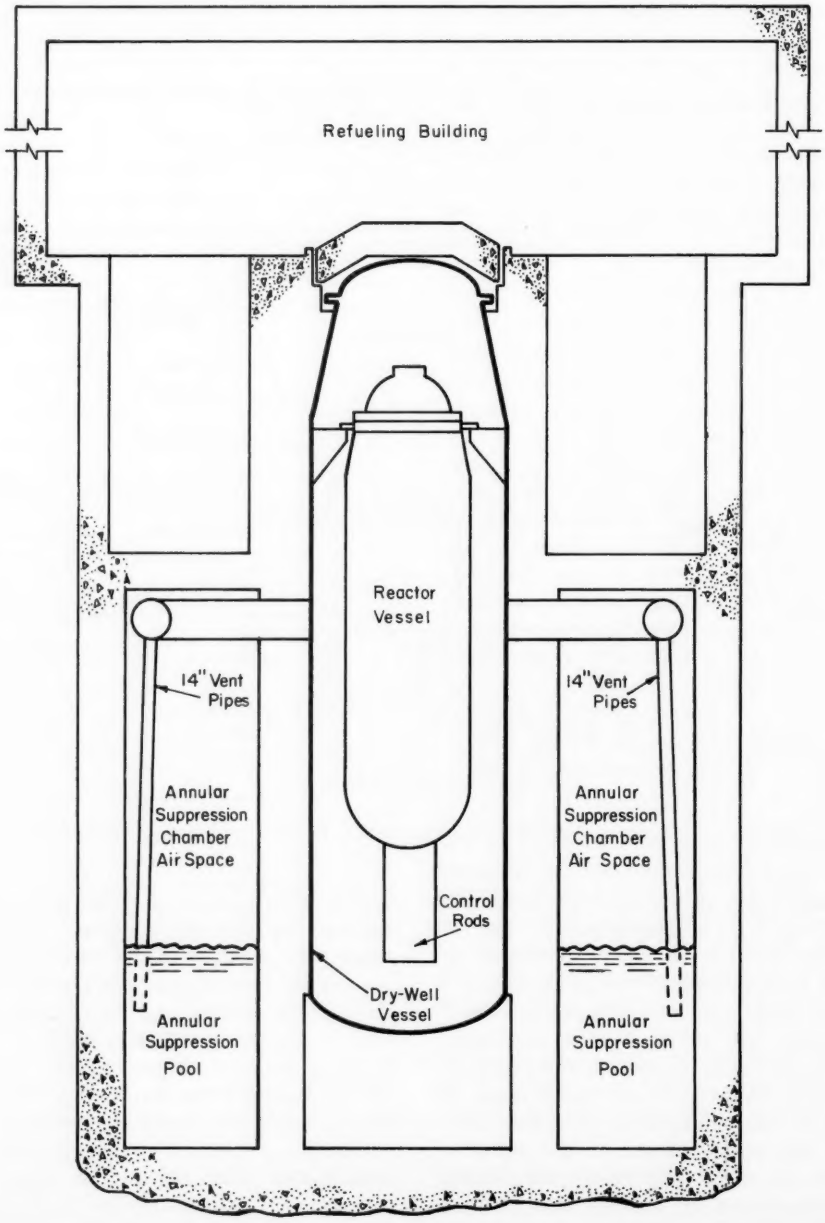

Fig. IV-6 Schematic representation of Humboldt Bay containment system.[4]

Pressure Suppression

It has been pointed out[5] that a brief general description of the pressure-suppression containment concept in *Power Reactor Technology*, 5(4): 29, gave a misleading impression with respect to the application of the concept in the Humboldt Bay plant. Figures IV-6 and IV-7 are presented here to correct this impression and to illustrate the Humboldt Bay application of the concept.

The reactor vessel is located within a steel, low-leakage (0.05% per day at design pressure) dry-well vessel that is designed for 72 psig. The dry-well vessel is vented to the annular suppression chamber, which is also a steel-lined low-leakage chamber (0.5% per day at 8 psig), through a pipe system that discharges beneath the water in the suppression chamber. The design pressures of the dry-well vessel and the suppression chamber are above the pressures that are calculated to result from a major break in the reactor coolant system. All pipes of the coolant system are enclosed by guard pipes from the dry-well vessel up to the point where a shutoff valve is installed in the coolant pipe. At that point the coaxial dry-well pipe is closed off by welding to the valve body, as indicated in Fig. IV-7. Thus the leakage at any break in a coolant pipe which occurs between the reactor vessel and the shutoff valve discharges into the dry-well vessel. Leakage from any break beyond the valve can, of course, be controlled by closing the valve.

During refueling operations (when the head of the dry-well vessel is removed), containment is provided by the refueling building, a reasonably airtight structure located over the dry well, suppression chamber, and fuel-handling area. Outleakage is minimized by holding the building at a slight negative pressure, and the building exhaust air is vented through cleanup equipment and a stack.

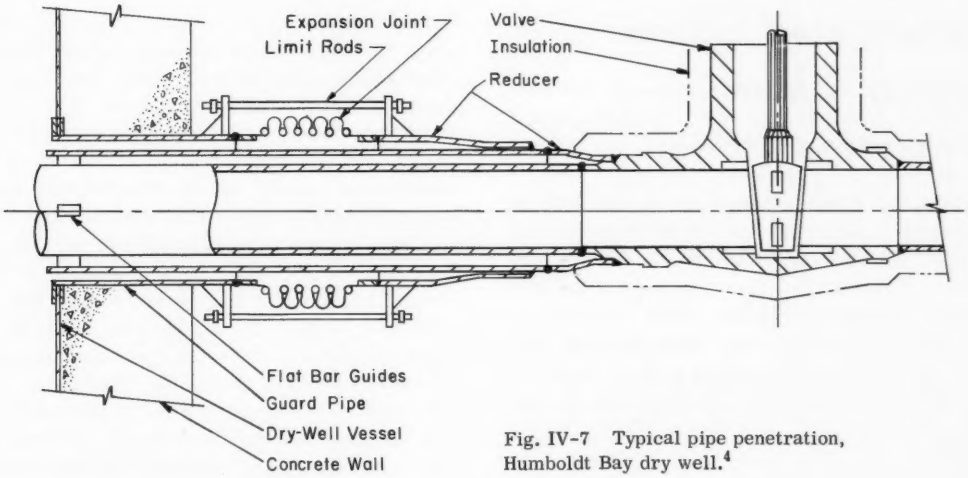

Fig. IV-7 Typical pipe penetration, Humboldt Bay dry well.[4]

References

1. G. H. Prigge, Application of Activated Carbon in Reactor Containment, USAEC Report DP-778, Savannah River Laboratory, September 1962.
2. J. B. Morris, R. A. Stinchcombe, M. D. Gray, and D. H. Logsdail, Removal of Iodine Vapour from Air by Metallic Copper, British Report AERE-R-4114, October 1962.
3. Consolidated Edison Company of New York, Inc., Ravenswood Nuclear Generating Unit A, Preliminary Hazards Summary Report, Docket 50-204, 1962, as follows:
   Vol. I, Chap. 1. Summary
   Chap. 2. Description
   Vol. II, Chap. 3. Safeguards
   Chap. 4. Accident Analysis
   Chap. 5. Control of Radiation
   Chap. 6. Research and Development Program
4. Pacific Gas & Electric Company, Humboldt Bay Power Plant Unit Number 3, Preliminary Hazards Summary Report, Docket 50-133, Apr. 15, 1959, and amendments.
5. C. C. Wheeler, Pacific Gas & Electric Company, personal communication.

Section

V

Power Reactor Technology

Design Practice

Consolidated Edison Nuclear Steam Generating Station

Consolidated Edison Company's nuclear steam generating station is located at Indian Point, Buchanan, N. Y. The reactor was designed by Babcock & Wilcox Co. The facility encompasses a large pressurized-water power reactor, an oil-fired superheater, and associated power-plant equipment. This review will be directed toward the reactor and its closely related equipment, with minimum attention given to the superheater. The information was taken from the safeguards report[1] and amended technical specifications for the plant.[2,3]

Fuel Elements (Rods)

The Consolidated Edison Thorium Reactor (CETR) is one of the few power reactors in the United States to be fueled with a mixture of thorium and uranium. This material, in the form of pressed and sintered oxide pellets, is clad with stainless-steel tubes. The core contains 1100 kg (±1%) of elemental U^{235} in oxide form with an enrichment of 93%; homogeneously mixed with this material is 17,200 kg of thorium oxide pellets of six different thorium-to-uranium ratios. The three radial zones within the core contain fuel assemblies of three different average thorium-to-uranium ratios to yield a flattening of the gross radial power distribution. Within any one type of assembly, fuel rods of several different thorium-to-uranium ratios are used to reduce the local power peaks due to water-hole effects. The distribution of the six different ratios is given in Table V-1, whereas the loading patterns of fuel rods and assemblies are indicated in Figs. V-1 and V-2.

Pellet dimensions	0.26 in. in diameter by 0.78 in. long (approximately)
Average pellet density	9.25 g/cm^3
Active fuel length (cold)	98.5 in.

Table V-1 FUEL-ELEMENT LOADING SUMMARY

Fuel-rod type	Mass of U^{235} per rod, g	Mass of U^{235} per fuel assembly, kg		
		Zone I	Zone II	Zone III
A	20.2 ± 0.4	0.384	0.081	0.040
B	28.8 ± 0.6	0.981	0.721	0.202
C	38.5 ± 0.8	5.345	1.538	0.846
D	52.1 ± 1.0	0	6.411	1.251
E	65.1 ± 1.3	0	0	8.921
F	13.5 ± 0.3	0.040	0.040	0.040
Total mass of U^{235} per assembly		6.750	8.791	11.300
Number of assemblies per zone		×32	×44	×44
Total mass of U^{235} per zone		216	387	497
Total mass of U^{235} in core		1100 (Zone I + Zone II + Zone III)		

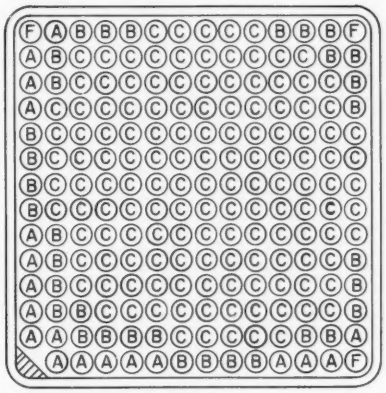

Zone I

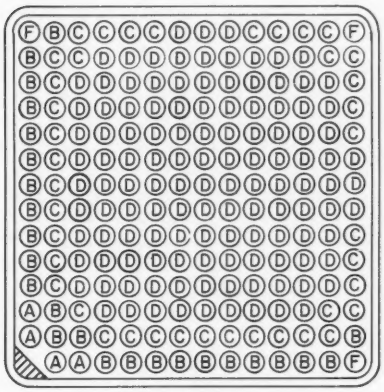

Zone II

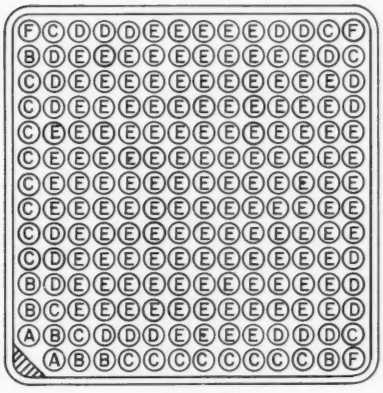

Zone III

Fig. V-1 Fuel-element loading patterns.[2] A, lowest; B, second lowest; C, third lowest; D, fourth lowest; E, highest; F, $\frac{1}{3}$ ThO_2 + $\frac{2}{3}$ concentration A.

Cladding material	Type 304 stainless steel
Cladding outside diameter and thickness	0.304 in. by 0.0205 in.
Pellet-jacket clearance (cold)	0.0015 in.
Filling gas	Helium
Total number of fuel rods in core	23,400
Number of pellets per fuel rod (approximately)	126
Total pellets in core (approximately)	2.95×10^6

The fuel rod is divided axially into six equal-length compartments. This is done with Kanigen-plated type 304 stainless-steel spacer disks held in place by crimping of the fuel tube and brazing. These disks are drilled with vent holes, and each compartment has a void space, for fission-gas accommodation, about 0.34 in. long (cold).

Fuel Assemblies

Each fuel assembly consists of a square bundle of 195 rods assembled on a square pitch with one corner fuel rod omitted. This is illustrated in Fig. V-3. The rod-to-rod spacing is maintained with stainless-steel ferrules, and the complete assembly, shown in Fig. V-4, is fabricated by brazing. Each fuel bundle is contained in a Zircaloy-2 fuel assembly. The bundle is spaced within the can by additional ferrules brazed to the outer row of fuel rods. An index strip is attached to one corner of the can to ensure proper orientation of the fuel bundle therein, and two Zircaloy-2 flow blocks are attached to each fuel assembly to reduce power peaking, to distribute coolant flow in a fixed shim-rod channel, and to ensure proper orientation of the fuel assemblies in the core. The can is fitted with transition pieces at each end; the upper of these contains a spring that holds the fuel bundle down against hydraulic forces while allowing for thermal expansion.

Total number of fuel assemblies	120
Number of fuel rods per assembly	195
Fuel-rod lattice geometry	Square
Fuel-rod lattice pitch	0.37 in.
Approximate core diameter	77.7 in.
Fuel-bundle can material	Zircaloy-2
Fuel-bundle can geometry	5.7 in. square
Overall length of fuel-bundle can	137.5 in.

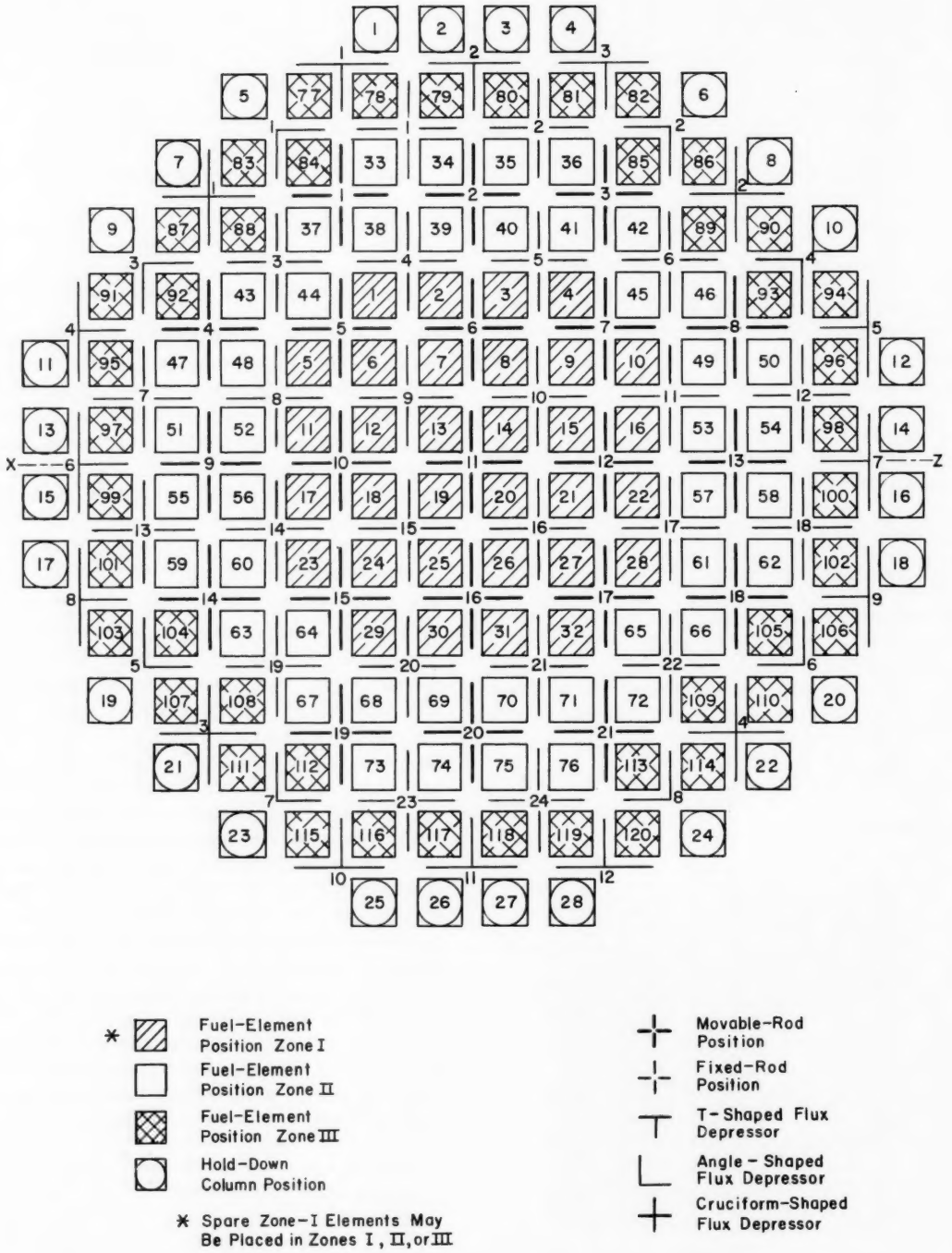

Fig. V-2 CETR core hardware position designations.[2]

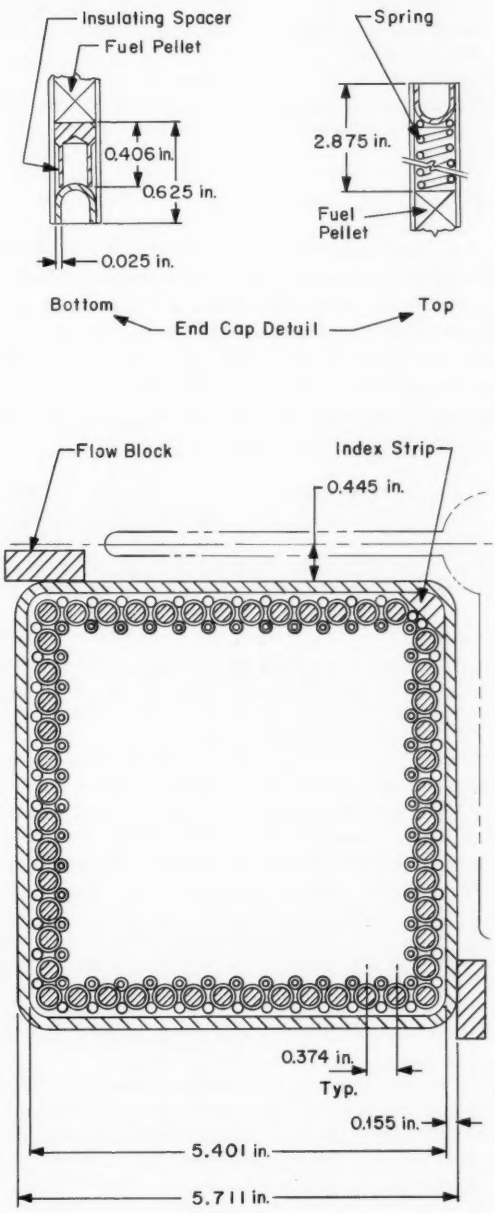

Fig. V-3 Fuel assembly cross section.[1]

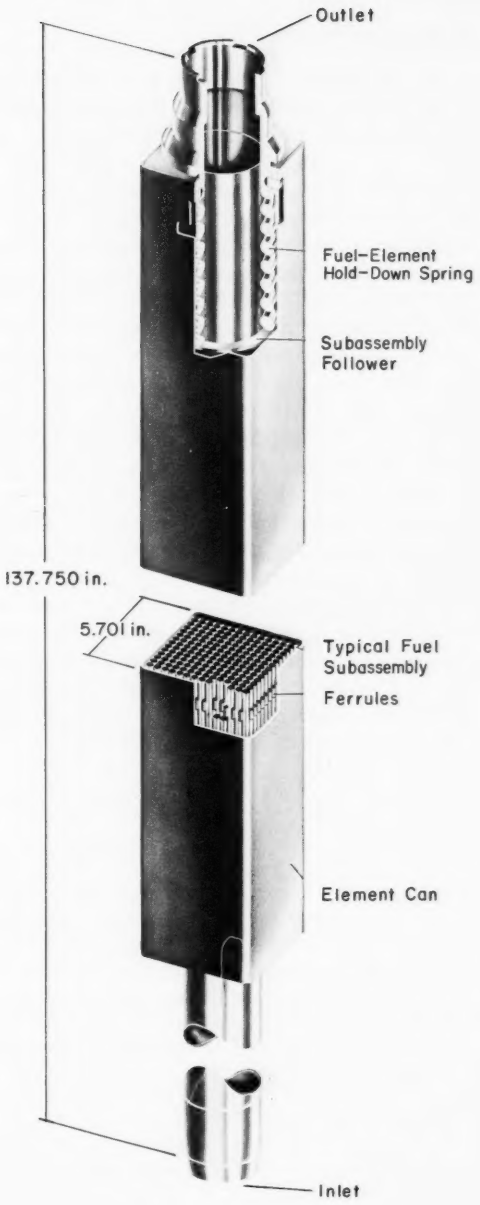

Fig. V-4 Schematic of fuel bundle.

Length of coolant channel	117 in.
Length of active core	98.5 in.

Reactivity Control

The reactivity of the CETR is controlled by control rods, fixed shims, a soluble poison, and a burnable poison in the fuel cladding. The control rods are made of hafnium, and each rod is followed by a Zircaloy-2 section. This follower, which has the same cruciform shape as the rod, moves up into the core as the hafnium portion is pushed into the space above the core region by the bottom-mounted drives. The boron–stainless steel cruciform-shaped fixed shims can be installed in as many as 24 positions in the core. The water channels at the periphery of the core are filled with type 304 stainless-steel flux depressors. Their position and shape are illustrated in Fig. V-2. The soluble poison is boric acid, which is added to the primary coolant after the reactor is scrammed and during cooldown of the primary system to less than operating temperature. The design criterion for the soluble poison addition is that it must provide sufficient negative reactivity to maintain the core subcritical at any temperature with the two control rods of greatest worth fully withdrawn. The burnable poison is natural boron alloyed with the fuel-cladding material.

Control rods	
Number	21
Material	95.4% hafnium 4.5% zirconium
Dimensions	Cruciform, 0.3 in. thick by 10.in. wide by 96.5 in. long
Follower material	Zircaloy-2
Follower dimensions	Identical to control rod
Travel	91 in. between full-in and full-out positions
Control rods driven from	Below
Fixed shims	
Number	Up to 24*
Material	Boron–stainless steel (type 304)
Composition	1 wt.% boron enriched to 80% B^{10}
Dimensions	Cruciform, 11.5 in. wide
Flux depressors	
Number	24
Material	Type 304 stainless steel
Shape and location	(See Fig. V-2)
Burnable-poison material	Natural boron
Burnable-poison location and concentration	Fuel cladding, 200 to 225 ppm per rod

*Spaces not occupied by boron–stainless-steel shims are occupied by Zircaloy-2 filler rods of the same geometry and dimensions as the boron–stainless-steel rods.

Core Structure

The internal structure consists of the lower grid-plate assembly, the core shroud and thermal shields, the hold-down columns, and the upper grid-plate assembly. These components are fabricated of type 304 stainless steel. With the exception of the thermal shields, they are readily removable. Reference 1 gives a concise description of the relation of the parts:

> The lower grid plate, the lower plenum chamber and the control rod guide tubes are bolted and doweled together to form the lower grid plate assembly. This assembly is supported by the reactor vessel by means of the core support ring, and in turn this assembly supports the core and the remaining internal structure of the vessel.
>
> The core shroud rests on the lower grid plate and acts as the inner thermal shield. It also restricts the amount of water which bypasses the core.
>
> The upper grid plate assembly holds the top of the core in position and distributes the flow of water to the outlet nozzles of the reactor vessel.
>
> The internal structure is held in place against hydraulic forces by the reactor vessel head. The force provided thereby is transmitted directly to the upper grid plate assembly. It is then transmitted from that assembly through the core shroud, the holddown columns and the fuel elements to the lower grid plate assembly. The force from the upper assembly to its related components is properly distributed by springs. These springs also accommodate the relative thermal expansions of the internal structure and the reactor vessel.
>
> The components of the internal structure are oriented with respect to the vessel and each other by a series of lugs, pins and dowels. Orifices at both the upper and the lower ends of the flow paths control the flow of water within the reactor vessel.

Data for the lower grid-plate assembly and for the core shroud and thermal shields are given below.

Lower grid-plate assembly	
Constituents	Lower plenum chamber, control-rod guide tubes, and lower grid plate

Method of assembly	Bolt and dowel
Method of support	Core support ring welded to vessel
Function	Support core and remaining internal structures except for two outer thermal shields
Core shroud and thermal shields	
Function	Shroud restricts bypass of coolant to thermal shields and thermal shields reduce fast-neutron and gamma dose to vessel
Inner thermal shield, inside diameter and thickness	7 ft 10 in. by 1 in.
Middle thermal shield, inside diameter and thickness	8 ft 8 in. by 1.75 in.
Outer thermal shield, inside diameter and thickness	9 ft 1½ in. by 1.75 in.

Fuel and Control Program

The treatment of this subject is complicated by the fact that the second core (core B) for the CETR may be entirely different from the original core (core A). The proposal for this core is discussed in Sec. VIII, this issue. This write-up will pertain to core A as designed.

The 21 movable control rods are divided into four groups of four rods each and one group of five rods. The rods are withdrawn or inserted during load changes in a preselected sequence depending on the number of fixed shims present in the core. As burnup proceeds the fixed shims are removed and replaced with the Zircaloy-2 fillers.

Maximum energy produced by core	355,000 Mwd
Burnup corresponding to maximum energy produced	22,000 Mwd/metric ton Th + U
Control-rod grouping (see Fig. V-2)	

Group designation	Rod numbers
A	6, 12, 16, 10
B	5, 7, 17, 15
C	2, 13, 20, 9
D	1, 8, 21, 14
E	3, 18, 19, 4, 11

Control-rod-withdrawal sequence	
With 12 fixed shim rods in core	Withdraw E, D, C, B, and A in order
With 4 or 0 fixed shim rods in core	Withdraw E, D, A, B, and C in order
Maximum reactivity worth (cold, clean)	
Control rods (all)	0.13
Control rods (1 group)	0.05
Burnable poison	0.03
Soluble poison	0.03
One fixed shim rod	0.02
One control rod	0.03
Entire control system	0.22
Maximum reactivity of core (cold, clean), no rods or fixed shims in core	0.13
Minimum cold shutdown margin	0.056

Spatial Distribution of Power

The following calculated peaking factors were taken from Ref. 4.

Gross radial	1.58
Local, hot channel	1.15
Local, hot spot	1.26
Axial	1.9
Total, hot spot	3.78

Heat Removal

Rated thermal power of reactor	585 Mw
Maximum transient thermal power of reactor	702 Mw
Average core heat flux at rated power	128,000 Btu/(hr)(sq ft)
Maximum local core heat flux at rated power	560,000 Btu/(hr)(sq ft)
Maximum temperatures (calculated)	
Pellet center	4850°F
Pellet surface	1750°F
Clad outer surface	605°F
Average rated power density	76 kw/liter of core
Total flow rate	52.8×10^6 lb/hr
Effective flow rate for heat transfer	45.7×10^6 lb/hr
Flow area for heat-transfer flow	12.35 sq ft
Average velocity along fuel rods	21.5 ft/sec
Average mass velocity along fuel rods	3.7×10^6 lb/(hr)(sq ft)

Active heat-transfer surface area	15,600 sq ft
Coolant temperatures	
Nominal inlet	486.5°F
Average rise in vessel	32.1°F
Average rise in core	36.9°F
Average in vessel	502.7°F
Average in core	505.2°F
Nominal outlet of hot channel	570.0°F
Saturation temperature at system pressure	596.2°F

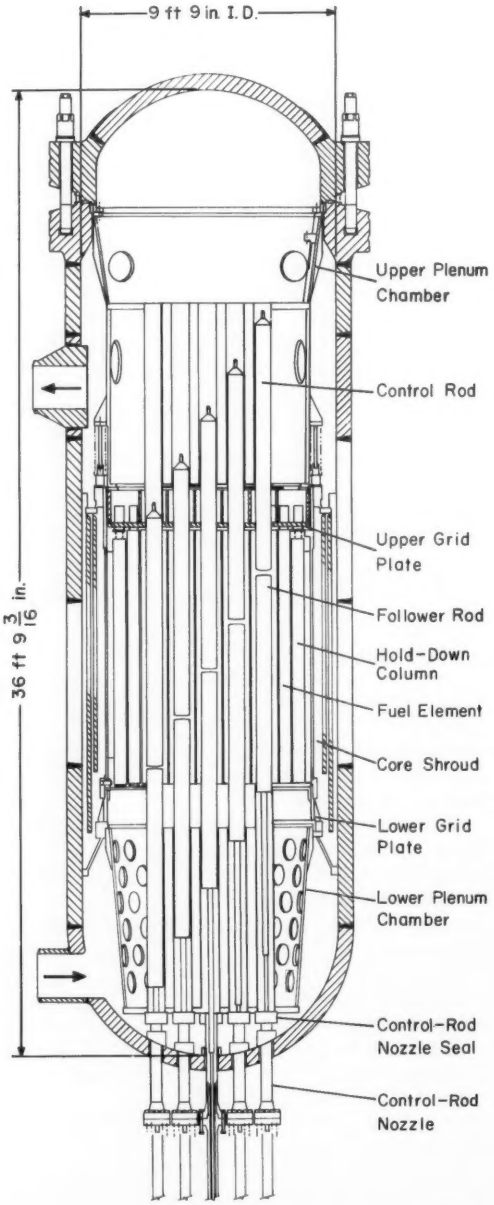

Fig. V-5 Vertical cross section through the CETR pressure vessel.[1]

Pressure Vessel (Fig. V-5)

Materials

Welded construction; reactor vessel is fabricated of SA-212 grade B carbon steel and is clad internally with type 304 stainless steel.

Dimensions	
Inside height	36 ft $9\frac{3}{16}$ in.
Inside diameter	9 ft 9 in.
Minimum wall thickness	6.95 in.
Operating pressure	1500 psia
Design pressure	1800 psig
Design temperature	650°F

Nozzle schedule

Type	Nominal size, in.	Quantity
Inlet	24	4
Outlet	24	4
Control rod	$3\frac{3}{4}$	21
Test and vent piping	$\frac{1}{2}$	3

Bottom head details

Hemispherical shape, attached by welding.

Top head details

Top head closure by bolted flange; sealed with two concentric seal rings with provision for seal welding if necessary. Space between seal rings provided with a leak-monitoring system. Space between outer seal ring and seal-weld canopy provided with leak-monitoring system also.

Reactor vessel nil ductility requirements

Before the vessel is irradiated it is not pressurized above 250 psig until the flanges have reached 130°F; after the vessel is irradiated it is not pressurized above 250 psig until the flanges have reached 130°F and the shell course adjacent to the core region has reached 180°F.

Reactor Instrumentation and Control

A block diagram of the nuclear instrumentation system for the CETR, published in *Power Reactor Technology*, 5(1): 41, may be consulted for details on the reactor instrumentation. The following information supplements this block diagram:

Locale of nuclear instrumentation detectors	External to vessel at three levels around the core

Range of operation—flux-level information

Channels 1 and 2	Source level to 10^{-6} × rated power
Channels 3 and 4	10^{-8} to 10^{-3} × rated power
Channels 5, 6, and 7	10^{-5} to 1 × rated power
Power-range group (18 channels)	10^{-3} to 1.5 × rated power

Range of operation—period information

Channels 1 and 2	10^{-9} to 10^{-6} × rated power
Channels 3 and 4	10^{-7} to 10^{-3} × rated power
Channels 5, 6, and 7	10^{-5} to 1 × rated power

Scram criteria for control rods

Effective insertion of all withdrawn control rods in the core within 1 sec after scram signal is received—fully inserted in 2.3 sec.

Fast-insertion criteria for control rods

Insertion time of 3.5 min on all withdrawn control rods.

Power-range instrumentation operation

Two-out-of-three coincidence to initiate scram at 120% of rated reactor power; two-out-of-three coincidence to initiate fast insertion at 115% of rated reactor power; three power-range channels used to compare power with primary coolant flow for scram purposes.

Additional conditions requiring scram

Reactor period of 10 sec.
High primary coolant pressure of 1800 psig.
Low primary coolant pressure of 1415 psig.
High reactor outlet coolant temperature of 540°F.
Low boiler-feedwater pressure of 465 psig.
Low control-rod drive hydraulic supply pressure of 790 psig.
Loss of control-rod-drive control power.
Loss of both sources of two-phase power to the control-rod-drive motors.
Scram of any one control rod.
High primary coolant fission and corrosion-product activity of 50% of the N^{16} activity level at 585 Mw.
Seismic disturbance of 0.1 g horizontal acceleration as measured on two seismic pendulum units.

Control-Rod Drives

The control rods are operated by 21 electromechanical–hydraulic drive mechanisms that also fix the control-rod positions in the reactor. These mechanisms, illustrated in Fig. V-6, are mounted to the bottom of the reactor vessel as part of a control-rod-drive line assembly. The control-rod drive consists of the following basic components: control rod, follower rod, snubber piston shaft, water snubber housing, seal shaft, buffer seal housing, and electromechanical–hydraulic drive mechanism. The

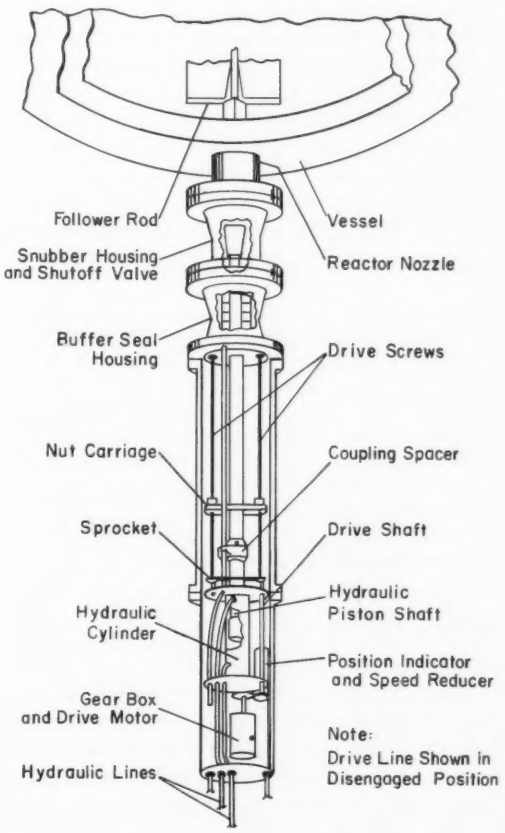

Fig. V-6 Schematic of a control-rod drive for the CETR.[1]

control rod and drive line are moved by the combined action of hydraulic pressure and an electric motor. To scram the reactor, the hydraulic pressure is rapidly reduced by the scram dump valve and its associated pilot valves to permit the pressure in the reactor to force the drive line downward. Scram movement is independent of the electromechanical drive mechanism. On scram the drive line accelerates to a maximum velocity that is controlled by an orifice in the hydraulic piping between

the scram dump valve and the balance piston. Drive-line deceleration at the end of the scram stroke is accomplished by the water snubber and by an oil snubber that is an integral part of the hydraulic cylinder. When the coupling spacer separates from the nut carriage, the drive motor automatically runs the nut carriage down to regain contact with the drive line. Nut-carriage position is continuously indicated on the control-room panel. During scram, or any other time when the coupling spacer is not in contact with the nut carriage, an alarm and a light on the control panel indicate that the hydraulic piston shaft is uncoupled from the positioning mechanism. Should there be a loss of power to the scram or a loss of hydraulic system pressure, the control rods are automatically inserted into the core by reactor pressure and gravity.

Hydraulic pressure supply for drive mechanisms	At least one of three separate high-pressure pumping units.
Auxiliary scram energy units	Four tanks charged with nitrogen at 900 psig; these are normally disconnected from the hydraulic system and are used only when the reactor pressure is below 200 psig.
Control-rod seal	Buffer type employing controlled leakage of seal water into reactor vessel.

Primary Coolant Circuit (Fig. V-7)

The primary coolant enters the reactor vessel near the bottom and flows upward through the core; the thermal shields, control rods, and shim rods are also cooled by water that is bypassed into appropriate regions. The heated coolant exits near the top of the reactor vessel to four boilers (termed "nuclear boilers"); steam is generated in these boilers for use in the turbine. The primary coolant is then returned to the reactor vessel by primary coolant pumps.

Primary coolant loops	
Number	4
Piping, outside diameter	24 in.
Piping, material	Austenitic stainless steel
Primary coolant pumps	
Number per loop	2
Capacity of each	16,400 gal/min

Reactor power vs. primary coolant pumps running

No. of pumps	No. of primary coolant pumps	Maximum scram setting*	
		% rated power	Mw(t)
8	4	120	702
7	4	111	648
6	4	103	603
6	3	95	556
5	4	94.5	553
5	3	87.0	509
4	4	90.5	529
4	3	77.1	451
4	2	67.3	394
3	3	68.5	401
3	2	53.5	313
2	2	39.0	228

Primary loop valves	Two 24-in. motor-operated gate valves, one at reactor inlet and one at outlet; 18-in. check valve in primary pump discharge pipe
Design primary coolant flow rate	13×10^6 lb/hr per loop; 33,000 gal/min per loop
Maximum primary coolant system warmup rate	40°F per hour
Safety valves	One spring-loaded relief valve per loop; capacity of 30 gal/min water at 1980 psig
Steam generators	
Number	4 (one per primary coolant loop)
Type	Shell and tube with primary coolant in shell side
Materials of construction	Shell, SA-212 grade B carbon steel clad with type 304 stainless steel on surfaces in contact with the primary coolant; tubes, type 304 stainless steel
Duty	500×10^6 Btu/hr
Primary system side design conditions	
Pressure	1800 psig
Temperature	650°F
Secondary system side design conditions	
Pressure	500 psig
Temperature	650°F

*Rated power is 585 Mw.

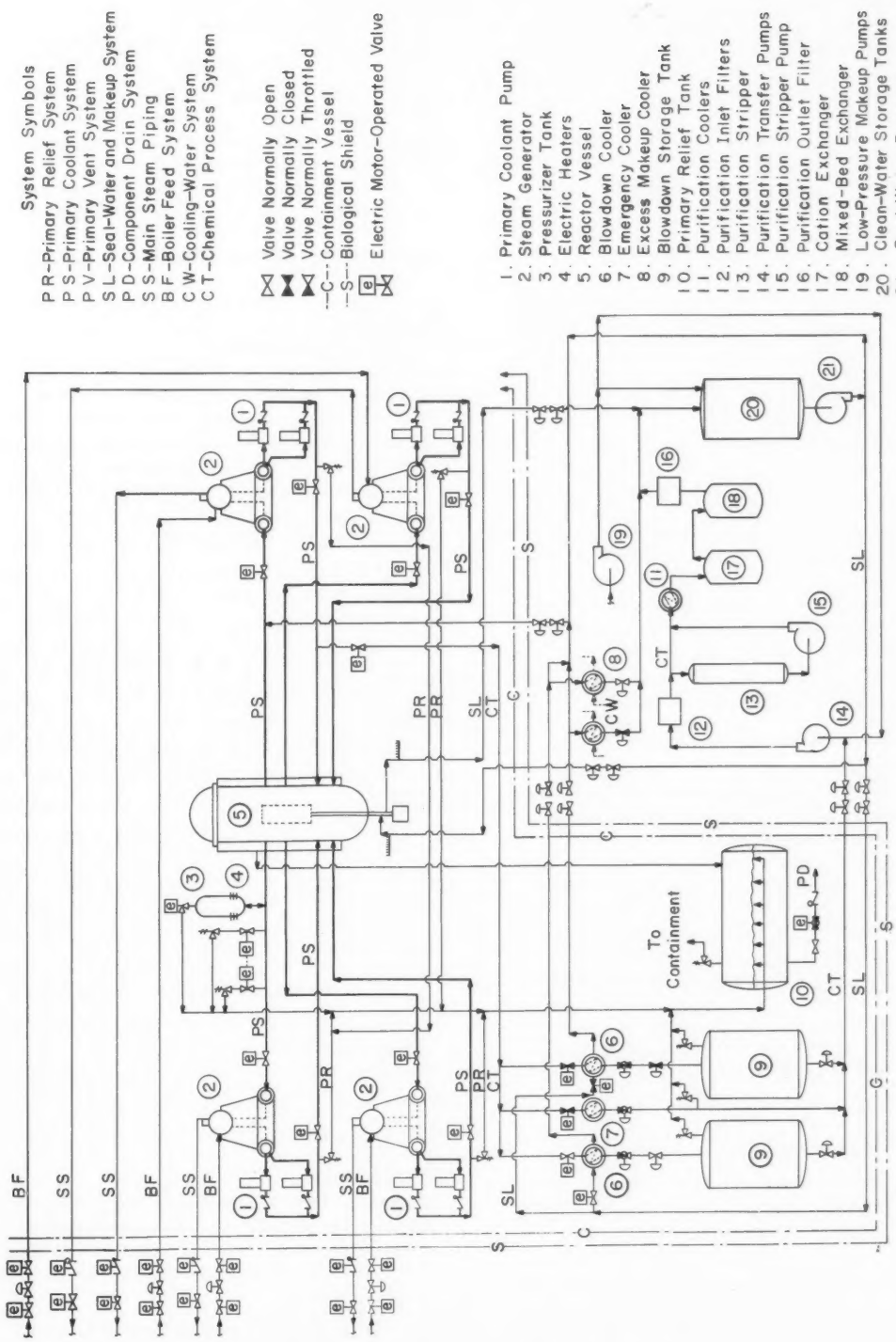

Fig. V-7 Simplified plant flow diagram for the CETR.[1]

Design flow rate of steam: 2.3×10^6 lb/hr

Feedwater temperature: 350°F

Pressurizer

Shape and size

Right circular cylinder with hemispherical top head and ellipsoidal bottom head, 6 ft inside diameter by 17 ft 9 in. inside height.

Materials of construction

SA-212 grade B carbon steel clad internally with SA-240 grade S stainless steel.

Heating system

Four bundles of 12 removable, immersion type electric heaters, horizontally mounted; 480 kw total capacity.

Spray system

Internal nozzle located in top head with capacity of about 54 gal/min

Pressurizer vessel penetrations

Number	Size	Purpose
4	9 in. inside diameter	Heater bundle nozzles
1	6 in.	Pipe surge line nozzle
1	6 in.	Pipe safety valve nozzle
1	15 in. inside diameter	Manway
1	2 in.	Pipe spray line connection
1	1 in.	Vent pipe connection
8		Instrument connections

Safety valves

Two pairs of spring-loaded pop type valves arranged in parallel; capacity of 45,000 lb/hr each at 1824 psig.

Primary relief tank

Accepts discharge from pressurizer and primary loop safety and relief valves; internally provides for sparging discharge under water.

Emergency cooling system

Method of operation: Natural circulation of primary coolant from reactor to steam generators (nuclear boilers)

Capacity: 10^8 Btu/hr

Treatment of Primary Water

Additives

Addition of hydrogen to protect stainless steels from corrosion.

Sample takeoff points

From each primary coolant loop, one reactor outlet, boiler water and saturated steam from each boiler, cooling water from fresh-water cooling system, and key streams in blowdown purification and waste disposal.

Primary coolant specifications

Material	Concentration
Total dissolved solids	1.0 ppm maximum
Dissolved oxygen	0.01 ppm maximum
Chloride	0.1 ppm maximum
Dissolved hydrogen	20 to 40 cm^3 STP per kilogram of water
Residual boric acid	Less than 40 ppm

Primary coolant blowdown and purification systems

Purpose

Maintain an equilibrium primary coolant activity of 4.2 μc per milliliter and meet primary coolant specifications.

Components

Regenerative blowdown coolers, two 3000-cu ft storage tanks for water to be treated, emergency blowdown cooler (nonregenerative), filters, ion exchangers, gas stripper, and three 5000-cu ft storage tanks for processed water.

Approximate blowdown rate: 84,000 lb/hr

Primary coolant boric acid requirements

Av. reactor water temp., °F	Required boric acid concentration, ppm
From Zero to 25 Equivalent Full-Power Days (EFPD) Operation	
>425	0
While cooling from 425 to 260	Add boric acid at minimum rate of 240 ppm/hr
<260	930
From 25 to 50 EFPD	
>425	0
While cooling from 425 to 260	Add boric acid at a minimum rate of 120 ppm/hr
<260	465
From 50 EFPD to End of Life	
Under all temperature conditions	0

Fuel and Shim Handling

Expected frequency

Twelve boron–stainless-steel fixed shims are used at the beginning of reactor operation; after a period of power operation either 8 or 12 shims are removed; the expected lifetime of the first core is 600 days.

Method of handling fuel and shims

Underwater by means of remote handling devices; core components to be removed or inserted into

core one at a time; irradiated core components stored under water in the Fuel Handling Building; irradiated fuel elements cooled by natural convection.

Fuel transfer system
Closed pool type; handling and storage pools covered with concrete and metal floors provided with sealed slots and openings for remote handling devices.

Containment

The containment vessel for the CETR is a 160-ft-ID steel sphere; the lower quarter of the sphere is surrounded by rock. This vessel is completely surrounded by a concrete structure referred to as the "outer biological shield"; this structure consists of $5\frac{1}{2}$-ft-thick concrete walls and a $2\frac{3}{4}$-ft-thick domed roof. The containment vessel and shield are shown in Fig. V-8. Penetrations of the outer biological shield, for personnel access, piping, electrical conductors, etc., are provided with supplemental shielding or labyrinths to ensure the effectiveness of the outer biological shield. The outer biological shield provides radiation protection under both normal operating conditions and in the event of a reactor accident within the containment vessel. While the reactor is critical, no personnel are allowed inside the containment vessel; access is permissible if the reactor is not critical or operating but the primary system is at temperature and pressure. The containment building is equipped with external and internal spray systems and vacuum breaker valves.

Diameter of containment building	160 ft
Material of construction	ASTM A-201 grade B fire box steel
Minimum free volume	1,745,000 cu ft
Design criteria for leakage	Total leakage rate of 0.1% of the volume in 24 hr at an internal pressure of 25 psig
Design criteria for containment building	Internal pressure of 27.5 psig; pressure differential (external over internal) of 1.25 psi
Vacuum breaker design criteria	Prevent occurrence of a pressure differential higher than 0.6 psi

Containment-vessel penetrations

Number	Type
1	Air lock (3 ft 6 in. by 6 ft 8 in. double door)
1	Personnel access hatch (7 ft in diameter)
3	Equipment doors (each 14 ft in diameter)
6	Emergency exits (each 4 ft in diameter)
1	Containment-vessel maintenance opening (4 ft in diameter)
316	Electrical penetrations
152	Piping penetrations
6	Ventilating ducts (four 48-in. and two 24-in. openings)
1	Fuel transfer tube (2 ft 6 in. in diameter)
487	Total

Pneumatic test pressure	25 psig
Maximum pressure attained during pneumatic test	31.25 psig

Missile protection
Intervening water and concrete and steel structures between reactor vessel (and piping) and containment vessel.

Condition of containment vessel during normal operation
Sealed with an internal pressure of 1 to 2 psig; containment-vessel pressure continuously monitored while sealed.

Spray systems
Internal and external spray systems located so that the water sprays impinge on the containment-vessel surface; spray systems supplied with water from a 30,000-gal tank with recirculation provided from the external spray system; external spray system activated by operator action when containment-vessel pressure reaches 10 psig; internal spray system activated by operator action if the containment-vessel pressure reaches 15 psig and the high-level-fission-product monitor trips or if the containment pressure reaches 20 psig.

Plant Control

The reactor control system provides for both automatic and manual adjustment of the reactor power level. The objective of the reactor control system during normal operation is to maintain the boiler steam pressure at approximately 405 psig. The reactor must be under manual control of the operator until the reactor power is about 15% of rated power; at that time control of the reactor may be transferred to the

automatic control system if desired. The automatic control system collects information from the nuclear and nonnuclear instrumentation. The nonnuclear data required are the average boiler steam pressure and total steam flow. The automatic controller utilizes these data to compute a power demand and compares this demand with the power information available from the nuclear instrumentation to generate a rod-velocity demand signal that is proportional to the reactor power change required to meet the steam-flow requirements and to reset the boiler pressure to the desired value. This rod-velocity demand signal is transmitted to one of the five control-rod groups through a sequence switching unit, and the signal is used to generate a rod-drive error signal to adjust the rod positions within the group selected. The maximum speed of each control rod is limited to 22.5 in./min.

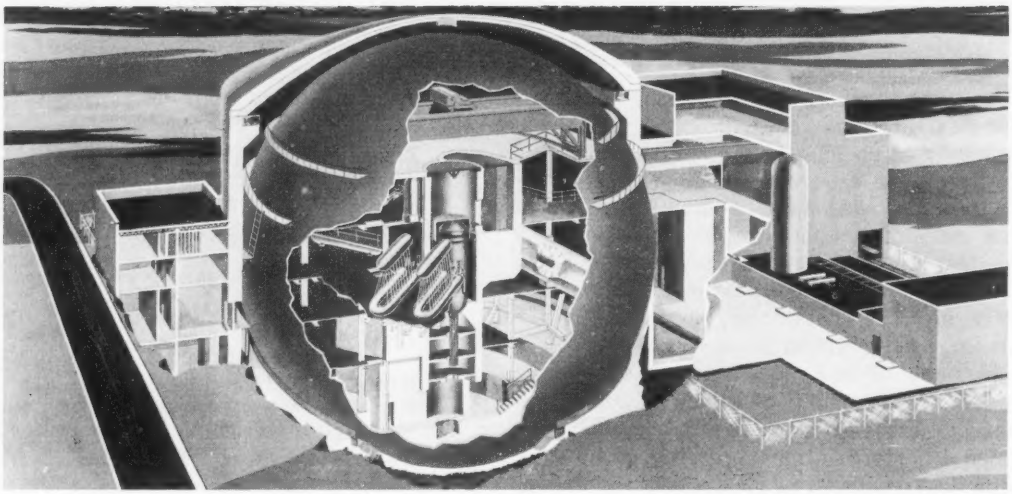

Fig. V-8 Pictorial view of the CETR.

Shielding

During normal operation the radiation levels in areas that are accessible are not to exceed 0.75 mr/hr. A neutron shield tank that surrounds the reactor provides an annulus of water 49 in. thick, cooled by two cooling coils located inside the neutron shield tank. Additional shielding is provided by a 3-ft-thick shield of ordinary concrete that surrounds the neutron shield tank. A concrete-walled pool above the reactor vessel is used to store reactor components and to provide shielding for the transfer of fuel elements and other components to the Fuel Handling Building. A 2-ft-thick concrete floor above this pool is used for refueling operations. Additional shielding is provided by the outer biological shield, discussed above.

Review of Nuclear Vessel Problems

In 1960 the Bureau Veritas of France completed a review[5] of the various problems associated with nuclear reactor vessels. In this review the main problems encountered and the solutions devised are presented and discussed briefly. Familiar problems, such as thermal stresses and strain cycling, are included. Reference 5 is a two-volume effort that includes a large bibliography; part of this bibliography is given as Refs. 6 to 61 at the end of this section. Reports of several nations are referenced, including England, France, Germany, Japan, and the United States. Where possible the author has utilized reactor-vessel information produced in France; however, the bulk of the information presented was produced in the United States by the ASME, by the Pressure Vessel Research Committee, and by the U. S. Navy program. The

review[5] is a thorough discussion of the theory and experiments that led to the tentative structural design basis given in Ref. 62.

Recent ASME Boiler Code Nuclear Cases

Since the review of codes and practice for nuclear pressure vessels in *Power Reactor Technology*, 4(4), several revisions have been made in the Nuclear Case Interpretations of the ASME *Boiler and Pressure Vessel Code*.

In revision 4 (Ref. 63) of Case 1270N (General Requirements for Nuclear Vessels), paragraph 2 was revised[64] to state that paragraph U-1(g) of Secs. I and VIII shall not apply to nuclear vessels. This paragraph allowed vessels of 5 cu ft volume or less and 250 psi design pressure or less to be exempt from inspection by a qualified inspector. Likewise, it allowed vessels of $1\frac{1}{2}$ cu ft volume or less to be exempt, with no limitation on design pressure. In revision 4, paragraph 2 was further amended to state that, where differences exist between nuclear code cases and Secs. I or VIII, the nuclear code case is to take precedence.

Paragraph 3 was changed to state that for nuclear vessels the nuclear cases replace paragraph UW-2 (Service Restrictions) of Sec. VIII. It was revised further to require that particular consideration be given to deterioration in service (due to corrosion, erosion, radiation effects, instability of material, or thermal stress) or mechanical shock and vibratory loading (this requirement previously appeared in Case 1273N). Previously this section dealt with specific details of new construction and exempted portions of primary vessels that are not in direct contact with primary coolant from certain nuclear cases. The reference to exemption was moved to Case 1273N, presumably to remove specific details from the case dealing with general requirements.

Paragraph 4 was amended to require jurisdiction over piping external to vessels up to and including the first circumferential weld. Previously the weld was not included.

Paragraph 5 was amended to include a definition of calandria vessels, not previously mentioned.

In revision 5 (Ref. 5) of Case 1270N, paragraph 3 was revised further to require that the purchaser's specification (for a nuclear vessel) incorporate requirements with respect to the in-service deterioration effects listed in revision 4 above.

In revisions 3 (Ref. 66) and 4 (Ref. 67) of Case 1272N (Containment and Intermediate Containment Vessels), the interpretation was enlarged to describe the type weld joint and the inspection required for each weld category as follows:

Category	Weld	Inspection
A and B	No. 1, double-butt or equivalent	Full radiograph
C	Fig. UG-34, UA-6, and/or UA-48 (Ref. 64)	Radiograph; by liquid penetrant, magnetic particle, or ultrasonics if non-radiographable
D	Fig. UW-16.1 (Ref. 64)	Same as C
Others		Liquid penetrant, magnetic particle, or ultrasonic

The section on allowable stresses was also enlarged to cover primary and secondary stresses not previously covered as follows:[67]

(f) Secondary stresses,* such as, for example, those which occur at changes in geometry of the structure or are produced by thermal gradients within the structure, shall be calculated on the assumption of elastic behavior, combined with the stresses calculated in accordance with Par. (5)(g) following, and

*Secondary stress, for the purposes of this Case, shall be defined as a stress developed by the constraint of adjacent parts or by self-constraint of a structure. The basic characteristic of a secondary stress is that it is self-limiting; local yielding or minor distortions can satisfy the conditions which cause the stress to occur, and failure from one application of the stress is not to be expected. Examples of secondary stresses are:

1 Discontinuity stress in the longitudinal direction at a head-to-shell or nozzle-to-shell junction, and

2 All thermal stresses acting on a shell except the effect of forces and moments produced by expansion of connected piping system.

the sum of such stresses shall be limited to three times the allowable stress values given in Table UCS-23.

(g) Primary stresses,* such as, for example, those which are produced by weight, pipe loads, wind, snow, or specified live loads, shall be combined with the primary stresses calculated by the formulas of Section VIII, and the sum of such stresses shall be limited for design conditions on final supports as follows:

(1) General membrane stresses to 1.1 times the allowable stress values given in Table UCS-23.

(2) Combined general membrane, general bending, and local membrane stresses to 1.5 times the general membrane stress values permitted by (5)(g)-(1).

In revision 5 (Ref. 68) of Case 1272N, item 5(a) was revised slightly to read: "(a) The requirements of Par. (1) or (2) of this case are met whichever is applicable," the statement "whichever is applicable" being added for clarity. Paragraph 1 deals with containment vessels and paragraph 2 with intermediate containment vessels.

In revision 6 (Ref. 69) of Case 1273N (Nuclear Reactor Vessels and Primary Vessels), the first paragraph of the reply was revised, relocating the reference to precedence of Code cases over Sections I and VIII in Case 1270N.

By paragraph 6 the requirement was added that, except as otherwise provided in paragraph 13 following, all welded joints of categories A and B (circumferential and longitudinal joints) are to be type No. 1 (double butt or equivalent) and are to be fully radiographed.

*Primary stress, for the purposes of this Case, shall be defined as a stress developed by the imposed loading which is necessary to satisfy the laws of equilibrium of external and internal forces and moments. The basic characteristic of a primary stress is that it is not self-limiting and therefore a primary stress which exceeds the yield strength may result in failure or gross distortion. Examples of primary stresses are:

1 General membrane stress in a shell produced by internal pressure or distributed live loads, and

2 Local membrane stresses in a shell produced by the external load and moment at a permanent support or nozzle neck, and

3 Local membrane stresses acting circumferentially at points of discontinuity, such as head-to-shell or nozzle-to-shell junctions.

By paragraph 7 the requirement was added that category C joints (flanges) are to be one of the following types:

Joint type	Example	Inspection
Double butt or equivalent	Details 6, 6a, and 6b of Fig. UA-48 (Ref. 64)	Full radiograph
Full-penetration corner welds	Figs. 5a, 5b, and 5c of Case 1273N-6*	Radiograph to standards of Par. UW-51 or P102 (Ref. 64) (special techniques)
Full-penetration corner welds	Figs. 5d, 5e, and 5f of Case 1273N-6*	Same as above, plus supporting ultrasonic inspection

*The joints of Fig. 5 in Case 1273N-6 were added as a part of revision 6.

By paragraph 8 the previous requirements for category D welds (nozzles and openings) were retained.

By paragraph 9 the requirement was added that all reactor and primary vessels of carbon and low-alloy steel are to be stress relieved in accordance with Secs. I or VIII.

By paragraph 13 the requirement was added that those portions of primary vessels not in contact with primary coolant shall be constructed in accordance with Secs. I or VIII except that the service restrictions of paragraph UW-2 do not apply and the following weld requirements must be met:

Weld category	Type weld	Inspection
A	Double butt or equivalent	Full radiograph
B	Double butt or equivalent; single butt with backing strip	Full radiograph

Also, the special requirements of Nuclear Cases 1271N, 1272N, 1273N, 1274N, 1275N, and 1276N do not apply to those portions of primary vessels which are not in contact with primary coolant.

In revision 7 (Ref. 70) of Case 1273N, paragraph 2, dealing with thermal stresses, was revised to read as follows: "Thermal stresses due to temperature distributions at any level of steady power operation shall be calculated on the assumption of elastic behavior and combined with the primary and secondary stresses produced by the design pressure. This combination of stresses shall not exceed three times the S value for the design temperature. This limitation does not apply to the stress in the cladding attached to the wall of a clad vessel (clad thickness less than 20 per cent of the base metal thickness) produced by differential expansion between the cladding and the base metal. Although stress concentrations produced by fillets, nozzles, notches, etc., should be minimized in order to reduce the possibility of fatigue failure, they are not intended to be included in the calculation of the stresses covered by the limitations of this paragraph." Formerly this section limited the combination of membrane stress and thermal stress to one-and-one-half times the S value. This is a very important and timely change since in the past it has been virtually impossible to design certain nuclear systems, such as emergency condensers, to meet the one-and-one-half S requirements.

In revision 5 (Ref. 71) of Case 1274N (Special Material Requirements), item 3(f), paragraph 2 was revised to delete the requirement that castings have identification markings. This section was also revised to describe in greater detail how the manufacturer is to inspect and certify castings used in nuclear vessels.

In revision 6 (Ref. 72) of Case 1274N, paragraph 6 was added, allowing nuclear vessels built and stamped under Sec. I to be fabricated of nickel-chromium-iron material using the rules in Sec. VIII, part UNF pertaining to ASME Specifications SB-166, SB-167, and SB-168. Also, the restriction was removed which formerly limited the quality factor to 0.95 for castings used for vessels designed under Sec. I.

Case 1276N (Ref. 73) (Special Equipment Requirements) was added to the nuclear cases as follows:

> Inquiry: May expansion joints meeting the requirements of Case 1177 be used on the secondary side of primary vessels intended for nuclear service, and if so, how shall they be attached to the vessel?
> "Reply: It is the opinion of the Committee that expansion joints may be used on the secondary side of primary vessels as well as on the secondary vessels, if bellows type expansion joints meeting the requirements of Case 1177 are used and providing the following two additional requirements are met:
>
> (1) All welded joints in the bellows portion of the expansion joint are of the double welded butt type as defined in Par. 3 of Case 1270N.
>
> (2) The bellows portion of the expansion joint is attached to the vessel nozzle or juncture by circumferential welds of a butt type having full fusion and penetration through the thickness of the bellows portion..." .

It was further required that:

> Following the completion of the butt type weld it shall be magnetic particle tested when a ferritic weld is made, or fluid penetrant tested when an austenitic weld is made. In addition, the joint shall pass a Halide leak detector test.
>
> In the present state of the art and pending further development in the design and testing of expansion joints, it is the opinion of the Committee that expansion joints shall not be used in the main shell and heads of nuclear reactor vessels and primary vessels.

In revision 1 (Ref. 74) of Case 1276N, paragraph 11 was revised to require that all welded joints in the bellows portion of the expansion joint be type No. 1 of Table UW-12 (Ref. 64) and be fully radiographed. This change was necessary since the weld definition was removed from Case 1270N by revision 4.

PM-1 Core Design

Although the PM-1 reactor is a small, highly enriched unit designed to fit a specific need for power and heat generation in the Army reactors program, it exhibits a number of unusual design features that are of general interest. Among these are (1) an unusual core configuration (Fig. V-9) and (2) the use of europium titanate as the absorber material for the control rods. The information summarized here is from Ref. 75. The gross characteristics of the reactor, which serves as the primary energy source for a plant producing 1000 kw of electricity and 7 million Btu/hr of thermal energy for space heating, are as follows:

Reactor type	Pressurized water
Reflector, coolant, and moderator	Light water
Reactor power, nominal	9.37 Mw

Operating pressure, nominal	1300 psia
Core life, nominal	17.4 Mw-year
Operating temperature, nominal	463°F
Core geometry	Right circular cylinder
Equivalent core diameter	22.74 in.
Active core length	30 in.
Structural material (all internals)	Modified AISI type 304 and type 347
Coolant flow rate	2125 gal/min
Average heat flux	71,200 Btu/(hr)(sq ft)

Local boiling is permitted in some high-flux regions, but bulk boiling is prevented.

Core Elements

Three types of core elements are included in each fuel bundle: fuel, poison, and dummy. These elements have identical end construction to permit complete interchangeability.

The tubular fuel element contains UO_2 dispersed in and clad with stainless steel. The fuel elements are assembled into bundles by use of end plates on grids; the elements have unfueled end regions of reduced diameter which fit into holes in the end plates. When an element is assembled into a fuel bundle, the beginning of the active fuel region lies 1 in. above the top surface of the lower positioning grid. This distance provides for equalization of flow after the element is orificed by the lower grid. Also, the diameter reduction of the tube end can thus start well away from the fuel–dead-end interface. The element characteristics are as follows:

Type	Tubular, clad cermet
Number in core	741
Diameter	
Outside	0.506 in.
Inside	0.417 in.
Length	
Overall	33¼ in.
Total active	30 in.
Average cladding thickness	0.0085 in.
Meat thickness	0.0285 in.
Meat composition	
UO_2	28 wt.%
Type 304 S. S.	72 wt.%
Loading per tube, U^{235}	40.13 ± 0.80 g

Lumped burnable-poison elements are substituted for fuel elements as required to provide the desired nuclear characteristics. These extend the capabilities of the control system enough to make possible the burnup of 9 kg of U^{235}, out of an initial loading of 29 kg. The elements are unclad and contain natural boron alloyed in stainless steel. The poison length may be varied easily by the use of unpoisoned, tubular "dead ends" which are mechanically locked to the boron–stainless-steel section. Normally the melting process for the boron–stainless steel cannot be controlled to provide a material composition tolerance much tighter than ±10% of the desired boron loading. With the unclad PM-1 element, the final machined diameter is varied slightly on the basis of the final material analysis to meet the prescribed loading with tolerances of approximately ±2%. The burnable-poison elements have the following characteristics:

Diameter	0.470 to 0.500 in., varied to compensate for actual boron loading attained
Material	Stainless steel, AISI type 304, modified 0.01 wt.% Co maximum and 0.03 wt.% Co plus Ta maximum containing 0.27 wt.% natural boron (nominal)
B^{10} per rod	0.383 g
Number	
Poison (30-in. length)	72
Poison (20-in. length)	18

Dummy core elements are incorporated into each peripheral bundle to fill in at the core periphery where the basic triangular element pattern ends and thus reduce the total core flow requirement. These elements are tubular with swaged ends to fit the upper and lower grids in a manner identical to that of the fuel elements. An orificed plug is entrapped within the tube to reduce the internal flow to a low level.

Fuel Assemblies

The active core within the shroud consists of seven fuel bundles: one hexagon-shaped center bundle and six identical pie-shaped bundles located around the periphery (see Fig. V-9). Each of the peripheral bundles is individually held and positioned within the core shroud. The center bundle rests upon the lower grids of the peripheral bundles, and it is positioned within their supporting guide-rail structure.

Each peripheral bundle is constructed basically from three control-rod guide rails, an upper and lower grid, a guide alignment structure, and the necessary core elements (fuel, poison, and dummy). The control-rod guides provide the fundamental structural connections for the bundle. They extend over the full length of the assembly and form a continuous track for the control-rod wear pads. The three guide rails are positioned relative to each other by fitting them into the alignment structure at their top and through the lower grid at the bottom. Correct upper alignment is achieved through the alignment structure, which fits over two alignment pins in the core shroud flange. Thus each control-rod guide rail in a peripheral bundle is aligned at its top and bottom, and the complete bundle is allowed free thermal expansion above its seat in the core shroud.

The guide rails fit through cutouts in the upper grid in a manner similar to the lower grid. The upper grid is located vertically by a shoul-

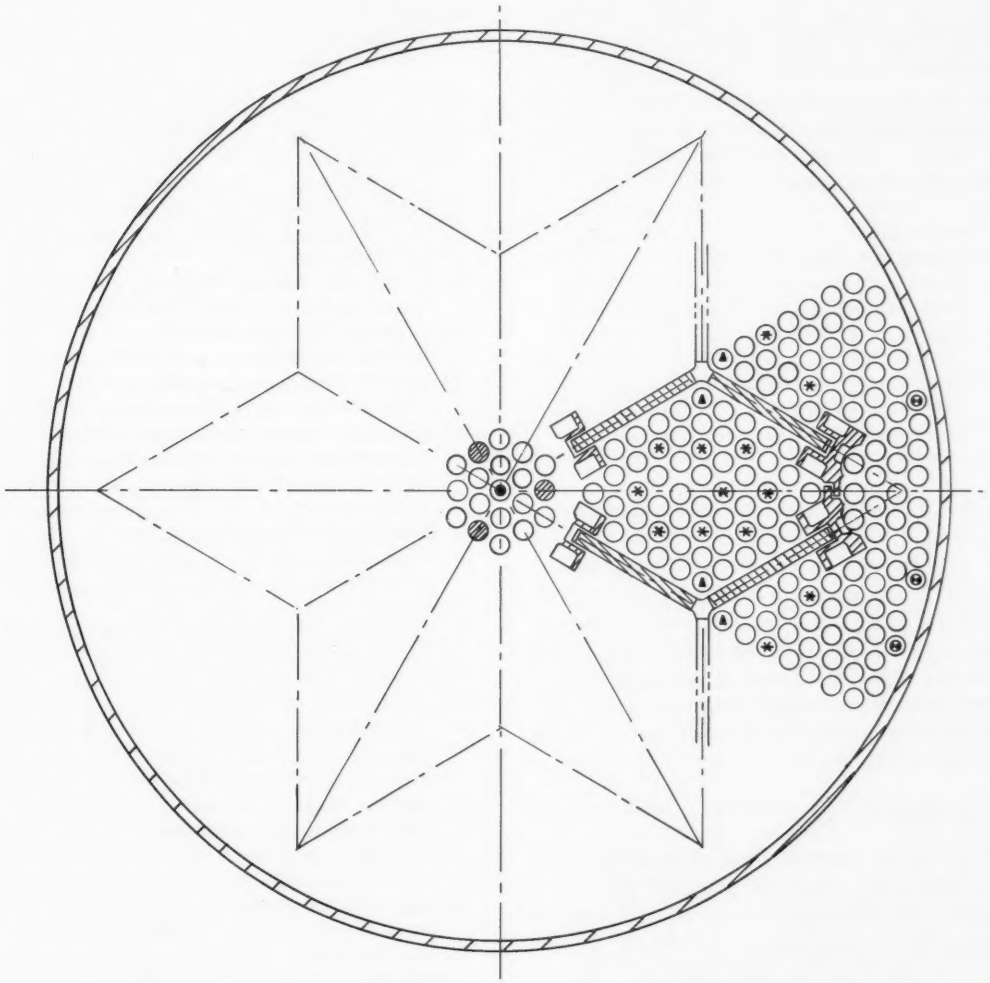

Denotes Location of Partial-Length Poison Rods.
Denotes Location of Primary Source.
Denotes Location of Fuel Tubes.
Denotes Location of Solid S.S. Support Rods.
Denotes Location of Dummy Element Tubes.
Denotes Location of Full-Length Poison Rods.

Fig. V-9 Cross section of the PM-1 reactor core.[75]

der on the guide rail and is secured by a sleeve fitting over the reduced portion of the guide rail which extends above the grid. When the alignment structure is locked into place at assembly, this sleeve extends at three points from the center-bundle lower grid to rest upon the peripheral-bundle lower grids. The center bundle is free to expand axially upward from this point, and top radial alignment is obtained by tabs bearing against the peripheral-bundle upper grids. The center bundle, because it can be replaced either with the core or can be removed and replaced separately through a port in the center of the reactor-vessel head, permits flexibility in future experimentation. The upper skirt assembly applies a hold-down force to the pickup plate of the center bundle and the guide-rail alignment structure of each peripheral bundle. The principal characteristics of the core are listed below:

Element pitch	0.665 in.
Elements in peripheral bundle	
Fuel	121
Poison (30-in. length)	12
Poison (20-in. length)	3
Dummy	3
Elements in center bundle	
Fuel	15
Poison	0
Dummy	0

This rather unconventional core construction, along with the Y configuration of the control rods, results in a very effective distribution of the control-rod absorber over the core volume. It no doubt plays an important part in meeting the stuck-rod specifications while using a total of only six rods. These specifications call for a positive shutdown margin with either one rod stuck completely out or two rods stuck in the operating condition.

Control Rods

Each control rod has a Y configuration so as to fit within the triangular element pattern of the core. The poisoned region of each control rod consists of europium titanate ($Eu_2O_3 \cdot 2TiO_2$) dispersed in stainless steel and is contained within cladding of nominal 0.030-in. stainless steel. The details are as follows:

Control-rod material	$Eu_2O_3 \cdot 2TiO_2$ clad with 30-mil stainless steel
Active control-blade dimensions	Each blade 0.250 in. by 3.5 in. by 32 in.
Number of control rods	Six Y-shaped control rods of three blades each
Control rods driven from	Top
Downward motion of rods	Decreases reactivity

References*

1. Babcock & Wilcox Co., Hazards Summary Report, Consolidated Edison Thorium Reactor, USAEC Docket 50-3, Exhibit K-5 (Rev. 1), January 1960.
2. Consolidated Edison Co. of New York, Inc., Provisional Operating License DPR-5, Appendix A, Technical Specifications, USAEC Docket 50-3, February 1962.
3. Consolidated Edison Co. of New York, Inc., Intermediate Decision, USAEC Docket 50-3, July 1961.
4. M. C. Edlund, R. M. Ball, J. C. Deddens, and R. F. Flickinger, Consolidated Edison Thorium Reactor. Core Assembly Physics and Zero Power Tests Report, Report BAW-163, Babcock & Wilcox Co., September 1961.
5. R. Mattera, Reactor Pressure Vessels, British Report DEG-Inf-Ser-259, 1962, a translation by G. R. A. Metcalfe from *Bull. Tech. Bur. Veritas*, 42(3): 37-59 (1960).
6. Murphy, Soderberg, and Rossheim, Considerations Affecting More Economic but Equally Safe Pressure Vessel Construction Utilizing Either Present-Day Ductile Materials or New High-Strength Less-Ductile Materials, presented at Proceedings of the American Petroleum Institute, Division of Refining, 35 (III), 1955.
7. D. R. Miller and W. E. Cooper, Safeguards Aspects of Reactor Vessel Design, *Welding J. (N. Y.)* (January 1958).
8. W. E. Cooper, The Scope of Pressure Vessel Codes and Activities Toward Improved Content, *Nucl. Eng. Sci. Conf. Preprint 78*, March 1958.
9. F. Plummer, R. Stout, E. Wenk, and I. Boberg, Ten Years of Progress in Pressure Vessel Research (1948-1958), *Welding Research Council Bull. No. 45*, December 1958.
10. Uniform Notation System for Pressure Vessel Shell Theory, Subcommittee of Design Division of P.V.R.C., *Welding J. (N. Y.)* (August 1955).
11. G. Salet, Stresses in the Ends of Pressure Vessels, Conference of the French Society of Mechanical Engineers, S.F.N., March 15, 1951.
12. Ch. Massonnet, Tensions in Pressurized Containers, Technical Note of the Commission for the Study of Metal Construction (C.E.C.M.).

*References 6 to 61 have been extracted from the bibliography of Ref. 5 for the convenience of the reader; they are not reviewed in this issue of *Power Reactor Technology*.

13. C. Kientzler and S. Borg, Observations of Strains Near Reinforced and Non-Reinforced Cone Cylinder Intersections, *Welding Research Council Bull. No. 45*, January 1959.
14. H. Fessler and R. Rose, Photo-Elastic Investigation of Stresses in the Heads of Thick Pressure Vessels, *Proc. Inst. Mech. Engrs. (London)*, 171(20): (1957).
15. G. Vossers, Jr., Fundamentals of the Behaviour of Ships in Waves, *International Shipbuilding Progress*, No. 63, November 1959; No. 64, December 1959 and following.
16. E. Kawashima, M. Sakao, and R. Tasaki, On the External Force Acting on the Marine Reactor Due to the Ship Motion in a Rough Sea, Conference Held at the Society of the Naval Architects of Japan, May 10, 1959.
17. F. P. Durham, Heat Transfer and Thermal Stresses in Nuclear Reactor Shells, USAEC Report LA-1590, Los Alamos Scientific Laboratory, September 1953.
18. L. G. Alexander, Application of the NDA Build-up Factors to the Calculation of Capture Gamma Heating in a Reactor Pressure Vessel, USAEC Report CF-55-4-140, Oak Ridge National Laboratory, Apr. 15, 1955.
19. G. Grass, Warmespannungen in Stahlwanden von Reaktordruckbehaltern unter Neutronenbeschuss bei eisenitijer Juhlung, *Atomkernenergie* (September 1959).
20. G. Sonnemann and D. M. Davis, Stress in Long Thick-Walled Cylinders Caused by Pressure and Temperature, *Am. Soc. Mech. Engrs., Paper 57-A-256*, 1957.
21. H. Kraus, Stresses in Hollow Cylinders Due to Asymmetrical Heat Generation, *Nucl. Eng. Sci. Conf., 5th, Cleveland, 1959, Preprint 31*, 1959.
22. E. Whalley, The Design of Pressure Vessels Subjected to Thermal Stress, N.R.C. No. 4006(56).
23. J. P. de Vries and R. C. Nicoll, Transient Thermal Stresses in Pressure Vessels. Part II: Thermal Stress Calculation, USAEC Report AECU-3643 (Pt. 2), Westinghouse Electric Corp., Advanced Design and Development Department, Apr. 30, 1958.
24. M. Heisler, Transient Thermal Stresses, USAEC Report NAA-SR-176, Atomics International, May 26, 1952.
25. R. Fritz, Evaluation of Transient Temperature and Stresses, *Trans. ASME*, 76(6): 913, Paper No. 53-A-75 (August 1954).
26. B. F. Langer, Thermal Stress Produced by Temperature Transients, USAEC Report WAPD-CE-41, Westinghouse Electric Corp., Atomic Power Division, July 29, 1955.
27. L. Coffin, A Study of the Effects of Cyclic Thermal Stresses on a Ductile Metal, *Trans. ASME*, 76(6): 931 (August 1954).
28. L. Coffin, Design Aspects of High-Temperature Fatigue with Particular Reference to Thermal Stresses, *Trans. ASME*, 78(3): (April 1956).
29. B. F. Langer, Working-Stress Criteria for Nuclear Power Plants, *Trans. ASME*, 77: 661-665 (July 1955).
30. B. Langer, Design Values for Thermal Stress in Ductile Materials, *Welding J. (N. Y.)* (September 1958).
31. G. Schoessow and L. Kooistra, Stresses in a Cylindrical Shell Due to Nozzle or Pipe Connection, *Trans. ASME*, 67: A-107-A-112 (1945).
32. P. Bijlaard, Stresses from Local Loading in Cylindrical Pressure Vessels, *Trans. ASME*, 77: 805-816 (1955).
33. P. Bijlaard, Stresses from Radial Loads in Cylindrical Pressure Vessels, *Welding J. (N. Y.)* (December 1954).
34. P. Bijlaard, Stresses from Radial Loads and External Moments in Cylindrical Pressure Vessels, *Welding J. (N. Y.)* (December 1955).
35. P. Bijlaard, Additional Data on Stresses in Cylindrical Shells Under Local Loading, *Welding Research Council Bull. No. 50*, May 1959.
36. P. Bijlaard, Computation of the Stresses from Local Loads in Spherical Pressure Vessels or Pressure Vessel Heads, *Welding Research Council Bull. No. 34*, March 1957.
37. P. Bijlaard, Stresses in a Spherical Vessel from Radial Loads and External Moments Acting on a Pipe. Influence of a Reinforcing Pad on the Stresses in a Spherical Vessel Under Local Loading, *Welding Research Council Bull. No. 49*, April 1959.
38. P. Bijlaard, Stresses in Spherical Vessels from Local Loads Transferred by a Pipe, *Welding Research Council Bull. No. 50*, May 1959.
39. E. Eberle, Stresses in Cylindrical Casings of Finite Length, *Sulzer Tech. Rev.*, No. 1, 1959.
40. R. Hicks, Theoretical Analysis of the Stresses Induced in a Spherical Pressure Vessel Due to the Constraining Effect of a Cylindrical Skirt, *Proc. Inst. Mech. Engrs. (London)*, 172(21): (1958).
41. H. de Leiris and A. Barat, On the Distribution of Stresses Around a Circular Opening, A.T.M.A., 1947.
42. E. Waters, Reinforcement of Openings in Pressure Vessels, *Welding J. (N. Y.)* (June 1958).
43. E. Waters, D. Hardenbergh, C. Taylor, N. Lind, J. Schweiker, F. Williams, and E. Auler, Theoretical Stresses Near a Circular Opening in a Flat Plate Reinforced with a Cylindrical Outlet. Stresses in Contoured Openings of Pressure Vessels. A Three-Dimensional Photoelastic Study of Stresses Around Reinforced Outlets in Pressure Vessels. Unreinforced Openings in a Pressure Vessel, *Welding Research Council Bull. No. 51*, June 1959.
44. V. Salerno, J. Mahoney, and L. Dragle, A Review, Comparison and Modification of Present Deflec-

tion Theory for Flat Perforated Plates. Correlation of Experimental Data with Theory for Perforated Plates with a Triangular Hole Array, *Welding Research Council Bull. No. 52,* July 1959.

45. G. Gallety, Analysis of Discontinuity Stresses Adjacent to a Central Circular Opening in a Hemispherical Shell, David Taylor Model Basin, Report No. 870, May 1956.
46. P. Cassidy, Higher Design Stresses for Pressure Vessels, *Welding J. (N. Y.)* (March 1951).
47. E. Orowan, Stress Concentrations in Steel Under Cyclic Load, *Welding J. (N. Y.)* (June 1952).
48. S. Tor, J. Ruzek, R. Stout, Repeated Load Tests on Welded and Pre-strained Steels, *Welding J. (N. Y.)* (May 1952).
49. J. Gross, S. Tsang, R. Stout, Factors Affecting Resistance of Pressure Vessel Steels, *Welding J. (N. Y.)* (January 1954).
50. J. Gross, D. Gucer, R. Stout, The Plastic Fatigue Strength of Pressure Vessel Steels, *Welding J. (N. Y.)* (January 1954).
51. T. Dolan, Fatigue as a Factor in Pressure Vessel Design, *Welding J. (N. Y.)* (June 1954).
52. C. Bowman and T. Dolan, Studies of the Biaxial Fatigue Properties of Pressure Vessel Steels, *Welding J. (N. Y.)* (January 1955).
53. J. Gross and R. Stout, Plastic Fatigue Properties of High-Strength Pressure Vessel Steels, *Welding J. (N. Y.)* (April 1955).
54. T. Dolan, Significance of Fatigue Data in Design of Pressure Vessels, *Welding J. (N. Y.)* (May 1956).
55. L. Kooistra, Effect of Plastic on Pressure Vessel Material and Design, *Welding J. (N. Y.)* (March 1957).
56. A. Weinstein and C. Zorowski, Internal Hydraulic Effects Resulting from Mechanical Shock of a Reactor Vessel, *Nucl. Eng. Sci. Conf., Preprint 202,* 1958.
57. A. J. Ulrich, Results of Recent Analyses of Borax II Transient Experiments, USAEC Report ANL-5532, Argonne National Laboratory, April 1956.
58. F. B. Porzel, Design Evaluation of BER (Boiling Experimental Reactor) in Regard to Internal Explosions, USAEC Report ANL-5651, Argonne National Laboratory, January 1957.
59. W. E. Baker and F. J. Allen, The Responses of Elastic Spherical Shells to Spherically Symmetric Internal Blast Loading, USAEC Report WASH-746, Ballistic Research Laboratories, November 1957.
60. F. B. Porzel, Some Hydrodynamic Problems in Reactor Containment, *Proceedings of the Second United Nations International Conference on the Peaceful Uses of Atomic Energy, Geneva, 1958,* Vol. 15, p. 434, United Nations, New York, 1958.
61. W. R. Wise, Jr., An Investigation of Strain–Energy Absorption Potential as the Criterion for Determining Optimum Reactor-Vessel Containment Design, U. S. Navy Report NAVORD-5748, Naval Ordnance Laboratory, June 30, 1958.
62. Tentative Structural Design Basis for Reactor Pressure Vessels and Directly Associated Components (Pressurized-Water-Cooled Systems), Report PB-151987, Revised Dec. 1, 1958.
63. *ASME Boiler and Pressure Vessel Code Interpretations,* p. 170, American Society of Mechanical Engineers, New York, 1959 (includes 1960 and 1961 revisions).
64. *ASME Boiler and Pressure Vessel Code,* American Society of Mechanical Engineers, New York, 1962.
65. *ASME Boiler and Pressure Vessel Code Interpretations,* p. 186, American Society of Mechanical Engineers, New York, 1959 (includes 1960 and 1961 revisions).
66. Nuclear Code Case 1272N-3, ASME Boiler and Pressure Vessel Code, *Mech. Eng.,* 83(8): 89 (August 1961).
67. *ASME Boiler and Pressure Vessel Code Interpretations,* p. 172, American Society of Mechanical Engineers, New York, 1959 (includes 1960 and 1961 revisions).
68. *ASME Boiler and Pressure Vessel Code Interpretations,* p. 187, American Society of Mechanical Engineers, New York, 1959 (includes 1960 and 1961 revisions).
69. *ASME Boiler and Pressure Vessel Code Interpretations,* p. 173, American Society of Mechanical Engineers, New York, 1959 (includes 1960 and 1961 revisions).
70. *ASME Boiler and Pressure Vessel Code Interpretations,* p. 198, American Society of Mechanical Engineers, New York, 1959 (includes 1960 and 1961 revisions).
71. *ASME Boiler and Pressure Vessel Code Interpretations,* p. 190, American Society of Mechanical Engineers, New York, 1959 (includes 1960 and 1961 revisions).
72. *ASME Boiler and Pressure Vessel Code Interpretations,* p. 201, American Society of Mechanical Engineers, New York, 1959 (includes 1960 and 1961 revisions).
73. Nuclear Code Case 1276N, ASME Boiler and Pressure Vessel Code, *Mech. Eng.,* 83(8): 90 (August 1961).
74. *ASME Boiler and Pressure Vessel Code Interpretations,* p. 184, American Society of Mechanical Engineers, New York, 1959 (includes 1960 and 1961 revisions).
75. R. O. Bagley, F. H. Cox, A. Carnasale, and H. Vener, PM-1 Reactor Core Final Design Report, USAEC Report MND-M-1866, Martin Co., January 1962.

Section

VI

Power Reactor Technology

Operating Experience

Shippingport Atomic Power Station

The Failed-Element Detection and Location System

The Shippingport Pressurized-Water Reactor (PWR) is equipped with a system for detecting and locating failed fuel elements. This is known as the failed-element detection and location (FEDAL) system. The system, diagramed in Fig. VI-1, operates by sampling the coolant at the outlet end of every blanket assembly, and each independent sample is analyzed for certain fission products that would be released in the event of a cladding leak. A total of 113 samples are continuously removed from the reactor, of which two are selected and sent to delayed-neutron monitors at any particular time and the rest are rerouted to the reactor. The various piping components are sized to provide sufficient time to allow for decay of N^{17} and thereby maximize the delayed-neutron counts received from the I^{137} and Br^{87} fission products. The activity detected is recorded in a predetermined program so that the data indicate which blanket element is being surveyed.

The FEDAL system was installed with the PWR core 1, and by mid-1958 it was functioning. References 1 and 2 give the operating experience with the FEDAL system through all of the seed 1 and seed 2 lifetimes and through part of the seed 3 lifetime. It became apparent that the background count of delayed neutrons was quite high; in fact, the background made it impossible to locate purposely defected rods while the reactor was operating at a steady-state power. The delayed-neutron background comes from several sources: (1) fissioning of natural uranium found as an impurity in core Zircaloy, (2) recirculating delayed-neutron activity, and (3) cosmic-ray and vacuum-tube noise. The natural-uranium content in the core Zircaloy for core 1 seed 1 was estimated as 2.54 ppm from the levels of fission products in the reactor coolant. In spite of the first unexpected source of delayed neutrons, it was found that the FEDAL system could detect pinhole leaks in the cladding if the channel was monitored during a reactor startup. This effect is attributed to "waterlogging" of the defected fuel element during shutdown. According to this concept, coolant enters the fuel element through the pinhole during shutdown and leaches some fission products from the oxide fuel. During startup the oxide temperature increases and the water within the fuel element boils, and the leached fission products are swept out through the defect and into the coolant stream. The resultant delayed-neutron-monitor counting rate during the transient behaves, typically, as shown in Fig. VI-2. These traces were obtained by holding the multiport valve on two sampling tubes during a startup. Fuel position K-8 contained a defective fuel element* but position I-10 did not. Another defective fuel rod was found in bundle J-5. These bundles were scheduled for removal at the time of refueling, and the metallurgical report on one of them is described later in this review.

Reactor Hydraulics

The inlet plenum mixing for the PWR has been extensively studied by a mockup con-

*The multiport valve actually was traveling in a direction opposite to the one intended during all of the seed 1 lifetime and part of the seed 2 lifetime. The discovery of this fact is an interesting detective story, for which the reader may wish to consult Ref. 1.

structed and operated by Battelle Memorial Institute.[3] The mockup utilized air as a carrier with SO_2 as a tracer to determine flows into various fuel elements under various operating conditions. The results given in Ref. 3 were checked by operation of the PWR under the same operating conditions as the mockup and by measuring pressure drops across flow-measuring nozzles. This is possible because the PWR core is quite highly instrumented, as indicated in Fig. VI-3. The results of the comparison are shown in Fig. VI-4: the two sets of data check within 5%. Another comparison was effected by operating two of the recirculation loops at an inlet temperature 22.5°F higher than the other two loops and checking various inlet water temperatures. Agreement was within 0.8°F.

Loss-of-flow studies were also performed. These were of particular interest since the power limit was believed to be set near the end of seed 2 lifetime by the flow through the core 3 to 5 sec after a complete-loss-of-flow accident (CLOFA). Data for the complete shutdown of all of the four operating pumps (CLOFA 4-O) are illustrated in Fig. VI-5. Data were also taken for a shutdown of three (of three operating) pumps.

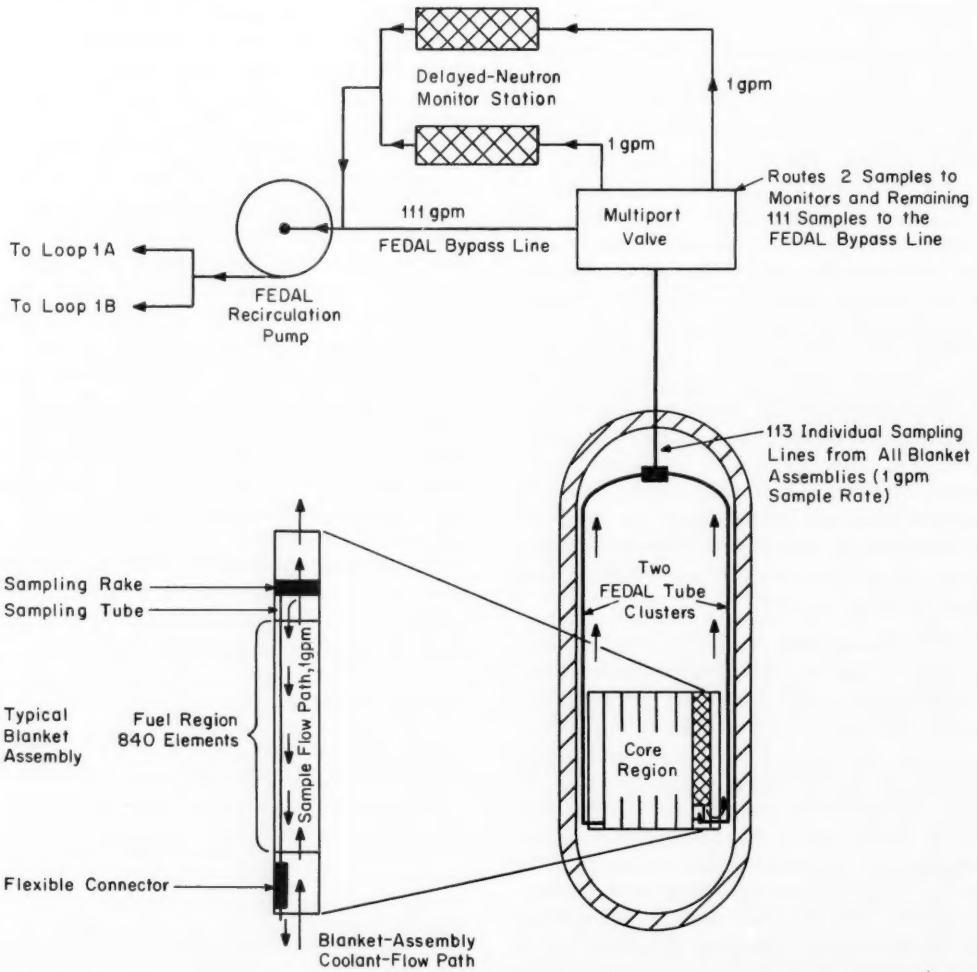

Fig. VI-1 Schematic diagram of the Shippingport core 1 failed-element detection and location system.[2]

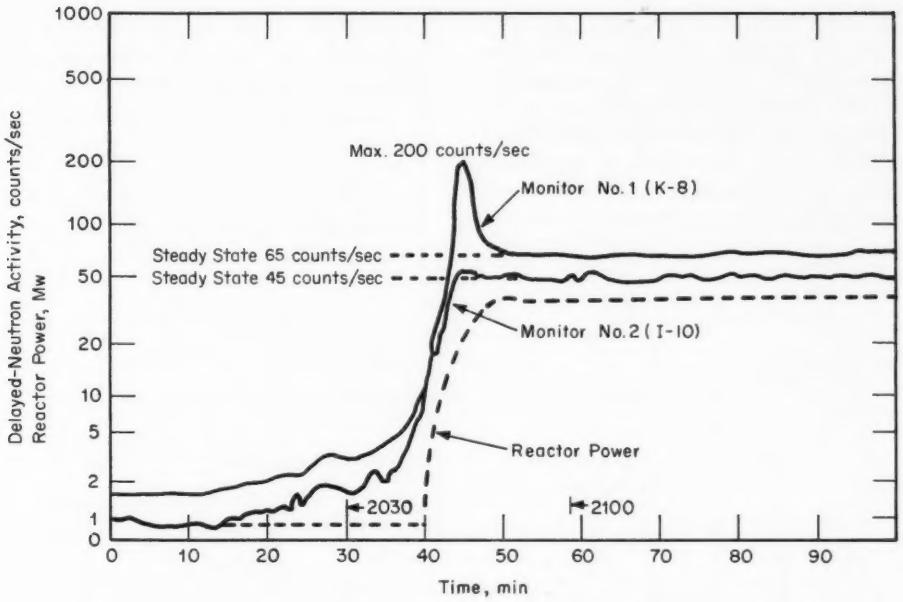

Fig. VI-2 The delayed-neutron activity traverses of Shippingport blanket assemblies K-8 and I-10 during a reactor startup transient performed on July 16, 1960.[2]

Fuel Canal Protective Coating

The fuel-handling canal for the PWR contains the reactor pit, fuel-storage pit, deep pit, shroud-storage pit, disassembly and transfer areas, crane lock, and various sumps. It was decided to coat the concrete walls and floors of these submerged areas to prevent the transfer of radioactive crud from the demineralized canal water to the concrete constructional material. Since 1957, when a polyester resin was first applied to the concrete surfaces, various other materials have been used for test patches because the performance of the polyester coating on the canal surface proved inadequate. The other materials undergoing tests were phenolic-epoxy, epoxy, and a phenolic coating. In general, none of the test patches proved entirely satisfactory, and continued work on the problem appears necessary.

Chemistry and Radioactive Contamination Experience

An important change in the PWR coolant-purification system was made in November 1960. The lithium hydroxide resin was changed from natural lithium hydroxide to a resin enriched in the Li^7 isotope. (The natural lithium contains 7.5% Li^6, which contributes tritium to the coolant via a neutron-alpha reaction.) The results are shown in Table VI-1. This reduction in the tritium level of the coolant was reflected in the total yearly tritium discharged from the plant to the Ohio River. These data are shown in Table VI-2. For the last four months of the seven-month period in 1961, the total tritium discharge was less than 2 curies.

The reactor coolant-water conditions, which are summarized in Table VI-3, had been extensively monitored during seed 1 operations. The frequency of most of the chemical analyses of the water coolant was reduced during seed 2 operation after it was discovered that the maintenance of the water specifications shown in Table VI-3 was not difficult. The revised and original schedules are shown in Table VI-4. In addition, it was found that many of the variables, such as primary coolant *p*H, change slowly and predictably with time and routine analyses thus become less important.

The Shippingport plant has operated for extended periods of time without primary coolant purifications, and a review of this mode of operation appeared in *Power Reactor Technology*, 6(2): 55-57. During seed 2 operation the reac-

tor vessel head was surveyed 13 times with portable survey instruments. These surveys encompassed the 32 control-rod-drive mechanisms, 10 fuel ports, the multiport valve in the FEDAL system, and various other instrumentation penetrations of the vessel. It was found that activity of the control-rod mechanisms varied considerably from survey to survey, particularly when the survey was conducted just after extensive rod motion and/or scram. Reference 1 gives the following conclusions:

1. Rod exercises will reduce radiation levels in the higher elevation and move crud to lower elevations.

2. Scrams are effective in reducing radiation levels in the lower elevations.

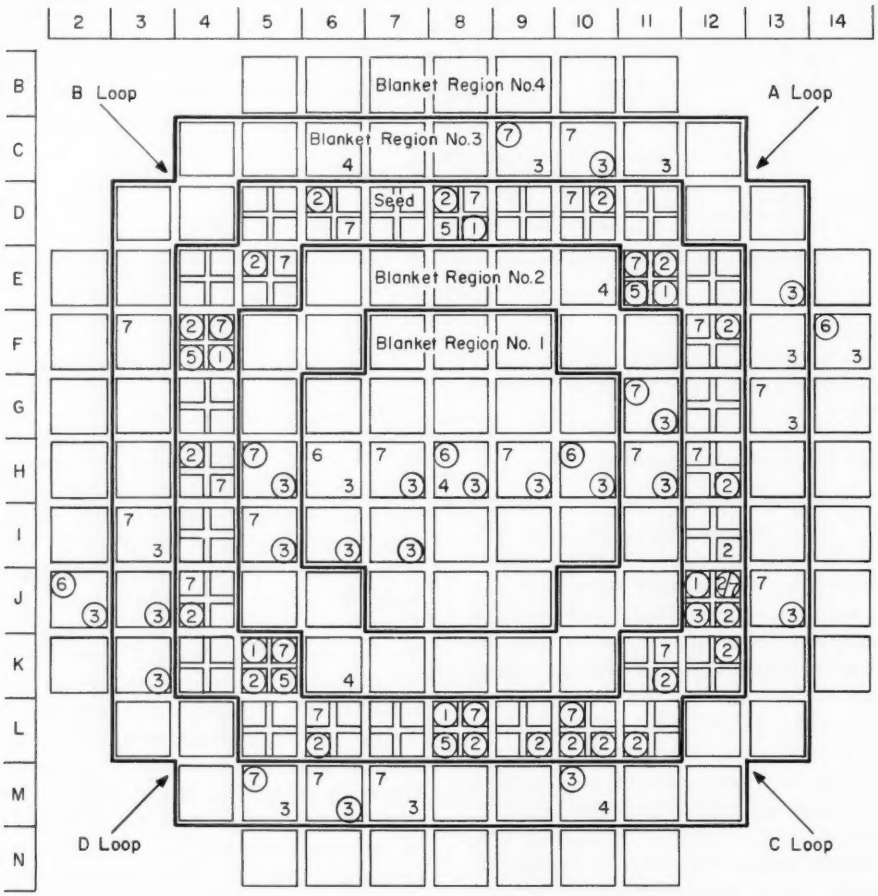
2 3 4 5 6 7 8 9 10 11 12 13 14
B C D E F G H I J K L M N
B Loop
A Loop
D Loop
C Loop
Blanket Region No.4
Blanket Region No.3
Seed
Blanket Region No.2
Blanket Region No. 1

1. Seed Fuel-Plate Thermocouple
2. Seed Exit-Water Thermocouple
3. Blanket Exit-Water Thermocouple
4. Blanket Inlet-Water Thermocouple
5. Seed Inlet-Water Thermocouple
6. Flow Nozzle
7. Modified Venturi

○ Operable Thermocouple or Calibrated Flow D/P Cell
No Circle Inoperable Thermocouple or Uncalibrated Flow D/P Cell Early in Seed 2 Life, July 1, 1960

Fig. VI-3 Shippingport PWR core 1 seed 2 instrumentation.[1]

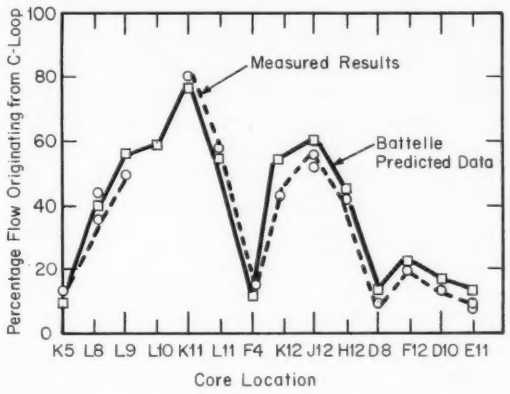

Fig. VI-4 Shippingport inlet-plenum mixing data that have been measured and predicted.[1]

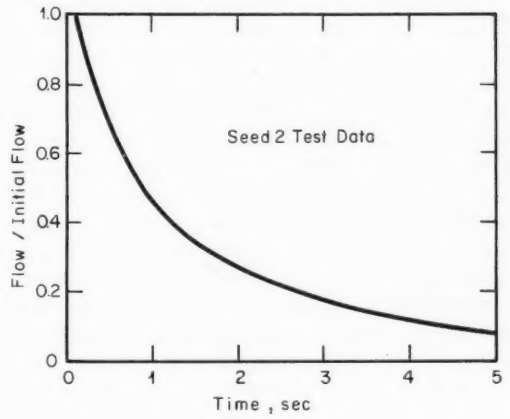

Fig. VI-5 Flow coastdown curve for shutdown of four pumps in the Shippingport PWR.[1]

Table VI-1 TRITIUM CONCENTRATION IN THE PRIMARY COOLANT AT PWR[1]

Date	Coolant-sample tritium, μc/liter
6/6/60	221
9/27/60	281
10/9/60	241
11/7/60	128
11/21/60	86
12/8/60	23
12/11/60	19.5
12/18/60	18.7
12/23/60	18.5
12/30/60	16.1
1/6/61	18.8
1/13/61	6.7
1/24/61	5.9
2/6/61	13.2
2/12/61	3.2
2/28/61	1.5
4/8/61	1.3
4/26/61	2.3

Table VI-2 TOTAL YEARLY TRITIUM DISCHARGES FROM SHIPPINGPORT[1]

Year	Curies discharged
1958	50
1959	64
1960	99
1961 (7 months)	12

Table VI-3 REFERENCE-WATER SPECIFICATIONS FOR SHIPPINGPORT[1]

	Conductivity, mmhos	pH at 25°C	Lithium conc., ppm	Dissolved oxygen conc.,* ppm	Hydrogen, cm^3/kg STP
Minimum	7.0	9.5	0.3	0.14	15
Maximum	75.0	10.5	2.3		60

*When the reactor coolant system is >200°F.

Table VI-4 REACTOR PLANT SAMPLING-AND-ANALYSIS SCHEDULE CHANGES[1]

Sample	Location	Determination	Frequency	
			Seed 1	Seed 2 and seed 3
Coolant charging	Primary storage tank	Conductivity	1/week	1/month
		Dissolved O_2		
		pH		
		Cl		
Reactor coolant	Laboratory analysis of 1AC or 1BD demineralizer influent	Conductivity	1/week	1/week
		pH	1/week	1/week
		Dissolved O_2	2/week	*
		H_2	1/week	Daily
		Total gas	2/week	Daily
		Inert gas	1/week	Daily
		Lithium and NH_3	1/week	1/month
Reactor coolant	Demineralizer influent crud	Crud weight	Daily	1/week
		% Fe in crud	Daily	
		Gamma spectrum		1/week
		Specific activity	Daily	1/week
Reactor coolant	Demineralizer effluent crud	Crud weight	1/week	1/week
		% Fe in crud	1/week	
		Gamma spectrum		1/week
		Specific activity	Daily	1/week
Reactor coolant	1AC or 1BD demineralizer influent	Total gas activity	2/week	2/year
		A^{41}	2/week	2/year
		H_3	1/week	Every 1000 equivalent full-power hours (EFPH)
Reactor coolant	Laboratory analysis of 1AC or 1BD demineralizer influent	Gross gamma activity (15 min)	Daily	Daily
		120-hr count	Daily	Daily
		Cs^{138}	Daily	3/week
		Kr^{88}	Daily	
		I^{131}, I^{133}	3/week	1000 EFPH
		Cs^{136}, Cs^{137}	Daily	1000 EFPH
		Br^{83}, Br^{84}	3/week	
		Xe^{133}	1/week	1000 EFPH
		Gross iodine decay curve for I^{131}, I^{132}, and I^{133}	3/week	
		Decontamination factor	Daily	1/week
Reactor coolant	Pilot demineralizer and crud probe	85% gamma ray; balance of major activity: Co^{60}, Co^{58}, Fe^{59}, Cr^{51}, Mn^{54}, Hf^{181}, Zr^{95}	†	1000 EFPH
Canal water	Demineralizer inlets and outlets	Conductivity	2/week	1/week
		pH	2/week	1/week
		Turbidity		1/week
		Gross gamma activity	Daily	1/week
Neutron shield tank	Eductor	pH	‡	2/year
		CrO_4		2/year
		Gross gamma activity		2/year
		K^{42}		
Hair-pin loop	Purification cubicle	Activity-level survey: I^{131}, Co^{58}, Cs^{136}, Cs^{137}, Te^{132}, Ba^{140}, Sr^{89}, Sr^{90}, Ce^{144}, Fe^{59}, Co^{60}, Zr^{95}, Ta^{182}, Ta^{183}, U	§	§
Valve operating system¶	Drain on water flush	Dissolved O_2	1/week	
Component cooling water	Component cooling-water-pump suction	pH	2/month	1/week
		CrO_4	2/month	1/week
		Conductivity		1/week
		Cl		1/week
		Gross gamma activity	2/month	1/week

*Not specified when hydrogen is present.
†Seed 1 was analyzed when activity had moved one-third of column length.
‡As frequently as access to sample point is possible.
§Performed as required for the AEC test program.
¶Dropped from schedule.

3. Most effective combination appears to be rod exercise followed by scramming the rods from their full height.

Since the reductions in the radiation levels ranged from about 20 to 50%, the effect could be a significant one. Over the operation periods of seed 1 and seed 2 it was found, on the average, that the external radiation levels of the reactor coolant piping increased at a rate of 2.5 to 3.0 mr/hr per 1000 EFPH of reactor operation.

PWR Fuel Rods

The failure of a blanket fuel rod was indicated by the detection system early in the operation of the Shippingport reactor.[4] The radioactivity released, however, was well within safety limits. The bundle was removed during refueling at the end of the second seed life after 13,700 EFPH. During operation the time-averaged heat flux was 98,700 Btu/(hr)(sq ft). The defective rod and some nondefective rods from the same bundle were closely examined visually and metallographically. In addition, nonirradiated rods, which had been originally fabricated from the same lot of tubing, were examined as above and by two eddy-current techniques. The first eddy-current test used a Probolog unit similar to that employed when the elements were fabricated. The second employed an eddy-current tester (RADAC) recently developed. It was found that, although the Probolog would not detect the defect that caused the failure, or similar defects in unirradiated cladding tubes, such defects could be found with the RADAC apparatus. Metallographic examination showed the failure to be a 50-mil-long crack starting on the inner surface and penetrating the tube through a 4-mil-diameter hole on the outside surface. This defect had been introduced in fabrication and was not the result of irradiation. Numerous similar but more shallow defects were found in the unirradiated rods, but their presence had only a minor effect on the mechanical properties of the tubes when they were tube-burst tested.

Although the defect in the failed element was small and had been present for a long exposure, it had not resulted in hydriding of the cladding or waterlogging of the fuel. The average hydrogen content of the cladding was only 125 ppm, and this would indicate a life of 30,000 EFPH to attain the limiting value for hydrogen content, given as 250 ppm.

Yankee Core Evaluation Program

The design of the Yankee Nuclear Power Station was described in *Power Reactor Technology*, 4(3): 47-55. Reference 5 is the first quarterly progress report of a program to evaluate the performance of the reactor core. Despite the early status of the program, there are several results of interest to the reactor designer. A total of 14 fuel assemblies and 3 control rods were inspected remotely at the Yankee site in the spent-fuel pit. Since some of the components will subsequently be examined in a hot-cell facility at Waltz Mill, Pa., the examinations at the Yankee site were primarily of a visual nature.

The results of the visual examination of the control rods are summarized by the following quotation:[5]

1. Large areas of all rods were devoid of nickel plating, based on the assumption that the silver-gray colored areas represented bare Ag-In-Cd alloy. Major losses of nickel were near the center of the control rod vanes; there was appreciably less apparent damage on the inboard areas of the vanes.

2. There was evidence of peeled nickel plate in several areas on two of the rods. This condition existed mainly at the boundaries between plated areas and apparently bare areas. Typical size of the individual peelings was about one square inch.

3. Vertical score marks were evident on all absorber rods. In addition, horizontal bands suggestive of rubbed areas were observed.

4. A silvery-white crystalline corrosion product was observed at the top interface between the stainless steel tie plates and the absorber section on several rods. The appearance and location of these deposits suggest that they were the result of galvanic corrosion. This corrosion was observed on three absorbers and over almost 50% of the length of each interface.

5. The appearance of Group 3 (intermediate neutron exposure) control rods was essentially the same as that of Group 1 and 6 rods.* There were large areas devoid of nickel plate and numerous score marks. Silvery-white crystalline deposits at the interfaces between the absorber section and the top tie plates were also evident. In addition, peel-

*Group 1 rods were fully inserted for approximately 2250 effective full-power hours; Group 6 rods were in the core only during initial testing to determine physics worth and thus received essentially no neutron exposure.

ing of nickel plate was observed at the edge of one vane. The surface appearance of this rod in comparison with the others would indicate that damage to the nickel plate was not influenced appreciably by core position and neutron exposure.

Punchings were made of the Group 1 and Group 6 control rods for metallographic and chemical analyses. These samples were circular in shape with a diameter of about 1 in. In general, they showed that the diffusion-bond layer did not protect the base metal and that, in the case of the Group 6 rods, the breakdown of the diffusion-bond layer occurred early in life. The rubbed and scored area on one rod (Group 1) showed a depth of about 15 to 20 mils. The breakdown in the diffusion-bond layer is attributed to either poor initial quality or excessive wear of the control-rod surface caused by rod movements during the test program. The chemical analyses of the punchings (two from each group) indicated that apparently some preferential leaching of cadmium had occurred during the corrosion of the Group 6 rods. The data are shown in Table VI-5. The variation of

Table VI-5 RESULTS OF CHEMICAL ANALYSES OF YANKEE GROUP 1 AND GROUP 6 CONTROL-ROD PUNCHINGS[5]

Rod designation	Sn, %	Cd, %	In, %	Ag, %
Group 6 (low neutron exposure)				
Sample Y-5	0.31	2.88	10.8	86.0
Sample Y-7	0.26	1.02	17.7	81.0
Group 1 (high neutron exposure)				
Sample Y-8	0.39	4.77	13.7	81.0
Sample Y-10	0.23	4.57	14.3	80.9
Nominal unirradiated		5.0	15	Balance

the indium content in the two Group 6 samples is interpreted to mean[5] that the indium diffused toward the surface of the control rod during either the annealing step after the nickel plating or during reactor operation. The presence of about the same amount of tin in both samples is also surprising since the two groups of rods experienced quite different neutron exposures. This is attributed[5] to the loss of tin by corrosion-product removal.

The general appearance of the 14 fuel assemblies is stated to be "good."[5] Some crud was observed at the top and bottom ends of several fuel assemblies, but the thickness was estimated at only 0.3 mil. This would cause sufficient fouling to raise the cladding temperature only 5 to 15°F. Two different types of scratches were observed on the cladding: oxidized and shiny. The oxidized scratches were probably formed during initial core-fueling operations and the shiny scratches during the refueling operations just preceding the writing of Ref. 5. The Yankee cladding thickness is 21 mils, and the reference states that a cladding scratch to a depth of 13 mils approaches the fracture threshold during operation. At least one loose piece of foreign matter was discovered lodged within a fuel bundle, but this was apparently too small to be of concern. The reference concludes that:[5] "More emphasis (should be placed) on the elimination of sharp corners and edges that may scratch the fuel cladding during maintenance operations, particularly as clad thicknesses are decreased in advanced cores."

References

1. C. N. Dunn and R. F. Stratton (Eds.), Shippingport Operations from Power Operation After First Refueling to Second Refueling, May 6, 1960 to August 16, 1961, USAEC Report DLCS-36402, Duquesne Light Co. and Westinghouse Electric Corp., Bettis Atomic Power Laboratory.
2. C. S. Abrams, P. W. Frank, O. D. Parr, and F. R. Vaughn, Evaluation of the PWR Core 1 Failed Element Detection and Location System, USAEC Report WAPD-TM-330, Westinghouse Electric Corp., Bettis Atomic Power Laboratory, November 1962.
3. H. R. Hazard and A. Rotkowitz, Studies of Mixing in the Lower Plenum of a Quarter-Scale Flow Model of the PWR Reactor, USAEC Report BMI-1172, Battelle Memorial Institute, Feb. 22, 1957.
4. L. R. Lynam, E. F. Losco, G. J. Salvaggio, and J. G. Goodwin, Fabrication Defects Observed in PWR Core 1 Blanket Fuel Rods, USAEC Report WAPD-TM-321, Westinghouse Electric Corp., Bettis Atomic Power Laboratory, September 1962.
5. Westinghouse Electric Corp., Atomic Power Department, Yankee Core Evaluation Program Quarterly Progress Report for the Period June 20, 1962 to September 30, 1962, USAEC Report WCAP-6052, Oct. 26, 1962.

Section

VII

Power Reactor Technology

Gas-Cooled Reactors

ANP Terminal Reports

With the cancellation of the Aircraft Nuclear Propulsion (ANP) program in early 1961, a decade of development of a direct-air-cycle nuclear turbojet ended. The program was comprehensive and required the advancement of technologies in practically every aspect of the overall power-plant concept. In the direct-air-cycle turbojet, the reactor receives air from a jet-engine compressor, heats this air, and then delivers it to the turbine. The hot air is exhausted through a nozzle, thus generating forward thrust. The temperatures that are required for the satisfactory operation of a system of this type are considerably higher than those required for attractive performance in current central-station nuclear power plants. Therefore, in addition to the problems in shielding, control, and remote handling which are inherent in the manned-nuclear-aircraft concept, the program embraced also the development of a high-temperature technology characteristic of the air-cycle environment.

The principal results of the program have been documented in a report that has recently been issued by AEC. The report, listed as Ref. 1, consists of 21 volumes that bear the generic title "Comprehensive Technical Report, General Electric Direct-Air-Cycle, Aircraft Nuclear Propulsion Program." A second report,[2] which consists of six volumes, is of a more general nature and contains only minimal reference to those problems or features unique to aircraft propulsion reactors. It is titled "Gas-Cooled High-Temperature Nuclear Reactor Design Technology." This report begins with basic concepts, proceeds to show the application of these concepts in simplified calculations that are intended to exclude nonworkable designs from further study, and then describes the more detailed assessments that are necessary to define the areas of final design and development activities. The detailed design sections of the report contain comparisons of the theoretical and experimental values of certain nuclear and thermal parameters. The design sections also describe tests of materials and mechanical assemblies, specify the areas in which computer analysis is useful, and describe the computer programs that were developed in conjunction with the ANP program.

Army Reactor Systems Program

Aerojet-General Nucleonics, under contract to the USAEC and the Department of the Army, is carrying out a development program that has as its objective the specification of a mobile nuclear power plant suitable for military field use[3] [*Power Reactor Technology*, 4(2): 7]. Thus far the program has led to the construction and operation of two reactor facilities at the National Reactor Testing Station: the Gas-Cooled Reactor Experiment (GCRE), and the Mobile Low-Power Plant No. 1 (ML-1) that is a prototype of a mobile nuclear power plant. The GCRE was built to investigate the operational and control characteristics of the reactor concept that was chosen for the mobile plant, and it consisted of a test reactor, a heat-removal system, and the required auxiliary and support equipment. The reactor was heterogeneous, water moderated, and nitrogen cooled and had a nominal power of 2 Mw(t). The first critical experiment was conducted in 1960. Testing was continued until April 1961 when there was a failure of the pressure vessel at the tube-to-tube-sheet joint. In January 1962 the decision was made to deactivate the GCRE, and this activity was completed by the end of June 1962.[3]

The ML-1 plant is a gas-cooled (nitrogen) water-moderated reactor. The plant is designed for an output of 3.3 Mw(t) and uses a gas turbine for power conversion.[4] A tabulation of ML-1 characteristics is presented in Table VII-1. The major components of the ML-1 power plant are housed in two skids or equipment packages: the reactor package, which consists of the reactor core, shielding, and most of the reactor auxiliary equipment; and the power conversion package, which includes the turbine-compressor set, recuperator, precooler, alternator, and electric switchgear. Each package weighs about 15 tons. During operation the packages are coupled together to form a complete power plant. The plant is operated from a control cab located several hundred feet from the reactor.

Table VII-1 CHARACTERISTICS OF THE ML-1 PLANT

Reactor power, Mw(t)	3.3 (2.9 into gas, 0.4 into water)
Net electric-power output, kw	330
Fuel inventory	49 kg, 93% enriched U (as UO_2)
Coolant	Nitrogen or air
Moderator	H_2O, 180 to 190°F, 34 psia
Average heat flux, Btu/(hr)(sq ft)	78,100
Heat-transfer area, sq ft	127
Approximate core length, in.	22
Active core equivalent diameter, in.	22
Reactor coolant flow, lb/sec	24.9
Reactor inlet temperature, °F	791
Reactor outlet temperature, °F	1200
Reactor inlet pressure, psia	313
Reactor outlet pressure, psia	289
Maximum cladding-surface temperature, °F	1750
Maximum fuel temperatures, °F	2160 (UO_2-BeO) 2650 (UO_2)

The ML-1 reactor is shown in Fig. VII-1. The reactor and shielding are located in a 9-ft-diameter tank in the reactor package. The tank is filled with borated water and serves as the major neutron shield during reactor operation. The ML-1 core contains 61 fuel elements that are held in type 321 stainless-steel pressure tubes. The tubes are joined at both ends to tube sheets and plenums to form the primary coolant pressure barrier. The tube sheets are cooled by moderator water that flows through internal passages within the sheets. The reactor is controlled by six pairs of semaphore type control blades that operate in the water between the pressure tubes. A lead-tungsten annulus, hexagonal in the plan view, encloses the active core and acts as a fast-neutron side reflector. When the reactor is shut down, biological shielding is provided by a lead annulus that surrounds the core and by another lead layer that encloses the pressure vessel. The shape of the reactor core, as defined by the side reflector, is hexagonal. An equivalent core is approximated by a cylinder having a radius of 11 in. and a height of 22 in. The spacing of the 61 fuel elements is varied to flatten the radial power distribution.

An ML-1 fuel-element cross section is shown in Fig. VII-2. The element consists of 19 pins surrounded by 5 concentric rings: namely, an inner liner, a layer of insulation, a foil liner of burnable poison, an outer liner, and a shim liner. The pin walls are Hastelloy X tubes and are 0.241 in. in outside diameter and 0.030 in. thick. They contain unequal fuel loadings to reduce differences in cladding temperatures. The center pin contains no fuel, the 6 inner pins contain highly enriched UO_2 pellets, and the 12 outer pins are filled with highly enriched UO_2-BeO pellets (70 wt.% UO_2). The inner liner of the element is Hastelloy X tubing that is 1.426 in. in inside diameter by 0.010 in. in wall thickness. The insulating ring is a 0.112-in. layer of Thermoflex (Al_2O_3-SiO_2) that surrounds the inner liner. The burnable-poison layer, which consists of cadmium alloy canned in stainless-steel foil, is attached to the inside surface of the outer liner and opposite the lower half of the fueled region. The outer liner is 0.012-in.-thick stainless-steel tubing, and it may be surrounded by a silver-plated stainless-steel shim liner. The fueled length of the element is 22 in., and the overall length is about 31 in. The pins are positioned in the inner liner by upper and lower spiders and by spiral wraps of 0.040-in.-diameter Hastelloy X wire. The nuclear design provides for a core lifetime of at least 10,000 hr; however, it is thought that corrosion of the fuel-pin cladding may limit the life of the first ML-1 core to about 3000 hr.

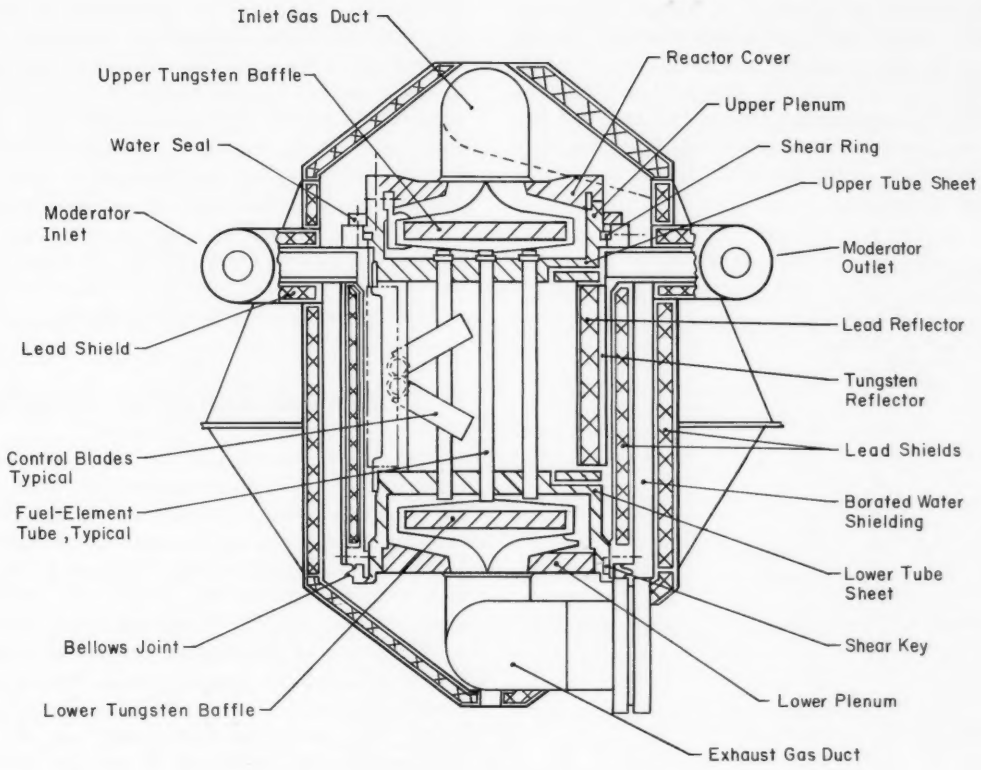

Fig. VII-1 The ML-1 reactor.[4]

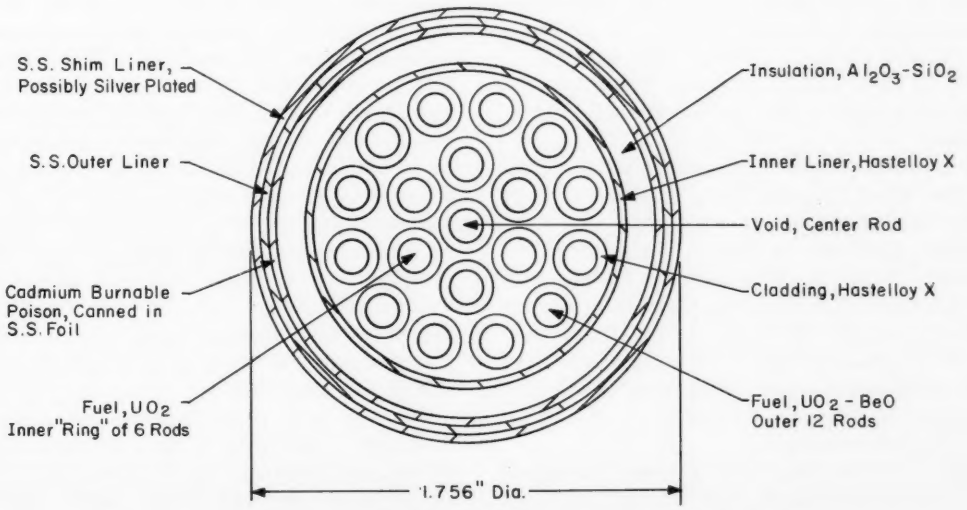
S.S. Shim Liner, Possibly Silver Plated
S.S. Outer Liner
Cadmium Burnable Poison, Canned in S.S. Foil
Fuel, UO_2 Inner "Ring" of 6 Rods
Insulation, Al_2O_3-SiO_2
Inner Liner, Hastelloy X
Void, Center Rod
Cladding, Hastelloy X
Fuel, UO_2 - BeO Outer 12 Rods
1.756" Dia.

Fig. VII-2 Cross section of ML-1 reactor fuel element.[4]

The ML-1 operates as a closed-cycle gas-turbine plant and uses either nitrogen or air as the working fluid. A schematic flow diagram of the plant, given in Fig. VII-3, shows temperatures and pressures around the loop for the design point conditions of 100°F ambient air temperature, nitrogen coolant, and a thermal power of 3.3 Mw.

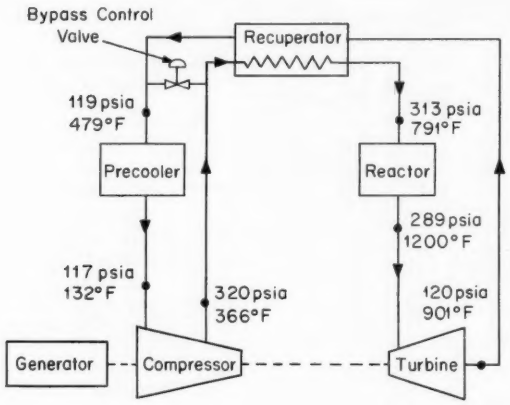

Fig. VII-3 ML-1 reactor power-plant cycle characteristics.[4]

Early in 1961 the ML-1 reactor skid was delivered to the National Reactor Testing Station for testing, and criticality was reached in March of that year. In June 1962 the power conversion skid was delivered, and preoperational testing was begun.[3] On Sept. 21, 1962, the ML-1 plant produced power for the first time.[5] After a short period of power operation, the plant was shut down for scheduled modifications.

In addition to the development of the GCRE and the ML-1, Aerojet-General is carrying out supporting activities for the Army Gas-Cooled Reactor Systems Program. These activities include a study to investigate the feasibility of an advanced gas-cooled high-temperature power plant that would represent improvements over the ML-1 design. Three reference designs have been established: a hydride-moderated reactor, a beryllium oxide-moderated reactor, and an unmoderated reactor.[3]

The failure of the GCRE pressure vessel at the tube-to-tube-sheet joint prompted a design review of the ML-1 pressure vessel. The objective of the review was to determine areas of possible improvement in the ML-1 design and with particular emphasis on improved configurations in the tube-sheet regions. Reference 6 presents the results of the review and describes the studies and experiments that were performed in an attempt to achieve a satisfactory uncooled-tube-sheet design. The uncooled concept was rejected as not feasible for a reactor of the ML-1 type, but an improved cooled-tube-sheet design, which eliminates all the potential problem areas in the ML-1 design, is judged to be a feasible development.

Advanced Reactor Studies

Preliminary designs for four integrated reactor-core and steam-generator units are described in Ref. 7. Figure VII-4, a vertical section through one of the units (the HGCR-3), shows an arrangement that typifies the basic layout of each of the four plants. The relative sizes of the major components vary, principally because of the differences in the reactor cores. The designs have resulted from a continuing study of reactors that utilize all-ceramic fuels. This study has been under way at Oak Ridge since the beginning of the gas-cooled-reactor program in 1957. A preliminary design study[8] of the GCR-2 reactor[9] (see Table VII-2 for characteristics) modified to use ceramic fuel elements was reported in 1959. The reactor defined by that study, the HGCR-1, operated with a contaminated cooling-gas circuit. The costs of the HGCR-1, when compared to those of its predecessor, the GCR-2, indicated that a reactor and steam-generator configuration of the Calder Hall type, on which both designs were based, was not economic for the ceramic-fueled contaminated-coolant plant. Subsequent studies were directed toward determining to what extent costs might be reduced by enclosing the reactor core with the steam generator in a single pressure vessel. The integrated concept has been employed in a series of four designs whose characteristics are compared to those of the GCR-2 and the HGCR-1 in Table VII-2.

For the past several years the Lawrence Radiation Laboratory of the University of California has performed a continuing study of advanced high-temperature gas-cooled reactors. In 1960 the study became a formal program known as the Advanced Reactors Studies (ARS)

program. Reference 10 contains a review of this program. The work being done is of a basic nature and is intended to be applicable to large high-temperature gas-cooled reactors in general rather than to a specific reactor concept. The program is divided into four principal areas: materials studies at elevated temperatures, criticality studies, reactor lifetime calculations, and cross-section measurements. About 80% of the effort is being expended in the first two areas.

Basically the work is directed toward high-temperature gas-cooled reactors that achieve high neutron economy through the use of low-cross-section moderators (graphite or BeO) without additional structural or cladding material and through the more or less continuous removal of fission products; the uranium-thorium fuel cycle is, of course, emphasized. The present concepts visualize large reactors of this general type which depend on high neutron economy and the continuous removal of fission products to obtain very long fuel exposures and high fuel utilization from fixed fuel. A reactor concept embodying these principles has been formulated as a focal point for

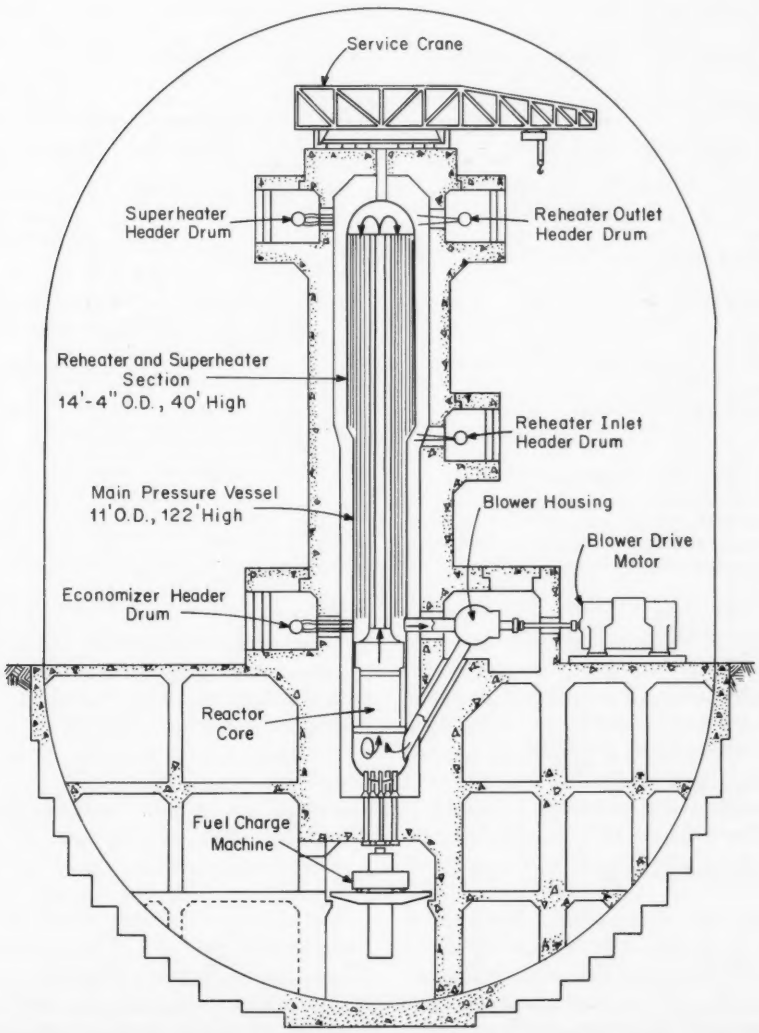

Fig. VII-4 Vertical section through the HGCR-3 BeO core and steam-generator unit.[7]

Table VII-2 CHARACTERISTICS OF GAS-COOLED REACTORS

	GCR-2	HGCR-1	HGCR-2	HGCR-3	HGCR-4	HGCR-5
Reactor output, Mw(t)	687	3095	1374	1130	1170	1170
Gross output, Mw(e)	252	1256	504	500	500	500
Net output, Mw(t)	225	1130	468	464	500	500*
Net overall efficiency, %	32.8	36.5	34.1	41.0	42.7	42.7
Thermal power density in core, kw/cu ft	49	219	97	2769	917	660
Reactor core						
Moderator and reflector material	TSF-grade graphite	Graphite	TSF-grade graphite	BeO	BeO	Graphite
Nominal core height, ft	20	20	20	10	10	10
Nominal core diameter, ft	30	30	30	7.7	12.5	15
Height of core plus reflector, ft	25	25	25	13	13	16
Diameter of core plus reflector, ft	35		35	10	15.3	20
Number of fuel channels	1597	1415	1597	1938	4850	5040
Pitch of channels, in.	8	8.5	8	2	2	2.25
Type of pitch	Square	Square	Square	Equilateral	Equilateral	Equilateral
Diameter of fuel channels, in.	345 at 3.45, 400 at 3.25, 852 at 3.05	4.5 × 4.5 square	345 at 4.0, 400 at 3.8, 852 at 3.6	1.34	1.20	1.51
Fuel element						
Slug outside diameter, in.	0.75 ± 0.005	0.372 × 4.5	3.9	0.875	0.80	1.1
Slug inside diameter, in.	0.32 ± 0.010		1.5	0.625	0.60	0.70
Slug length, in.	0.50 ± 0.003		24	10	10	12
Maximum slug internal temperature, °F	2200	~2095	1680	1945	2050	1900
Approximate slug average surface temperature, °F	1000		1350	1600	1500	1000
Slug maximum design surface temperature in hot zone, °F	1200	2000	1660	1850	2000	1800
Average power density in fuel element, watts/cm^3	45.9	82.5	15.3	1000	537	208
Average surface heat flux, Btu/(hr)(sq ft)	52,000	124,400	69,400	455,000	225,000	169,000
Pressure vessel						
Shape	Sphere	Sphere	Cylinder	Cylinder	Cylinder	Cylinder
Outside diameter, ft	50	50	38	10.7	18	22
Material	SA-212 grade B steel	Same	Same	Same	Same	Same
Vessel height, ft	5		108	122	102	99
Thickness, in.	3.250	3.25	4.5	4	4.0	4.0
Working pressure, psig	300	300	300	1000	625	500
Maximum temperature, °F	650	650	650	650	650	650
Coolant						
Gas	He	He	He	CO_2	CO_2	He
Working pressure, psia	300	300	300	1000	640	515

*The plant electric-power consumption is very small because both the feedwater pumps and the gas-circulating blowers are driven by steam turbines.

(Table continues on next page.)

Table VII-2 (Continued)

	GCR-2	HGCR-1	HGCR-2	HGCR-3	HGCR-4	HGCR-5
Coolant (continued)						
Normal total flow, lb/sec	972	2400	1972	5430	6970	1530
Reactor inlet temperature, °F	460	525	480	665	665	665
Reactor outlet temperature, °F	1000	1500	1220	1350	1250	1250
Circuit pressure drop, psi	6.61	12.6	6.6	65	40	14
Coolant blowers						
Type	Axial	Axial	Axial	Centrifugal	Axial	Axial
Number per reactor	4	8	4	3	3	3
Power for all blowers, Mw	18.3	53.7	18	26.8	15	30
Steam generator						
Type of generator	Once-through	Once-through	Once-through	Once through	Once-through	Once-through
Number per reactor	4	8	1	1	1	1
Gas inlet temperature, °F	1000	1500	1220	1350	1250	1250
Gas outlet temperature, °F	450	525	470	650	650	650
Feedwater inlet temperature, °F	324	445	324	520	520	520
Feedwater pressure, psia	1020	1688	1020	2450	2450	2450
Steam outlet temperature, °F	950	1050	950	1050	1050	1050
Steam outlet pressure, psia	950	1450	950	2400	2400	2400
Containment vessel						
Height, ft		220	214	214	179	179
Diameter, ft		220	140	140	114	114
Shape		Sphere	Cylinder with spherical top and elliptical bottom	Cylinder with spherical top and elliptical bottom	Cylinder with spherical top and elliptical bottom	Cylinder with spherical top and elliptical bottom

the general research. It is a one-region homogeneous graphite-moderated thermal breeder, 15 to 30 ft in diameter, initially loaded with thorium and U^{235}. The provision for fission-product removal is inherent in the core concept. The core is formed from blocks that consist of a homogeneous mixture of carbon, thorium, and U^{235}. Two groups of passages for two separate gas loops penetrate the blocks. One set of passages is used for heat removal and is lined with some substance such as zirconium carbide. It also has a high rate of gas flow. The other passages are unlined and provide for a low-flow gas stream to remove the volatile fission products. Conceptually this does not differ greatly from the schemes used in the Peach Bottom reactor and the British Dragon.

The operating temperature of the core is conceived to be about 2000°K in order to obtain adequate fission-product diffusion rates and to ensure the volatility of most of the important fission products. It is expected that this high temperature will induce a self-annealing effect in the core structure which will anneal out radiation damage. The desired power density in the core is at least 3 Mw/cu ft, and the core lifetime is projected as about 20 years at 2000 Mw(t). Although it has been necessary to define the reactor concept in order to plan the research and development work effectively, the significant part of the program is, as the reference[10] points out, the basic work on fission-product diffusion, fission-product cross sections, and reactor physics.

Progress Reports

The Peach Bottom Atomic Power Station will employ concepts of fission-product control and removal rather closely related to those discussed above. The work performed in the research and development program for this high-temperature gas-cooled graphite-moderated reactor, known also as the HTGR, during the period from Jan. 1, 1962, through Mar. 31, 1962, is described in Ref. 11. A half-scale clear-plastic nonnuclear flow model of the HTGR reactor vessel and internals was operated during the period from January 1961 through October 1961. The model was used to determine the pressure-drop characteristics of the reactor internal flow paths, to study the flow patterns in the gas-coolant passages, to measure how effectively the inlet gas would cool the reactor vessel wall, and to check the stability of the core and core-restraining capabilities of the tilting reflector blocks. Descriptions of the test facility, the methods of testing, and the results obtained are given in Ref. 12.

Reference 13 presents the results of a study of the economics of a cycle that incorporates a gas-cooled nuclear reactor, a gas turbine, a regenerator, a cooler, a two-stage compressor, and an intercooler. The result of this study was the writing of a computer code that aids in the selection of the optimum cycle within the somewhat limited scope of the code. Although the overall program is quite simplified and is usable with only a specific system, it may serve as a source of information concerning basic relations and certain interactions of the components of the turbine type power plant.

Plans to build the Pebble-Bed Reactor Experiment (PBRE) have been dropped, but apparently Oak Ridge National Laboratory will continue to work on fuel that could be used with this concept.[14] Two recent progress reports for the Oak Ridge gas-cooled reactor program[15,16] contain descriptions of the PBRE design that was being evolved prior to the cancellation of the construction program. The reports describe the work that is being performed in support of the Experimental Gas-Cooled Reactor (EGCR) project and in the advanced reactor design and development program. Mention is also made of the successful operation of two Bristol Siddeley gas-bearing compressors.

References

1. D. H. Culver and G. Thornton, Comprehensive Technical Report, General Electric Direct-Air-Cycle, Aircraft Nuclear Propulsion Program, 21 vols., USAEC Report APEX-901 to APEX-921, June 1962, as follows:

   APEX-901, Program Summary and References
   APEX-902, P-1 Nuclear Turbojet
   APEX-903, Core Test Facility
   APEX-904, Heat Transfer Reactor Experiment No. 1
   APEX-905, Heat Transfer Reactor Experiment No. 2
   APEX-906, Heat Transfer Reactor Experiment No. 3
   APEX-907, XMA-1 Nuclear Turbojet
   APEX-908, XNJ 140E Nuclear Turbojet
   APEX-909, Aircraft Nuclear Propulsion Systems Studies
   APEX-910, Aircraft Nuclear Propulsion Application Studies
   APEX-911, Remote Handling
   APEX-912, Controls and Instrumentation
   APEX-913, Metallic Fuel Element Materials
   APEX-914, Ceramic Reactor Materials
   APEX-915, Shield Materials
   APEX-916, Moderator Materials
   APEX-917, Organic, Structural, and Control Materials
   APEX-918, Reactor and Shield Physics
   APEX-919, Aerothermodynamics
   APEX-920, Applied Mechanics
   APEX-921, Nuclear Safety

2. General Electric Company, Flight Propulsion Laboratory Department, Gas-Cooled High-Temperature Nuclear Reactor Design Technology, six volumes, USAEC Report APEX-800, Parts A to F, June 1962, as follows:

   Part A: 1. Introduction; 2. Influence of Performance Requirements on Power Plant Component Specifications; 3. Reactor Design
   Part B: 4. Cellular Metallic Fuel Reactors
   Part C: 5. Ceramic Reactors
   Part D: 6. Folded-Flow Reactors } (Classified)
   Part E: 7. Shield Design
   Part F: 8. Control Design Factors

3. Aerojet-General Nucleonics, Army Gas-Cooled Reactor Systems Program, Semiannual Progress Report, January 1 through June 30, 1962, USAEC Report IDO-28590, Aug. 17, 1962.
4. Aerojet-General Nucleonics, Army Gas-Cooled Reactor Systems Program, Final Hazards Summary Report for the ML-1 Nuclear Power Plant, USAEC Report IDO-28560, November 1960.
5. *Nucleonics Week*, 3(39): (Sept. 27, 1962).
6. Aerojet-General Nucleonics, Army Gas-Cooled Reactor Systems Program, Design Report for an

Improved ML-1 Pressure Vessel, USAEC Report AGN TM-398, September 1962.

7. A. P. Fraas, Preliminary Designs for Four Integrated Gas-Cooled Ceramic-Fueled and -Moderated Reactor Core and Steam Generator Units, USAEC Report ORNL-2752, Oak Ridge National Laboratory, Dec. 12, 1962.
8. W. B. Cottrell, C. M. Copenhaver, H. N. Culver, M. H. Fontana, V. J. Kelleghan, and G. Samuels, The HGCR-1, A Design Study of a Nuclear Power Station Employing a High-Temperature Gas-Cooled Reactor with Graphite-UO_2 Fuel Elements, USAEC Report ORNL-2653, Oak Ridge National Laboratory, July 28, 1959.
9. Oak Ridge National Laboratory, The ORNL Gas-Cooled Reactor, Parts 1 to 4, USAEC Report ORNL-2500, Apr. 1, 1958.
10. R. Fox, The LRL Advanced Reactors Studies Program — A Review, USAEC Report UCRL-6863, University of California, Lawrence Radiation Laboratory, Apr. 3, 1962.
11. General Atomic Division, General Dynamics Corp., 40-Mw(e) Prototype High-Temperature Gas-Cooled Reactor Research and Development Program, Quarterly Progress Report for the Period Ending March 31, 1962, USAEC Report GA-3132, September 1962.
12. S. Ross, E. A. Day, and R. A. Skeehan, Tests on Half-Scale Flow Model of 40 Mw(e) Prototype HTGR (Peach Bottom Atomic Power Station), USAEC Report GA-2963, General Atomic Division, General Dynamics Corp., June 20, 1962.
13. R. V. Miskell, Effects of Major Parameters on Cycle Efficiency and Cost for a Gas-Cooled Reactor Turbine Power Plant, USAEC Report Y-1396, Union Carbide Nuclear Company, June 19, 1962.
14. *Nucleonics Week*, 3(39) (Sept. 27, 1962).
15. Oak Ridge National Laboratory, Gas-Cooled Reactor Program Quarterly Progress Report for Period Ending December 31, 1961, USAEC Report ORNL-3254, Apr. 6, 1962.
16. Oak Ridge National Laboratory, Gas-Cooled Reactor Program Quarterly Progress Report for Period Ending March 31, 1962, USAEC Report ORNL-3302, July 16, 1962.

Section

VIII

Power Reactor Technology

Pressurized-Water Reactors: Proposed Second Core for Indian Point

The Consolidated Edison Thorium Reactor (CETR) at Indian Point, Buchanan, N. Y., has been described in detail in Sec. V of this issue. Recently the Consolidated Edison Company submitted to the AEC Division of Licensing and Regulation a conceptual design of a proposed second core (prepared by the Westinghouse Electric Corp.).[1] This core differs considerably from the first core. If adopted, the new core would be installed after the normal life of the first core and would be used with presently existing control-rod drives, fuel-handling tools, instrumentation, etc. The fuel elements are composed of low-enrichment uranium oxide pellets jacketed in thin-walled cold-worked stainless-steel tubing. The control rods are composed of cadmium-indium-silver alloy with Zircaloy followers.

In this design the fuel is rather finely subdivided (pellets are 0.313 in. in diameter). Flux peaking has been depressed (1) by minimization of water holes in the core, (2) by arranging the fuel axially in one continuous length (instead of using periodic steel spacers in the fuel element, as in the first core) and (3) by the use of three different fuel enrichments in three radial zones. There is no brazing operation on the fuel jacket; therefore cold-worked tubing, with its higher allowable stress levels, is employed. Advantage of this is taken to specify a considerably thinner wall (0.012 in.) than has been required for previous designs in which the jackets have been annealed in a furnace-brazing cycle; in spite of the thin wall, the fuel jacket is expected to be "free standing."

In order to obtain maximum lifetime, the control rods are supplemented by soluble poison in the reactor coolant during shutdown and initial stages of power operation, allowing the enrichment to be increased over that which would be feasible otherwise. The reactor would be first brought to power with dissolved poison of reactivity equivalent to equilibrium xenon, and the poison would then be removed as xenon builds up. Complete removal of the soluble poison is expected to occur during a period of 100 hr at full power.

The reactor core is divided radially into three zones of equal size (Fig. VIII-1), with the initial fuel enrichment increasing progressively from the inner to the outer zones. Refueling is accomplished by (1) removing fuel from the inner zone, (2) moving the remaining fuel inward one zone, and (3) inserting new fuel in the outer zone.

Fuel Elements

The typical fuel element consists of sintered uranium oxide pellets enclosed in a stainless-steel tube with stainless-steel caps welded at each end. An aluminum oxide insulating washer and spring above the pellet stack complete the element. There are no intermediate spacers or other interruptions in the fuel column. The main characteristics of the fuel elements are

Fuel pellet diameter, in.	0.313
Fuel column length, in.	101.5
Cladding outside diameter, in.	0.341
Cladding thickness, in.	0.012
Nominal pellet-clad clearance (cold), in. diametral	0.004
Ratio of jacket thickness to outside diameter	0.035
Total number of elements per core	20,760
Total length of fuel column, ft	1.76×10^5

Fuel Assemblies

The fuel rods are held in place by a series of eggcrate spacers that have integral leaf springs

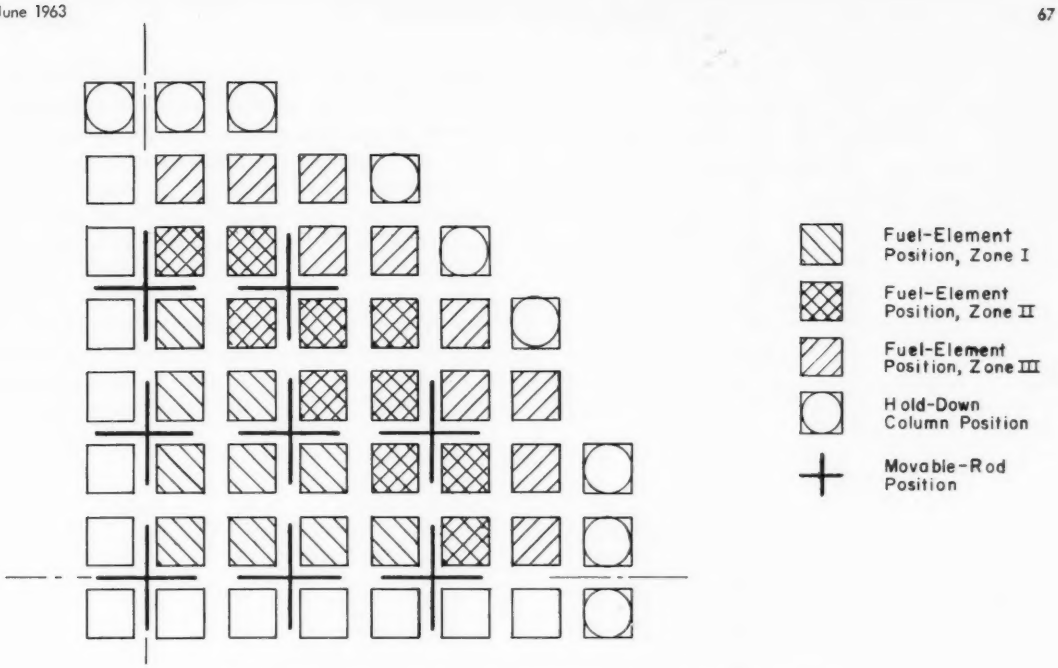

Fig. VIII-1 Cross section of the proposed core B for the CETR.[1]

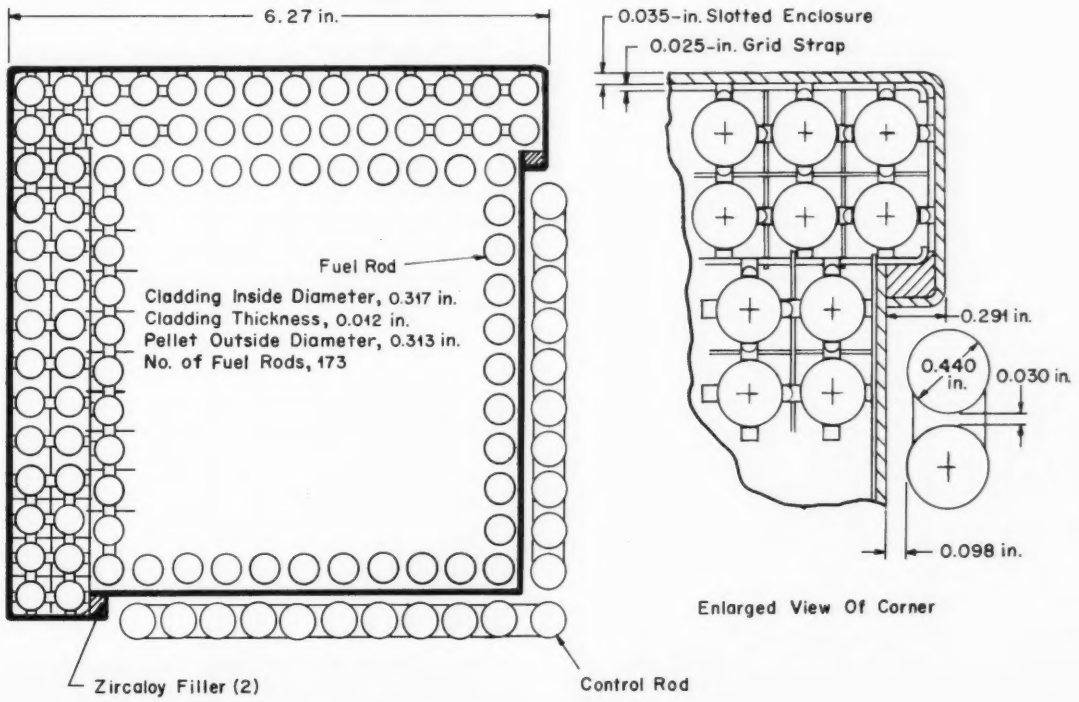

Fig. VIII-2 Cross section of proposed fuel element in the conceptual design of core B for the CETR.[1]

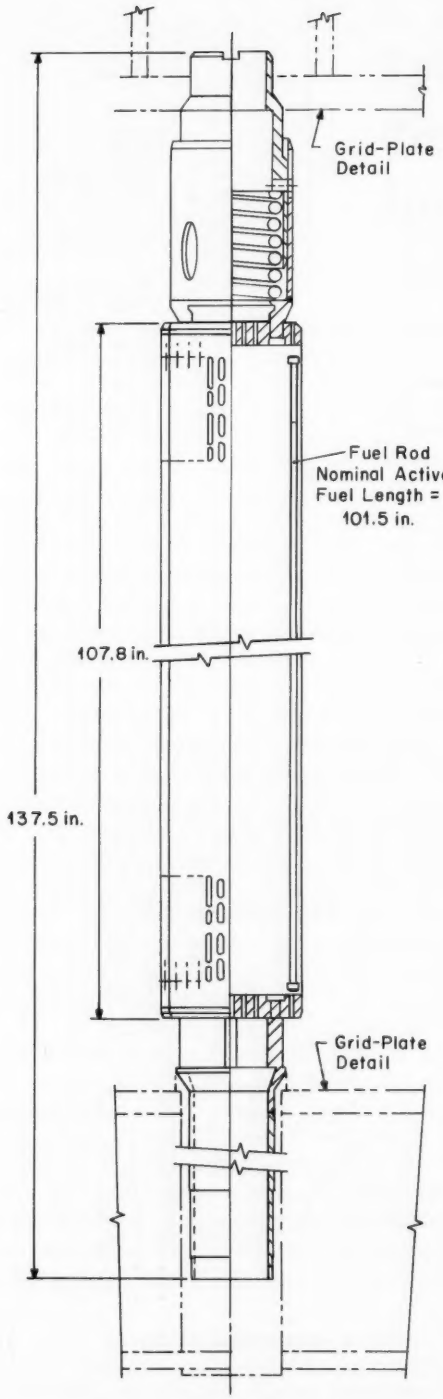

Fig. VIII-3 Proposed fuel element in the conceptual design of core B for the CETR.[1]

in each cell (Fig. VIII-2). Stainless-steel stampings, 0.024 in. thick, are assembled and furnace brazed at all intersecting joints to form the eggcrate spacers. The fuel assembly is formed by locating spacers at 11-in. intervals inside a perforated stainless-steel shroud and inserting the fuel rods. It is completed by the addition of end plates (drilled for coolant passage) and flow nozzles to fit existing structures (Fig. VIII-3). The spacing of the nominally square lattice is modified in the two rows of fuel rods farthest from the control rod. The more important characteristics of the fuel assemblies are

Number of fuel rods per assembly	173
Fuel-rod lattice	Square
Lattice spacing (rods farthest from the control rod), in.	0.441
Lattice spacing (rods nearest the control rod), in.	0.453
Cross-sectional dimensions of assembly, sq in.	6.27
Method of spacing fuel rods	Eggcrate spacers
Total fuel assemblies	40 in each zone; 120 total

Control Rods (Fig. VIII-4)

The poison section of the typical cruciform control rod is composed of round rods of silver-indium-cadmium alloy inside cladding tubes. A Zircaloy follower completes the rod. The required control-rod channel width is minimized by use of a flexible joint that will allow some translation between the poison section and the follower. The rods are designed to operate with existing core internals. Important characteristics are

Poison material	Cadmium-indium-silver alloy in cladding tubes
Absorber-tube dimensions	0.440 in. in outside diameter by 100 in. long
Control-rod shape	Cruciform, 10-in. span
Follower-rod length	100 in.

Reference

1. Westinghouse Electric Corp., Conceptual Design of Core B, Consolidated Edison Company, Indian Point Nuclear Facility, USAEC Docket 50-3, September 1962.

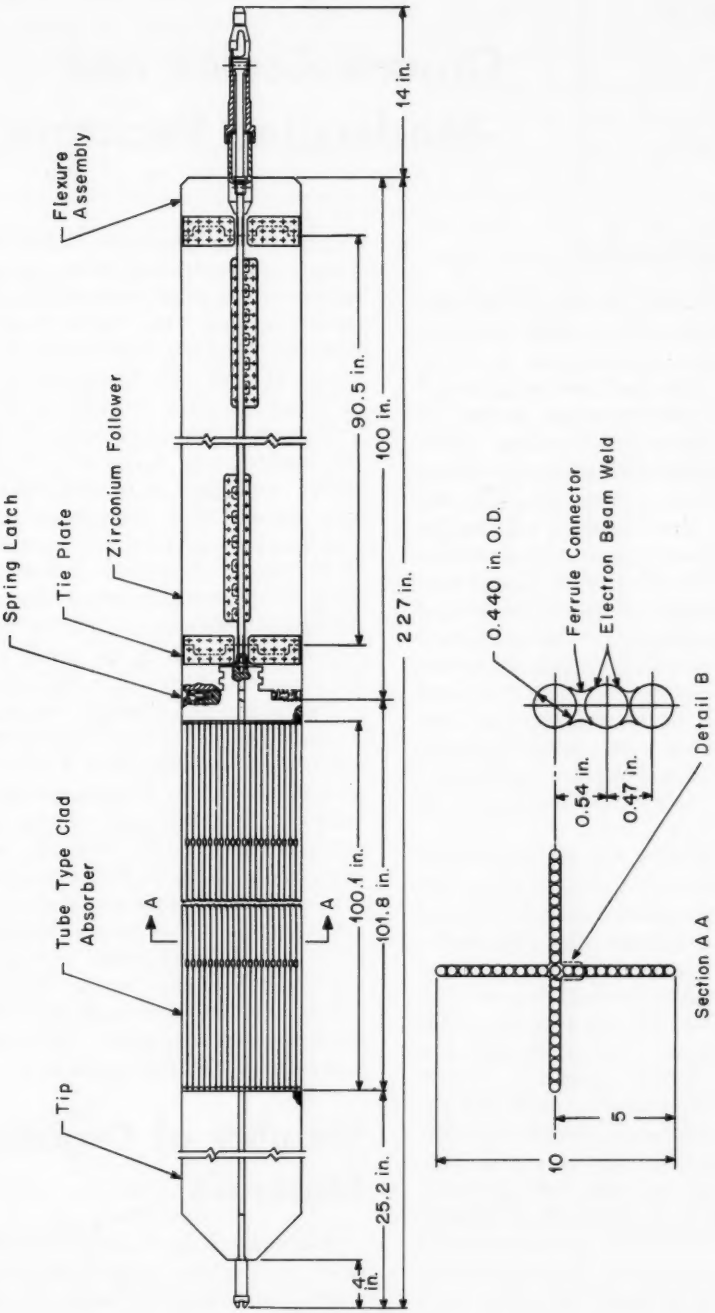

Fig. VIII-4 Proposed control rod in the conceptual design of core B for the CETR.[1]

Section

IX

Power Reactor Technology

Organic-Cooled and -Moderated Reactors

Coolant Treatment

The descriptions and experimental results arising from the operation of four Piqua prototype systems were reviewed in *Power Reactor Technology*, 4(2): 82-88. The systems were coolant purification, coolant degasification, waste-gas disposal, and high-boiler (HB) handling. Additional data on the HB-handling system were reviewed in *Power Reactor Technology*, 5(3): 56-59. A recent publication[1] reports information obtained with the coolant-purification, degasification, and waste-gas and water-treatment systems. It describes work done under the Advanced Organic-Moderated Reactor (AOMR) research and development program, although the equipment used was that designed, constructed, and operated to develop the Piqua systems. Some changes have been made in the equipment to provide for better operation; however, the flow diagrams given in the review cited above are still essentially correct.

The purification system was modified by the addition of a larger model return pump (the pump that transfers material from the HB and distillate tanks to the surge tank) and an increase in the reboiler heating capacity from 6 to about 15 kw. Operation with the modified system revealed that a large fraction of the ceramic-tower packing in the flash still was broken, presumably from bumping and slugging during operation. The ceramic packing was replaced by steel Raschig rings. After these modifications were made, the system, with little operator attention, was operated continuously for periods up to 21 days to prove its reliability. Agreement between calculated and experimental purification results was good. The system was able to reduce the HB concentration from about 20% in the feed to about 1% in the overhead and to concentrate the HB to 80 to 100% in the bottoms.

In previous operation of the degasification system, difficulty had been experienced in determining the water concentrations in the various process streams and/or in obtaining representative samples. Accordingly a considerable period of time was devoted to the development of water-analysis procedures and to the improvement of the instrumentation and control of the experimental equipment. Automatic, unattended operation of the degasification system was accomplished for periods up to 21 days. The results indicated that the system was able to reduce the water concentration to satisfactorily low levels when water-containing organic (Santowax OMP) was fed to it, although unexplained variations in the water content within the acceptable range were observed.

The waste-gas system was operated as a service facility for the purification and degasification systems, and it was not subjected to detailed testing. Previous work had indicated, however, that the gas-scrubber recirculating water formed a stable emulsion, and the operations reported on in Ref. 1 were accomplished with a modified waste-gas system that incorporated a screen filter to break the emulsion. This filter was located in the recycled-scrubbing-water line, but the clarified water was pumped to the clarified-water tank and a portion recirculated to the scrubber. Diatomaceous earth was used as the filter medium.

Stability of Organic Materials

Reference 2 is of particular interest in the field of organic-coolant stability because it treats the combined effects of temperature and radiation. The materials used were biphenyl, isopropyl biphenyl, metaterphenyl, and Santowax R. Irradiation was accomplished by an ac-

celerator or in-pile, with sample temperatures being held to within 2°C. Typical data presented in Fig. IX-1 illustrate the effect of temperature on various *G* values for Santowax R in-pile irradiations. The conclusions of general interest are quoted as follows:[2]

1. With the exclusion of two cases, that of *G* (→HBR) for biphenyl under electron bombardment, and *G* (→HBR) for isopropyl biphenyl subjected to pile radiation, which gave a constant activation energy, the effective activation energy for *G* (gas) and *G* (→HBR) [was] found to rise with increasing temperature. This may indicate the participation of more than one decomposition process as the temperature rises.

2. At low temperatures (<300°C) the activation energies for *G* (gas) and *G* (→HBR) were low (<1 k.cal.) and at higher temperatures the relative increases of gas production were, in general, greater than those for conversion to HBR. This indicates that at these temperatures gas and polymer production occur by different processes.

3. At temperatures of 390–420°C, about 20–30°C below those where thermal decomposition becomes important, the curve of *G* (→HBR) against temperature showed a steep rise. At temperatures of 415 and 419°C the increased *G* value was much larger than could be explained simply by the contribution of the thermal decomposition.

4. Since the sharp increase in *G* (→HBR) with temperature may result in limitations on the bulk coolant temperature in a reactor, this region seems to require further investigation. Important parameters for variation appear to be the intensity and type of the radiation.

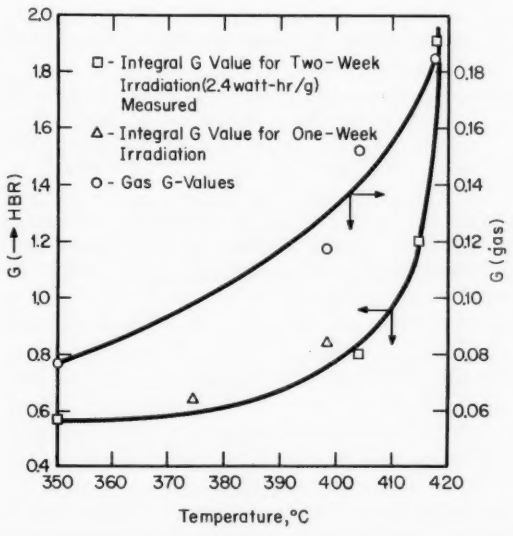

Fig. IX-1 Effect of temperature on *G* (gas) and *G* (→HBR) for Santowax R.[2]

An extensive investigation of the radiation stability of organic fluids, conducted at the Department of Nuclear Engineering, Massachusetts Institute of Technology, is reported in Refs. 3 to 5. This work was the basis for a paper presented at a meeting of the American Nuclear Society[6] which has been previously reviewed [*Power Reactor Technology*, 6(1): 69-70]. References 3 to 5 contain considerable additional information.

The loop used for the studies was located in the central fuel-element position of the MIT reactor. A special fuel element was provided with 8 of the normal 18 fuel plates removed. In the resulting space was located an aluminum thimble ($1\frac{1}{4}$ in. in outside diameter and with a 0.035-in. wall) that contained a stainless-steel capsule with a volume of 205 cm^3 for the organic under study. Organic fluids were pumped into the steel capsule for irradiation and were returned to the out-of-pile portion of the loop for sample taking and heating or cooling. A $\frac{5}{16}$-in.-OD aluminum tube was placed adjacent to the exterior of the aluminum thimble for instrumentation to monitor the radiation dose rate throughout each in-pile run, and the loop was equipped with an in-pile organic-leak detector. This loop was used to obtain the results published in Ref. 6.

The test loop was run from August until October of 1961 with Santowax OMP at a temperature of 600°F and under a pressure of 100 psig. No new organic was added during this period, and the degradation-product concentration increased to about 39% during the test period.*

Heat-transfer measurements were made on the recirculating organic coolant during the in-pile test. The measurements were made by determining the heat-transfer coefficient and the out-of-pile fouling characteristics of the organic material. An electrically heated test section was incorporated in the out-of-pile portion of the loop. The film coefficients were determined by measuring wall temperatures and bulk coolant temperatures, whereas a graphical method was used to infer the extent of fouling of

*The degradation products arising from the irradiation of organic materials are discussed in some detail in Ref. 3, and the degradation-product concentration is computed as 100 minus the total weight percent of orthoterphenyl, metaterphenyl, and paraterphenyl remaining.

the heat-transfer surfaces from the thermal results. The authors conclude that the coefficients of heat transfer for forced convection are correlated within ±10% by conventional relations and that no fouling of the out-of-pile heat-transfer surfaces existed.

Table IX-1 OPERATING CONDITIONS FOR FOULING LOOP[7]

	OMRE	OMRE replica cell	Deep channel cell
Bulk coolant temperature, °F	600	730	750
Radiation surface temperature, °F	750 to 850	900	850
Coolant velocity in radiation channel, ft/sec	15	3.0 to 9.0	1.0
Operating pressure, psig	200	200	200
Beta-current flux, $\mu a/cm^2$	0.2	29.5	22.4
Fast-neutron flux, neutrons/(cm^2)(sec)	8.9×10^{13}		
Coolant channel thickness, in.	0.134	0.134	1.75
Test period, hr		56	18

An out-of-pile circulating loop with electron irradiation for fouling studies is described in Ref. 7. The loop consists of a 6-Mev 4-kw linear accelerator (Linac) delivering electrons to an irradiation cell that simulates a fuel-element coolant channel. Organic is pumped through the cell and undergoes irradiation under controlled conditions. Typical operating conditions are given in Table IX-1. Some published experimental results were obtained using clean Santowax OMP and core II coolant from the OMRE. The conclusions are quoted as follows:

> The test results indicate that the circulating loop generates film under moderate temperatures in a radiation field. This out-of-pile loop closely reproduced reactor fouling experience in the following ways: (*a*) clean coolant did not foul; (*b*) reactor coolant (Core II) with particulates fouled; (*c*) heaviest film was found in the radiation area; and (*d*) lower fouling occurred at higher velocity.

References

1. W. N. Bley, J. A. Vanderlip, and R. R. Stiens, Development of Prototype Process Systems for OMR, USAEC Report NAA-SR-5675, Atomics International, Oct. 15, 1962.
2. W. G. Burns, C. R. V. Reed, R. W. Wilkinson, and J. A. Winter, The Radiation and Thermal Stability of Some Potential Organic Moderator-Coolants, Part VI. The Effect of Temperature on the Radiolysis of Biphenyl, Isopropyl Biphenyl, Metaterphenyl and Santowax R, British Report AERE-R-3989, August 1962.
3. D. T. Morgan and E. A. Mason, The Irradiation of Santowax OMP in the M.I.T. In-Pile Loop, Part I. Summary to October 5, 1961, USAEC Report MITNE-21, Massachusetts Institute of Technology, May 1962.
4. D. T. Morgan and E. A. Mason, The Irradiation of Santowax OMP in the M.I.T. In-Pile Loop, Part II. Equipment Design, Procedures and Results of Irradiation to October 5, 1961, USAEC Report MITNE-22(Bk. I), Massachusetts Institute of Technology, May 1962.
5. D. T. Morgan and E. A. Mason, The Irradiation of Santowax OMP in the M.I.T. In-Pile Loop, Part II. Equipment Design, Procedures and Results of Irradiation to October 5, 1961, USAEC Report MITNE-22(Bk. II), Massachusetts Institute of Technology, May 1962.
6. E. A. Mason, D. T. Morgan, W. N. Bley, T. W. Carroll, J. P. Casey, E. Sefchovich, and A. Turricchia, In-Pile Irradiation of Santowax OMP, *Trans. Am. Nucl. Soc.*, 5(1): 106 (June 1962).
7. R. A. Mengelkamp, P. S. Hudson, and J. C. Hillyer, An Out-of-Pile Electron Irradiation Circulating Loop for Fouling Studies, USAEC Report IDO-16801, Phillips Petroleum Co., Aug. 1, 1962.

Section

X

Power Reactor Technology

Supercritical Water Reactors

Power-generating cycles that utilize working fluids in the supercritical pressure and temperature condition are capable of achieving efficiencies of about 45% at fluid temperatures of around 1100°F. Several fossil-fueled steam power plants that operate in the supercritical region have been built in the United States [*Power Reactor Technology*, 4(2): 78-81], and the apparent success of these plants is attested by the current design and construction of other such plants. Although the incentives for high efficiency are somewhat different in nuclear plants than in fossil-fueled plants—just as the problems of supercritical steam generation are different and probably more difficult—there is considerable interest in the development of nuclear plants that operate in the supercritical pressure region. Recent reports prepared by General Electric[1] and Westinghouse[2–4] describe activities that have been directed toward determining the potential benefits and problem areas of supercritical pressure power reactors.

Reference 1 presents the results of a design study and economic evaluation of the 300-Mw(e) Supercritical Pressure Power Reactor (SPPR) carried out under an AEC contract at Hanford. The estimated[1] SPPR plant capital costs and power costs, calculated in accordance with the Nuclear Power Plants Cost Evaluation Handbook, are $175/net kw and about 6.09 mills/kw-hr, respectively. The reactor is cooled and moderated by light water. The plant operates on a direct cycle and attains a net thermal efficiency of 43%. It is similar in concept to an earlier supercritical water plant studied at Hanford which was included in the review mentioned above. The turbine throttle conditions are 3515 psia and 1050°F, and double reheats to 1000°F are employed. The core is 10 ft high and about 12 ft in diameter. It is made up of clusters of two-pass fuel elements suspended in a pool of unpressurized light water that serves as the moderator. The coolant water enters and leaves at the top of the elements, and it makes passes through three groups of elements in series. It enters the reactor as feedwater at 540.3°F and about 4500 psig. The fluid temperature at the

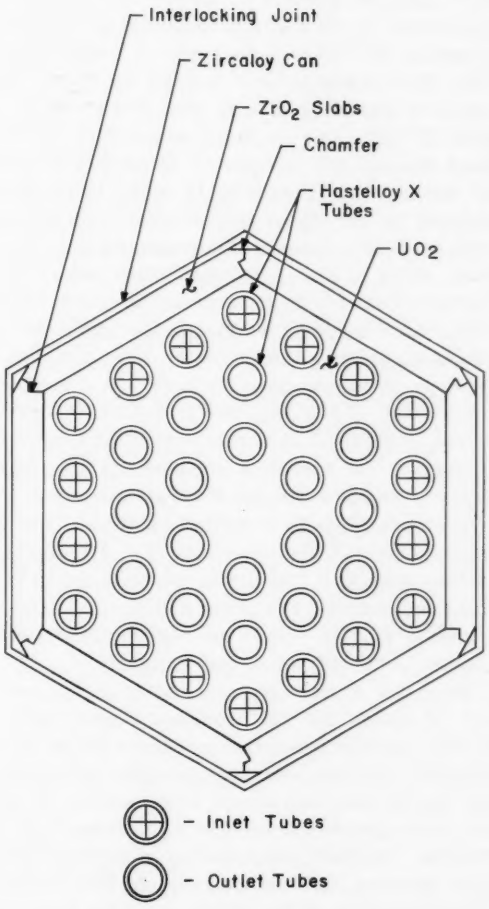

Fig. X-1 Cross section of SPPR fuel element.[1]

end of the first pass is 805°F. The discharge from the first pass is immediately taken through the core again, where the fluid temperature is raised to 1050°F. The discharge from the second pass flows through the reheat heat exchangers, where heat is transferred from the 1050°F fluid to the exhaust steam from both the high-pressure and first-reheat sections of the turbine. The reheat steam temperature is raised to 1000°F, and the temperature of the fluid from the second pass of the core is lowered to 821°F. The 821°F fluid is returned to the reactor for final heating in the third pass, after which it enters the high-pressure section of the turbine at 1050°F and 3515 psia.

The fuel element, a cross section of which is shown in Fig. X-1, is a hexagonal block of UO_2, 10 ft long and about 2 in. across the flats. It is penetrated by 36 coolant channels that are the pressure members of the primary coolant system. The channels are formed by $^3/_{16}$-in.-ID tubes of Hastelloy X with wall thicknesses of about 27 mils. The incoming coolant flows downward through the peripheral 18 tubes and back up through the remaining 18 tubes to be discharged at the top of the element. The fueled region of the element is surrounded by $^1/_2$-in.-thick slabs of ZrO_2 insulation which reduce the thermal losses to the surrounding unpressurized light-water moderator. The entire assembly is contained within a thin Zircaloy outer can. Fabrication of the element is based on vibratory compaction of the UO_2, and UO_2 densities of 90 to 92% of theoretical are predicted for the given geometry. The elements are intended for exposures of 25,000 to 40,000 Mwd/metric ton.

The core consists of 85 fuel clusters, each of which contains 7 fuel elements. The fuel cluster is the basic unit for piping connections to the main coolant inlet and outlet headers, and a distribution system within the cluster apportions coolant to the individual fuel elements.

Since the design is a conceptual one, a number of questions and problems remain unresolved. Among these the problems of the fuel element, including thermal stresses, corrosion, and deposition, may be the most severe. These and other problems, including problems of flow and the "whistle" phenomenon in supercritical flow systems, are summarized in Ref. 1. The characteristics of the SPPR plant are given in Table X-1.

References 2, 3, and 4 describe work at the Westinghouse Atomic Power Department on an AEC program with the goal of developing a 1000-Mw(e) supercritical steam-generating station for a target date of 1975. The program includes experimental investigations of hydraulic and heat-transfer characteristics and the corrosion-erosion behavior of selected fuel-cladding materials as well as the conceptual design and evaluation of the reactor portion of the plant.

Most of the experimental work will be performed in a single supercritical water loop that furnishes the following conditions:

Steam pressure, psia	2400 to 4000
Maximum system flow rate, lb/hr	2200 at maximum test-section heat input
Test-section power input, kw	5 to 600
Test-section flow rate, lb/hr	4 to 2200
Maximum test-section outlet temperature, °F	1100
Test-section flow areas, sq ft	1.36×10^{-5} to 1.09×10^{-3}
Heat flux range, Btu/(hr)(sq ft)	0.2 to 1.5×10^6

The objectives and prime areas of interest in the experimental heat-transfer program, as taken from Ref. 2, are listed below in order of interest and priority:

1. To obtain a forced convection heat-transfer correlation in the vicinity of the critical region over the range of expected reactor operating conditions
2. To obtain once-through heat-transfer data over a wide range of variables to determine the quality and pressure effect on the heat-transfer coefficient; under similar thermodynamic conditions, to compare the difference in heat-transfer characteristics between heating one side of an annulus and heating two sides
3. To investigate the heat-transfer behavior of superheated steam over a limited pressure range
4. To study the conditions under which "whistle" phenomena occur and to interpret the data with the objective of predicting the inception of this effect within the limits of the experiments

The loop was expected to be operational in the latter part of 1962.[3]

Two supercritical reactors were evaluated to determine the preferred concept for continued development: the Supercritical Once-Through Tube Reactor (SCOTT-R), in which metal-clad fuel is contained in pressure tubes, and the Fuel-Bearing Graphite Reactor (FBGR), in which the fuel is located in graphite external to

Table X-1 CHARACTERISTICS OF THE CONCEPTUAL SUPERCRITICAL PRESSURE POWER REACTOR (SPPR) PLANT[1]

Power	
Thermal, Mw(t)	698
Electric, Mw(e)	300
Efficiency, %	
Net	43.0
Gross	44.9
Auxiliary power, Mw	2.83
Equivalent main feed pump power, Mw	9.93
Fuel material	Enriched UO_2
Weight of UO_2 in core, lb	88,655
Density of UO_2, g/cm^3	9.98 (91% TD)
Enrichment, % U^{235}	
Initial	4.08
Final	1.27
Specific power, Mw/metric ton of U	
Average	19.62
Maximum	65.5
Moderator space between fuel elements, in.	1.75
Volume of H_2O/volume of UO_2 in core	
Without coolant	2.32 : 1
With coolant cold	2.61 : 1
With coolant hot	2.38 : 1
Number of fuel elements	595, in 85 clusters of 7
Fuel element	Hexagonal, internally cooled, 2 in. on flats
Number of coolant tubes per fuel element	36
Coolant tube	
Material	Hastelloy X
Wall thickness, in.	0.027
Inside diameter, in.	3/16
Fuel-element active length, ft	10
Lattice spacing, in.	5.22
Fuel-jacket material	Zircaloy-2
Thickness, in.	0.030
Core diameter, ft	11
Number of control rods	85
Reactor vessel	
Material	AISI 304 S.S.
Inside diameter, ft	13
Height, ft	30
Wall thickness, in.	0.5
Effective heat-transfer area in coolant tubes, sq ft	10,500
Heat flux, Btu/(hr)(sq ft)	
Maximum	755,000
Average	228,000
Average core power density, kw/liter	25.0
Maximum fuel temperature, °F	4800
Maximum fuel-jacket surface temperature, °F	
Hastelloy	1300
Zircaloy	200

Characteristics of coolant passes	First	Second	Third
Number of fuel elements	~217	~168	~210
Inlet temperature, °F	540.3	805	821
Outlet temperature, °F	805	1050	1050
Inlet pressure, psig	4550	4450	4100

Turbine throttle pressure, psig	3500
Coolant flow rate, lb/hr	1,880,000
Coolant cycle time (from pump to turbine), sec	45
Coolant *p*H	8.7 to 9.0
Average fuel irradiation level at discharge, Mwd/metric ton	30,771
Fuel enrichment, % U^{235}	
Initial	4.08
Final	1.27
Total final plutonium concentration, g/kg	6.8
Excess reactivity, mk	
Burnup	115
Other	110
Total	225
Power peaking factor	
Static	2.67
Transient and overpower	1.25
Moderator	H_2O
Inlet temperature, °F	90
Outlet temperature, °F	
Average	165
Maximum	200
Reactor heat in moderator, %	5.62
Turbine type	Cross compound, 2 reheats
High-pressure stage conditions	1050°F, 3515 psia
First-reheat conditions	1000°F, 912 psia
Second-reheat conditions	1000°F, 299 psia
Exhaust pressure, in. Hg	3.5
Condenser size, sq ft	110,000
Number of feedwater stages, including deaerator	10 with 1 spare
Feedwater pumps	
Steam-driven	1 at 4600 psi, 400 gal/min
Electrically driven	1 at 4600 psi, 2000 gal/min
Generator No. 1 (high-pressure unit)	
Speed, rpm	3600
Rating, kva	224,000
Voltage, kv	20
Generator No. 2 (low-pressure unit)	
Speed, rpm	1800
Rating, kva	160,000
Voltage, kv	20

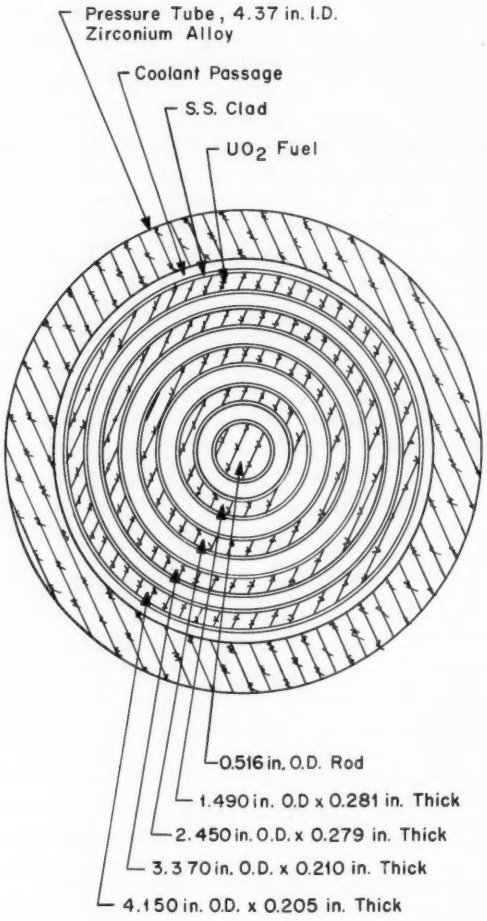
Pressure Tube, 4.37 in. I.D.
Zirconium Alloy
Coolant Passage
S.S. Clad
UO_2 Fuel
0.516 in. O.D. Rod
1.490 in. O.D x 0.281 in. Thick
2.450 in. O.D. x 0.279 in. Thick
3.370 in. O.D. x 0.210 in. Thick
4.150 in. O.D. x 0.205 in. Thick

Fig. X-2 1000-Mw(e) SCOTT-R pressure-tube fuel assembly.[2]

coolant tubes. The selection was made on the basis of fuel-cycle cost comparisons, reactor capital cost comparisons, and feasibility comparisons. "Near-term" and "advanced" versions of each reactor were considered; the near-term versions would utilize materials for which a considerable developmental background exists, and the advanced versions would utilize materials that require development.

The conceptual SCOTT-R is graphite moderated and has several hundred vertical pressure tubes that contain fuel and coolant. The core, with an active equivalent diameter of 29.5 ft and an active height of 20 ft, is housed in a low-pressure tank, and the graphite is maintained under a helium atmosphere. The fuel is UO_2 clad with austenitic stainless steel. Direct-cycle steam is generated at 1050°F and 3500 psig in a once-through system. The reactor employs annular-ring fuel elements, one of which is shown in cross section in Fig. X-2. Coolant flow progresses in four consecutive passes outside to the center of the fuel assembly, the last pass taking place in two parallel channels.

The conceptual FBGR is graphite moderated and has vertical fuel-bearing graphite assemblies that contain coolant tubes (Fig. X-3). The active equivalent diameter of the core is 53.5 ft, and its active height is 45 ft; it is contained in a low-pressure vessel in which a helium atmosphere is maintained. The heat-transfer system and the turbine cycle are similar to those of the SCOTT-R, and the overall efficiency is in the same range, 43 to 45%. A cross section through a fuel-coolant cell of the reactor is shown in Fig. X-3. Each cell contains eight coolant tubes which are located in a removable sleeve of graphite and which provide the in-core primary system pressure barrier. The coolant flow is two-pass: downward in four of the tubes and upward in the remaining four. External to the coolant-tube sleeve, which also

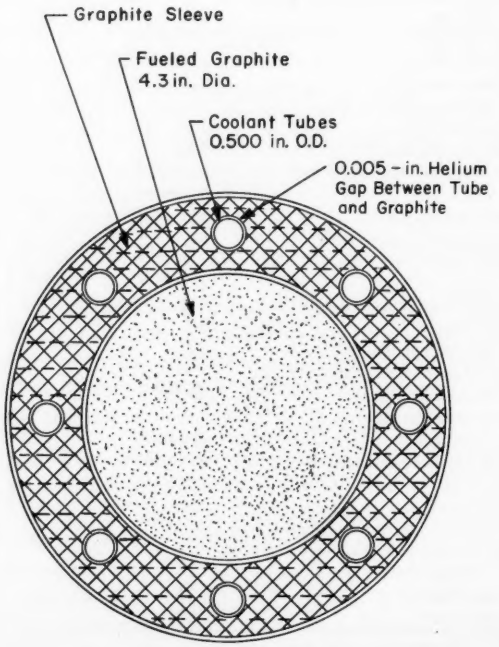

Fig. X-3 FBGR unit cell.[2]

serves as moderator, is the major portion of the moderator graphite, and the region surrounded by the sleeve contains a fuel slug composed of 50 wt.% uranium in the form of UC_2.

As a result of the comparative evaluation[4] the SCOTT-R concept was selected as the one for continued development, primarily on the basis of lower estimated capital costs, a lower estimated fuel cost for the near-term case, and a somewhat higher feasibility rating. The principal characteristics of the SCOTT-R concept[3] are listed in Table X-2.

The supercritical reactors represent the next step beyond nuclear superheat for the attainment of high-performance steam conditions with direct-cycle steam. When it is recognized that a number of the more difficult problems of nuclear superheat have their counterparts in the supercritical systems and that there are, in addition, problems peculiar to the supercritical approach, it is easy to believe that the 1975 target date for the development of a large supercritical reactor is not an overly conservative one.

Table X-2 SUMMARY OF PLANT DATA FOR THE CONCEPTUAL SUPERCRITICAL ONCE-THROUGH TUBE REACTOR (SCOTT-R)

Power	
Thermal, Mw(t)	2297
Electrical, Mw(e)	1000
Net plant efficiency, %	43.5
Auxiliary power, Mw	10
Reactor coolant	H_2O
Reactor inlet	
Temperature, °F	506
Pressure, psia	3750
Coolant flow rate, lb/hr	7,772,000
Turbine throttle	
Temperature, °F	1050
Pressure, psia	3500
Throttle flow, lb/hr	6,749,000
Reactor vessel	
Inside diameter, ft	35.5
Height, ft	42.0
Material	SA-212B steel
Thickness, in.	1.30
Design pressure, psia	115
Temperature, °F	230
Pressure-tube assembly	
Number	540
Tube inside diameter, in.	4.37
Tube outside diameter, in.	
Near-term SCOTT-R	5.37
Advanced SCOTT-R	5.17
Inside liner thickness, in.	
Advanced SCOTT-R	0.025
Material in near-term SCOTT-R	
Strength member	Zr–2.5 Nb
Material in advanced SCOTT-R	
Strength member	Zr–3 Al–0.5 Nb
Inside liner	Zr–0.3 Ta–0.13 W
Design pressure, psia	4000
Design temperature, °F	
Near-term SCOTT-R	680
Advanced SCOTT-R	700
Reactor core	
Active equivalent diameter	29.5
Height, ft	20
Lattice pitch, in.	13.5
Total uranium loading, kg of U	
Near-term SCOTT-R	121,900
Advanced SCOTT-R	124,200
Reactor core (continued)	
Average specific power, kw(t)/kg of U	
Near-term SCOTT-R	18.9
Advanced SCOTT-R	18.3
Fuel enrichment in near-term SCOTT-R, at.%	
Initial	3.03
Final	1.49
Fuel enrichment in advanced SCOTT-R, at.%	
Initial	2.77
Final	1.29
Burnup, Mwd/metric ton of U	16,500
Moderator material	Graphite
Reactor energy in moderator, %	4.1
Moderator to fuel	
Volume ratio	44 : 1
Atom ratio C/U	80 : 1
Peak to average power ratio	3.31
Reflector material	Graphite
Reflector thickness	
Axial, ft	2.5
Radial, ft	2.0
Total graphite height	25.0
Maximum diameter, ft	33.5
Fuel-assembly geometry	4 rings and rod
Fuel material	UO_2
Cladding material	310 S.S.
Fuel thickness, in.	0.205 to 0.281
Cladding thickness, in.	
Near-term SCOTT-R	0.012
Advanced SCOTT-R	0.010
Fuel compact density, g/cm^3	9.31
Length, ft	20
Heat flux, Btu/(hr)(sq ft)	
Average	122,000
Maximum	404,000
Total number	540 (1 per pressure tube)
Reactor control	137 B_4C rods

References

1. H. Harty, J. J. Regimbal, K. G. Toyoda, and R. D. Widrig, Economic Evaluation of a 300-Mw(e) Supercritical Pressure Power Reactor USAEC Report HW-68420(Rev.), Hanford Atomic Products Operation, June 1961.

2. Westinghouse Electric Corp., Atomic Power Department, First Quarterly Progress Report (Jan. 5, 1962–Mar. 31, 1962) for 1000 Mwe Supercritical Pressure Nuclear Reactor Plant Study, USAEC Report WCAP-2009, May 1962.

3. Westinghouse Electric Corp., Atomic Power Department, Second Quarterly Progress Report (Apr. 1, 1962–June 30, 1962) for 1000 Mwe Supercritical Pressure Nuclear Reactor Plant Study, USAEC Report WCAP-2070, August 1962.

4. Westinghouse Electric Corp., Atomic Power Department, 1000 Mwe Supercritical Pressure Nuclear Reactor Plant Study Selection of Preferred Reactor Concept, USAEC Report WCAP-2042, July 1962.

Section

XI

Power Reactor Technology

Physics

Resonance Absorption

As part of the Heavy-Water Lattice Research Project, the thermal column of the Massachusetts Institute of Technology Research Reactor has been used to investigate the neutron capture of U^{238} in a 1.010-in. natural-uranium rod in heavy-water lattices of 4.50-, 5.00-, and 5.75-in. spacing.[1] Experimental techniques, based on (1) a direct determination of the cadmium ratio and (2) the direct measurement of the ratio of U^{238} captures to the number of U^{235} fissions, were intercompared through the conventional initial conversion ratio. For the three lattices investigated, the discrepancy noted between the two values of conversion ratio ranged from near perfect agreement for the largest lattice spacing to a difference of $5 \pm 4\%$ for the smallest. This discrepancy is sufficiently large to suggest further investigation in tighter lattices to determine any systematic error in either of the two experimental techniques.

Measurements of the effective resonance integral for the 1.010-in. fuel rods agreed well with the accepted single-rod value, although a significant depression of the asymptotic $1/E$ flux, near energies corresponding to the lower U^{238} resonances, was noted. As in the case of the conversion ratio measurements, this effect would be more significant in tighter lattices.

Reference 1 also contains a large bibliography comprising most of the important papers related to the general subject of resonance capture. These references are arranged in chronological order under each of several subheadings.

The results of an experimental investigation of the resonance absorption of thorium in semihomogeneous thorium-graphite mixtures, covering the range of carbon-to-thorium ratios from 10 to 2000, is given in Ref. 2. An activation technique was employed, with irradiation of the samples in the British reactor Zenith. Corrections for thermal absorption were obtained independently by irradiating identical samples in the thermal column of the British reactor Nestor, with copper foils for cross-normalization of the thermal-neutron absorption. The derived resonance capture in thorium for the homogeneous carbon-thorium mixture has been correlated with the single parameter, σ_p', the equivalent scattering cross section per absorbing atom. For the semihomogeneous thorium-graphite system used, which involved elements of a thorium-graphite mixture embedded in pure graphite (as in the Dragon-reactor core), the equivalent scattering cross section per absorbing atom was approximated by

$$\sigma_p' = \sigma_p + \sigma \frac{S}{M} = \sigma_p + \frac{S}{4VN}$$

where σ_p is the scattering cross section per absorbing atom of the thorium-graphite mixture, S and V are the surface and volume of the thorium-graphite lump, and N is the number of thorium atoms per unit volume in the lump.

The variation of the resonance integral with σ_p' was found to be

$$RI = 1.4 + 80.9 \sqrt{\frac{\sigma_p'}{\sigma_p' + 2000}} \text{ barns} \qquad (1)$$

which has been normalized to an infinite-dilution resonance integral for thorium of 82.3 barns. For $\sigma_p \ll 2000$ barns, Eq. 1 reduces to

$$RI = 1.4 + 1.81 \sqrt{\sigma_p'} \qquad (2)$$

For the case of completely segregated thorium and graphite, this would correspond, in terms of S/M, to

$$RI = 1.4 + 17.8 \sqrt{S/M} \qquad (3)$$

The latter equation, which would apply for thorium-metal rods, agrees well with the form derived on a theoretical basis by Nordheim[3] [*Power Reactor Technology*, 5(4):19] as follows:

$$RI = I_h + 1.37 + 17.9\sqrt{S/M} \qquad (4)$$

where I_h is a small contribution from high-energy resonances.

Critical and Exponential Experiments

Calculations of the fission ratio for rod clusters in graphite-moderated reactors generally involve some degree of homogenization of the individual fuel rods over a portion of the fuel channel. For purposes of comparison with theoretical models to determine the degree to which the homogenization process is justified, measurements of the U^{238}-to-U^{235} fission ratio have been made[4] in slightly enriched oxide rod clusters covering a broad range of cluster geometries. The catcher-foil technique was used. Individual clusters were positioned in a 4.5-in.-diameter channel penetrating a 56-in. cube of graphite adjacent to the Nestor source reactor. The fuel rods consisted of 1.135 wt.% enriched UO_2 pellets which were 0.299 in. in outside diameter and which were clad with 0.378-in.-OD aluminum tubing. Foil packages, each containing two enriched (1.135 wt.%) or depleted (384 ppm by weight) uranium-metal foils, separated by an aluminum catcher foil, were irradiated in representative elements of each rod cluster. The uranium foils were 0.003 in. thick, whereas the catcher-foil thickness was 0.001 in. Since no effort was made to remove the oxide layer from the surface of the uranium foils, the effect of this oxide layer on the activity of the catcher foils was determined by separate calibrations in a thermal-neutron flux.

The report is devoted primarily to discussions of the experimental techniques and accuracies, but a comparison of experimental and calculated values of δ, the fission ratio, is given for four cases, covering clusters of 3, 7, 18, and 37 rods, with values of δ ranging from about 0.01 to 0.035. The agreement is considered reasonable.[4] Insofar as the measurements could establish a trend, it appeared that the calculated values tended to be higher than the experimental values at small fission ratios and lower than the experimental values at the large ratios.

Reference 5 contains a description of the critical studies carried out in the Zero Power Reactor III (ZPR-III) fast critical facility (National Reactor Testing Station, Idaho) for the Enrico Fermi Atomic Power Plant. The Enrico Fermi Atomic Power Plant is a sodium-cooled fast breeder reactor with intermediate sodium loops, sodium-to-water steam generators, and associated turbine generator. The reactor-core region consists of the central fuel portion of 91 subassemblies plus 10 control-element channels. The fuel is in the form of partially enriched uranium-molybdenum alloy pins, 0.148 in. in diameter and 30.95 in. long, clad by coextrusion with 0.005 in. of zirconium and arranged in the subassembly on a 0.199-in.-square matrix. The axial blanket portions of the 91 core subassemblies and the remaining 548 radial blanket subassemblies consist of stainless-steel-clad depleted uranium-molybdenum alloy in the form of 0.443-in.-OD rods on a 0.483-in.-square matrix. The regulating and safety control rods employ boron carbide as a poison.

The objectives of the program include determination of the uranium enrichment required for criticality, the effect of minor variations in core and blanket composition, reactivity coefficients, control- and safety-rod characteristics, power distribution, spectral indices, and the reactivity worth and wave shape of the oscillator rod. The experimental program was separated into two phases. The first phase involved investigations of a clean assembly, which was a simplified and homogenized core and blanket geometry constructed for ease of experimental manipulation and analysis. The second phase involved experiments on the engineered, or "as designed" core. This assembly included such details as control- and safety-rod channels, core end gaps, and a precise reconstruction of the core outline. In each phase the core (and blanket) was mocked up by loading drawers with the proper combination of fissionable, structural, and simulated or canned coolant materials and by inserting the drawers into the square matrix tubes of the ZPR-III structure. The critical experiment data were used to establish the U^{235} enrichment of the fuel alloy, worths of fuel subassemblies, and the B^{10} enrichment of the control and safety rods.

Reference 6 contains a summary of work performed on the Spectral Shift Control Reactor

(SSCR) Basic Physics Program during the eighth contract quarter. Briefly, the SSCR Basic Physics Program is designed to study the nuclear properties of clean uniform lattices of slightly enriched oxide fuels moderated by D_2O-H_2O mixtures. Presently the variables consist of 4 and 2.46% enriched UO_2, nonmoderator-to-moderator ratios of 0.7, 1.0, and 1.2, and D_2O concentrations in the range from 0 to about 90%. In the eighth contract quarter, data were obtained on three cores, i.e., cores XIII, XIV, and XV, using fuel elements of the 2.46% enrichment at a nonmoderator-to-moderator ratio of unity. The D_2O content of the moderator was 0, 70, and 50%, respectively, in the three cores. Typical measurements included determination of the clean critical loading, critical moderator levels (h), $\partial\rho/\partial h$, radial and axial flux plots for critical buckling determinations, thermal-disadvantage factors (dysprosium-aluminum foils), the cadmium ratio for U^{235} (Oralloy-aluminum foils) and the cadmium ratio for U^{238} using both chemical separation and thermal-activation techniques. In the thermal-activation technique, the epithermal activity of U^{239}, as measured by the chemical separation method, was related to the thermal activity of dysprosium in the lattice; the results were calibrated by measuring the uranium-to-dysprosium activity ratio following irradiation in a thermal-neutron flux. Thus perturbations by cadmium were eliminated in the in-core uranium-foil measurements, and good agreement with the results of the chemical separation technique was obtained. The initial criticality was achieved in the small lattice experimental facility. This facility employs the Lynchburg Source Reactor as an annular driver in application of the Physical Constants Testing Reactor technique to small epithermal systems of the SSCR type.

Theoretical predictions of temperature coefficients for the SNAP Experimental Reactor (SER) and the SNAP Developmental Reactor (SDR), based on hydride thermalization models which appeared to be substantiated by TRIGA-reactor experiments, were found to be in disagreement with SNAP experimental data. Reference 7 presents a brief description of experimental measurements carried out on the SER and SDR systems, the method of analysis employed in evaluating the fuel-moderator temperature coefficient from these measurements, and an interim report on the development of a hydride thermalization model. To date, isothermal temperature-coefficient and power-coefficient measurements for the SER and SDR systems, as well as zero-flow transient experiments on the SER, have been completed. The isothermal temperature-coefficient experiments consisted of measuring the reactivity defect as the system was heated uniformly over a broad temperature range. Some power-coefficient data were obtained for the SER and a variety of coolant temperature and flow conditions were investigated for the SDR. The magnitude and temperature dependence of the thermal-spectrum temperature coefficient in SER and SDR have been obtained from transient experiments and verified by power-coefficient and isothermal measurements.

Thermal-neutron spectral effects are calculated[7] for SNAP systems by a one-dimensional, multiregion, multigroup diffusion-theory code that allows both upscatter and downscatter of neutrons in the thermal-energy range and only downscatter in the epithermal (and fast) energy range. A phenomenological model for the calculation of thermal-energy transfer cross sections in zirconium hydride is developed with neutron interactions in zirconium and hydrogen treated separately. For zirconium, a crystal phonon scattering formulation is used which includes phonon emission and absorption processes due to neutron interactions with the crystal lattice. The hydrogen cross-section formulation is similar to that employed for zirconium except that Bose-Einstein phonon statistics are replaced by Fermi-Dirac statistics to describe properly the initial proton energy states and allowed transitions between states. Broadening of the excited vibrational state is described by a frequency-distribution function that is calculated from experimental differential-scattering data. The temperature dependence of the hydrogen scattering cross sections is, to first order, determined by the statistical occupation numbers for the proton vibrational states. The use of Fermi-Dirac statistics to describe the proton-excited energy states in zirconium hydride was verified by comparing the SDR and SER experimental spectral temperature coefficients with those predicted by models employing Fermi-Dirac, Boltzmann, or Bose-Einstein statistics. Good agreement between measured and calculated zirconium hydride spectra is attributed to the use of frequency-distribution functions derived from experimental data and the treatment of the

zirconium crystal lattice with a Debye spectrum.

To better define the effects of rod spacing, temperature coefficient, and coolant removal in heavy-water-moderated (and cooled) systems, a series of exponential measurements[8] on 19-rod clusters of natural UO_2 rods in D_2O was carried out at the Subcritical Experiment and Pressurized Subcritical Experiment facilities of the Savannah River Laboratory at temperatures between 20 and 220°C. The fuel rods consisted of 0.500-in.-OD pellets which had a mean density of 10.4 g/cm^3 and which were clad in type 6063 aluminum tubing that was 0.547 in. in outside diameter. The pertinent geometric variables consisted of the following: (*a*) rod-to-rod spacings of 0.025 and 0.100 in., (*b*) triangular lattice pitches of 7.00, 8.08, 9.24, and 12.12 in., (*c*) a mean-square lattice pitch of 8.00 in., and (*d*) aluminum-housing tubes that were 4 and 5 in. in outside diameter. The latter were employed either individually or concentrically at each cluster to permit the use of different void geometries. Values of the material buckling were evaluated from the relaxation length of the axial flux distribution for selected combinations of the geometric variables. In addition, data for evaluation of the fast-fission factor, resonance escape probability, surface effectiveness for resonance neutron capture (i.e., Dancoff effect), and intracell thermal-flux profiles were measured for a more restricted set of geometric variables. Comparisons are made in the reference[8] between experimentally determined parameters and the predictions of calculational models. Intracomparisons between the experimental and critical (Process Development Pile) buckling measurements were in agreement for flooded lattice configurations but, for voided lattice configurations, corrections for anisotropic diffusion were required.

Reference 9 contains the results of measurements of control-element worth by the pulsed-neutron technique in a broad range of thermal reactor types. Control elements in the form of slabs, angles, cylinders, and tubes were fabricated with such absorber materials as Cd, Ag, B_4C, B_2O_3, Dy_2O_3, boral, Ag-Cd, and B_4C-Dy_2O_3. The worths of individual elements and arrays of elements of a given geometric shape and composition were measured in 11 basic cores by determining the prompt-neutron decay constant, α, and the decay constant at delayed critical, α_c, with the elements fully inserted and removed, respectively. The basic cores used four types of moderator, namely, H_2O, D_2O, graphite, and an organic mixture, in a tank 6 ft in diameter and 6 ft high. Three fuel enrichments, namely, 1.3% (UO_2), 3.0% (UO_2), and 93.2% (uranium-aluminum), were used in rod type elements that were approximately 0.5 in. in diameter. Uniform square lattices of the fuel rods were used with the various moderators in the following combinations:

Moderator	Enrichment, %	Temp., °C	Fuel-rod pitch, cm
H_2O	1.3, 3, 93.2	20	2.032
D_2O	1.3, 3, 93.2	20	4.064
Graphite	1.3, 3, 93.2	20	5.08
Organic	1.3, 3	40	2.032

The graphite core region was driven by an H_2O-moderated annular region. Reactivity control in all cores was achieved by varying the liquid moderator level. The prompt-neutron decay constant was measured in each basic core (without control rods) as a function of geometric buckling (water height) to permit adjustment of the decay constants measured with control elements inserted to a constant value of geometric buckling and to permit an extrapolation to delayed critical buckling for an evaluation of α_c.

After a burst of neutrons has been injected suddenly into a subcritical multiplying system, the thermal-neutron density at any point in the system will quickly reach a maximum and then will decay according to the relation

$$n(l) = n_0 e^{-\alpha l} + n_d(l)$$

where l, on the time scale that describes thermal-neutron decay, may be considered to be zero at the time of the effectively instantaneous burst. The symbol α designates the prompt-neutron decay constant. The term $n_d(l)$ describes the decay of the delayed neutrons. Since the number of delayed neutrons is small and since they are emitted over a long period of time (relatively), the prompt decay can be measured over a large decrement, and α can be determined, without interference from the delayed neutrons so long as the reactor is subcritical. The prompt decay constant (α) has a positive value for all reactivities below prompt

critical. At or above delayed critical, however, a large background of neutrons will normally be present, and α cannot be evaluated by observing the decay of a small additional prompt burst. This difficulty can be circumvented, and the value of α at delayed critical (α_c) can be determined, by obvious extrapolations from measurements made on the slightly subcritical reactor.

If two control elements, a standard and an unknown, yield prompt decay constants α_{std} and α_x when inserted, separately, in the same initially critical reactor, the ratio of the reactivity worths (R_x/R_{std}) is given by

$$\frac{R_x}{R_{std}} = \frac{\alpha_x - \alpha_c}{\alpha_{std} - \alpha_c}$$

The reference gives values of α_c for the critical assemblies listed above, as well as the values of α which result when many different absorbers and groups of absorbers are inserted into the assemblies.

In support of the Army Nuclear Power Program (ANPP) Code Development Program, experiments[10] employing water-moderated arrays of uranium and stainless steel have been carried out to generate the necessary data for testing the general code. Twelve plate type cores containing between 9 and 25 fuel assemblies were investigated; metal-to-water ratios ranged between 0.265 and 0.383, and equivalent full-core (45 assemblies) boron loadings varied between 0 and 470 g of natural boron. Each fuel assembly contained 18 laminated bundles of fully enriched uranium-metal strips sheathed in stainless steel plus a sufficient number of stainless steel and boron stainless-steel strips to provide the desired core composition. Typical measurements consisted of the following: (1) determination of critical mass and core size, (2) axial and transverse buckling determinations based on flux profiles measured with thorium, cadmium-covered gold, and dysprosium-aluminum foils, (3) intracell and reflector activation mappings with dysprosium foils, (4) evaluation of the percentage of fissions by subcadmium neutrons, (5) determination of fuel and boron reactivity worths, (6) temperature coefficient of reactivity between 20 and 65°C, (7) homogeneous fuel-assembly substitution experiments, and (8) pulsed-neutron experiments for an evaluation of the prompt-neutron lifetime and control-rod worth.

Shielding

Thermal-Neutron Distribution

One of the most difficult problems in the design of the thermal and biological shields for a nuclear reactor is the prediction of the thermal-neutron distribution beyond the reactor core. The problem is important because usually the bulk of the shield heating results from neutron capture and because most of the gamma energy emerging from the biological shield is in the form of neutron-capture gammas produced in the shield. Several methods have been developed for calculation of the thermal-neutron distribution. These methods have had varying degrees of success, but none has been capable of handling all degrees of heterogeneity which may arise in a shield design. Most of them combine semiempirical neutron-removal theory with neutron diffusion. Several of these methods were reviewed in *Power Reactor Technology*, 3(2): 40 and 5(3): 28-29.

A multigroup method for multilayer shields is described in Ref. 11. It is an extension of one of the methods previously reviewed which gave satisfactory results when checked against measurements in graphite-iron-water shields but which did not give good results in water and iron-water shields. The modified method makes use of an energy-dependent removal cross section in a removal flux kernel which describes the neutron-source distribution for the slowing-down process. Slowing down is described by a 10-group age-diffusion formulation. The novel approach in the method is to advance the slowing-down source that results from a removal collision with hydrogen to a point beyond the position of the actual collision. This correction was introduced because the scattering by hydrogen is highly anisotropic in the laboratory system, whereas the slowing-down theory assumes the sources arising from these collisions to be isotropic. A previous study of this method in water showed that a constant multiplicative factor, independent of neutron energy, could be used to convert the removal collision density to the source for the neutron slowing-down procedure.[12] The calculated subcadmium neutron distributions were compared with experimental measurements made in the Panel C facility of the LIDO reactor. The shield configurations investigated consisted of single slabs of iron, from 2.41 to 21.87 cm thick, in water,

as well as multiple iron-water layers of various thicknesses. The calculations underpredicted the reaction rates due to subcadmium neutrons by about 50% in the water regions and on the surfaces of the iron slabs. Larger deviations occurred in the interiors of the thick iron slabs. Another interesting result[11] is the comparison of the 10- and 17-group calculations; these showed only a 10% difference, suggesting that 10 groups are sufficient to describe the neutron slowing-down procedure.

A Bulk Shielding Code

The computer code MAC is an IBM-7090 code for calculating the neutron and gamma attenuation through reactor shields.[13] It calculates the following quantities as functions of distance through the shield assembly:

1. Neutron fluxes for 35 energy groups
2. Neutron dose rates
3. Approximate neutron spectrum
4. Gamma fluxes for seven energy groups
5. Total gamma dose rate, with a breakdown of the contribution from each region in the shield
6. Approximate gamma spectrum

The calculation of the neutron distribution in space and energy is done by a combination of neutron removal theory with diffusion theory. The removal cross section, which differs from that usually used in shielding calculations, is defined as

$$\Sigma_r = \Sigma_{tot} - \bar{u}\,\Sigma_{sc}$$

where Σ_r = removal cross section
Σ_{tot} = total cross section
$\bar{u}$ = mean cosine of the elastic scattering angle in the laboratory system
Σ_{sc} = elastic scattering cross sections

The gamma calculations are done for slab sources with the buildup expressed in terms of the sum of two exponentials commonly called Taylor buildup factors.

The code has been tested by comparing calculations with experimental data obtained in the Hanford Bulk Shield Facility. The materials tested include iron-masonite, ferrophosphorus cements, iron–serpentine concrete, and ordinary concrete. The shield thicknesses are from 210 to 250 cm, with attenuation factors in the range of 10^{12} and 10^{11} for neutrons and gammas, respectively. The calculated neutron fluxes and gamma dose rates, as functions of distance, are compared[13] with the experimental values. Good agreement is obtained in some shields, whereas in others the method tends to underpredict the intensities. The gamma dose-rate predictions, for the most part, agree with the measured rates, whereas the calculated neutron fluxes, in general, agree very well near the source but tend to fall below the measured values as the distance from the source increases.

Pathfinder Shield Analysis

A report on the shielding analysis of the Pathfinder Atomic Power Plant has been published.[14] It includes the shield design criteria, a description of the biological shields throughout the plant, a presentation of the methods used to determine the sources and their strengths, and a brief description of the method used to calculate the attenuation of the radiation through the shields. The sources of radiation considered are the operating-core gammas and neutrons, the shutdown-core gammas 4 hr after shutdown, the gaseous fission-product activity in the coolant, and the N^{16}, N^{17}, and O^{19} activity produced in the recirculating water. The calculated dose rates from all sources are presented both in tabular form and in illustrations that show the gross dose rates expected in various areas of the plant. Safety factors are used in the design to cover uncertainties in (1) the gamma and neutron sources and source spectra, (2) the absorption and attenuation coefficients, (3) the buildup factors, and (4) the adequacy of the geometric representation of the shielding and related structures.

Radiation Survey on N.S. Savannah

A report on the detailed radiation survey of the nuclear ship *Savannah* is of special interest because calculated and measured dose rates can be compared.[15,16] The measured dose rates were taken using the ORNL Mobile Radiation Shielding Laboratory No. 1. The results of the detailed survey show that the design dose rate of 0.5 rem/year in the passenger access areas is not exceeded. In the areas restricted to crew access, the design dose rate of 5.0 rem/year is exceeded only in the water-sampling room, where access can be controlled. A comparison of the measured total dose rates with the calculated total dose rates shows the measured

values to be, in general, lower than the calculated values. Of the totals, the measured neutron dose rates are generally a little higher than the calculated rates, whereas the measured gamma rates are for the most part much lower than the calculated rates.

Experimental Breeder Reactor II Design

Reference 17 covers the shield design of the Experimental Breeder Reactor II (EBR-II). It includes a description of the shields, along with the resulting neutron and gamma-flux distributions, as well as a brief description of the plant and reactor. Of special interest is a section of the report which enumerates and discusses the major shield-design problems, most of which are peculiar to a sodium-cooled reactor of the EBR-II design.

From the point of view of shielding, the EBR-II can be described briefly as an unmoderated, heterogeneous, sodium-cooled reactor, which consists of a central region made up of stainless-steel-jacketed fuel pins containing enriched uranium, and a surrounding blanket region made up of fuel rods containing depleted uranium. The reactor proper is surrounded by what is referred to as the neutron shielding and by a reactor vessel. The latter, in turn, is surrounded by a much larger tank (the primary tank) that contains liquid sodium, the primary heat exchanger, and a spent-fuel storage rack. The arrangement is shown in Figs. XI-1 and XI-2. The liquid sodium in the primary tank serves as the primary coolant for the reactor. The primary coolant is pumped through the core and then through a sodium-to-sodium primary heat exchanger, after which it is discharged

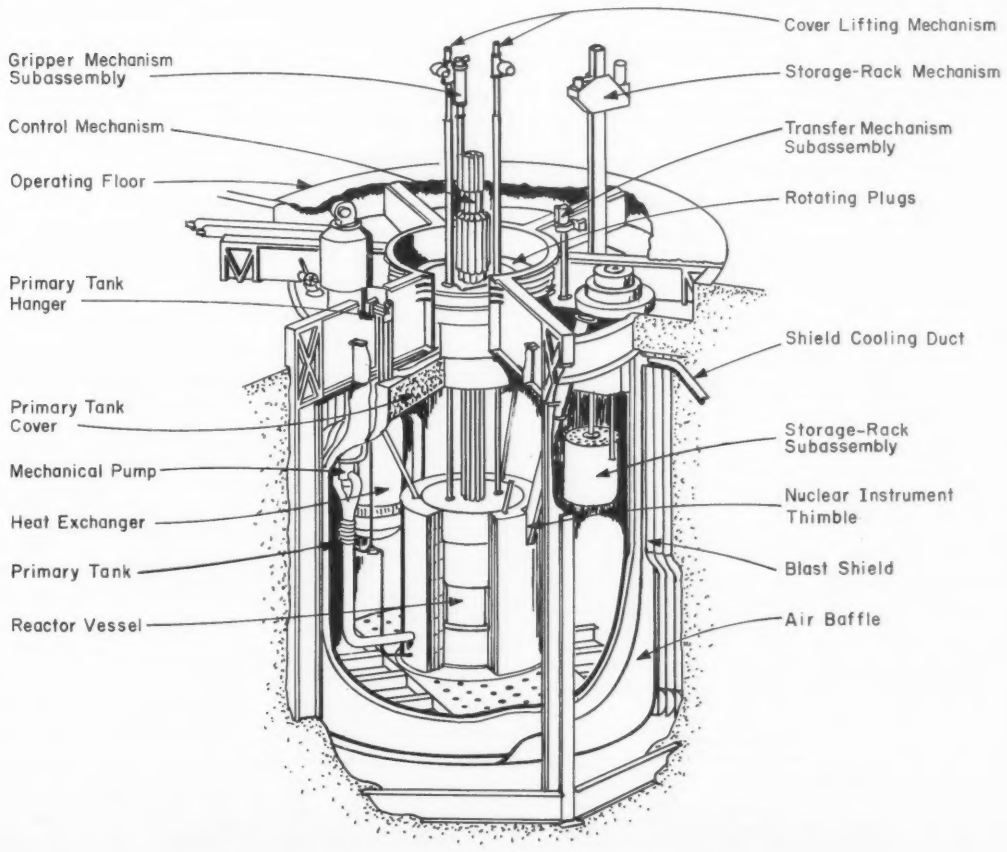

Fig. XI-1 Cutaway view of the EBR-II reactor.[17]

into the primary tank. The secondary sodium from the primary heat exchanger is piped from the reactor containment building to an adjacent building that houses the boiler.

One of the shielding problems was to minimize the activation of sodium in the secondary coolant loop. Activation is possible because of the proximity of the primary heat exchanger to the reactor core. The neutron flux, primarily thermal, is reduced in the radial direction by approximately 20 in. of neutron shielding composed of seven rows of 4-in.-square stainless-steel cans filled with graphite. Figure XI-2 shows the location of these cans. The fifth and seventh rows of cans contain 3 wt.% boron carbide in the graphite. To further reduce the activation of the secondary loop, a 1-in.-thick stainless-steel plate containing 1.5 wt.% boron was placed on the side of the heat exchanger closest to the reactor core, and a 0.5-in. plate with 1.1 wt.% boron was placed on the other side of the heat exchanger. The calculations show that the thermal-neutron flux in the heat exchanger is reduced by about a factor of 6 by the addition of the boron in the neutron shield and around the heat exchanger. The report gives complete results showing the variation of the calculated thermal-neutron flux in the heat exchanger with changes in boron concentration.

For the neutron-distribution calculations, both by position and energy, a multigroup diffusion code, STAR, was utilized. For these particular calculations, 10 energy groups were used.

Duct Studies

The transmission of thermal and fast neutrons along air-filled ducts in water has been experimentally and analytically studied by the United Kingdom Atomic Energy Authority. The results have been published in two reports, one dealing with fast neutrons and the other with thermal neutrons.[18,19] Both of the experiments were done in the LIDO Panel C facility, using three

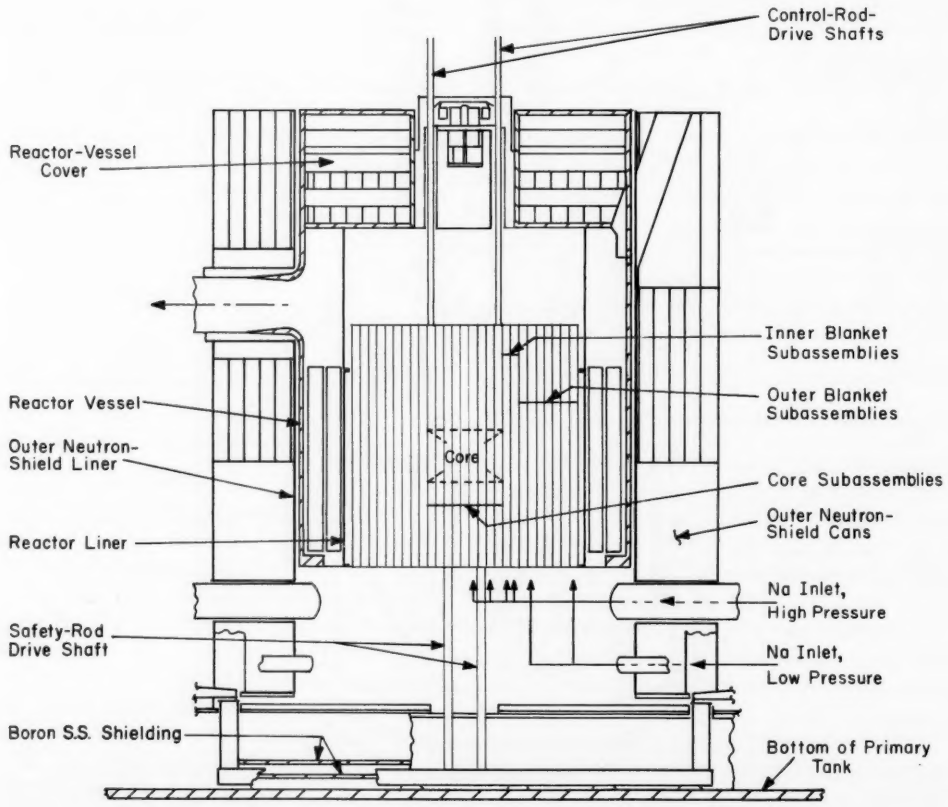

Fig. XI-2 Schematic of the EBR-II shielding.[17]

13-ft-long aluminum ducts with outside diameters of 1, 2, and $3\frac{3}{4}$ in. The ducts were horizontal and normal to the face of the reactor. Although the results are not directly applicable to typical power-reactor shield designs, the experimental results and the analysis do suggest possible methods of calculating the transmission of neutrons along straight ducts.

The fast-neutron flux was determined by measuring the activity produced in sulfur pellets by the $S^{32}(n,p)P^{32}$ reaction. The reaction threshold is about 2 Mev; however, this does not yield an ideal detector since the main interest in duct transmission is the fast-neutron dose rate, of which a significant part is produced by neutrons below 2 Mev.

The method of calculation is best described as a line-of-sight method employing a point-source attenuation kernel derived from results of the moments method.[20] The total neutron-flux incident on the detector is found by integrating over the core volume. The activation of the detector was considered to consist of two components: (1) the activation due to the neutrons entering the duct through the front face and (2) the activation due to neutrons entering the duct through the side walls. Another possible source of activation, the neutrons that scatter out of the duct and subsequently reenter the duct, was neglected. This component should be insignificant because most neutrons will be degraded in energy below the S^{32} threshold if they are scattered back into the duct. Further, these neutrons are implicitly considered to some extent in the moments-method results.

The calculated results gave good agreement with experiment for the three duct sizes. The largest disagreement, approximately a factor of 2, occurred when the detector was closest to the reactor core. The results show that the agreement improves as the detector is moved farther from the source. Further, it is apparently sufficient to take into account only the flux penetrating the end of the duct if the duct is more than 100 cm long.

The experimental measurements of the transmission of thermal neutrons were carried out in the same facility with the same ducts, and with the use of manganese foils as detectors. The measurements included the thermal-neutron flux as a function of distance from the end of the duct. The flux components due to thermal neutrons entering through the end and through the walls were separated by covering the walls and the end of the duct, alternately, with cadmium sheet.

The theoretical analysis of the thermal flux at a point in the duct was resolved into three components:

1. Thermal neutrons that enter the end of the duct and are attenuated geometrically down the duct, commonly called the streaming component
2. Neutrons of all energies which enter the end of the duct and penetrate the duct wall before diffusing back into the duct as thermal neutrons, commonly called the albedo component
3. Thermal neutrons which enter the duct through the duct wall and which have not previously passed through the end of the duct at any energy, commonly called the leakage component

The details of the calculational methods are described in Ref. 19.

In general, the agreement of the calculated and measured thermal-neutron fluxes was very good. For the bare ducts, without cadmium covers, the agreement improved as the distance from the source increased. In this region of agreement the streaming component was the important one. The comparison of the calculated and measured streaming components (duct wrapped with cadmium) gave agreement within a factor of 1.5 for penetrations of the order of 200 radii from the entrance for all three duct diameters. However, a straight-line fit to a logarithmic plot of flux as a function of distance gave a slope of about -2.35 for all three ducts, whereas theory predicted a slope of about -2.0. The difference between prediction and measurement was unexplained but was investigated. With the end of the duct covered with cadmium, the calculated results underpredicted the thermal-neutron flux by up to a factor of 4. The agreement was poorest for the largest duct.

In conclusion it can be said that, for straight ducts of the length usually present in power-reactor shields, the streaming component predominates for both fast and thermal neutrons. Consequently calculation methods can be simplified for most practical cases, and the transmission by ducts is not strongly dependent on the surrounding materials.

References

1. A. Weitzberg, I. Kaplan, and T. J. Thompson, Measurements of Neutron Capture in U^{238} in Lattices of Uranium Rods in Heavy Water, USAEC

Report NYO-9659, Massachusetts Institute of Technology, Jan. 8, 1962.
2. L. I. Tirén and J. M. Jenkins, Resonance Shielding in Thorium-Graphite Mixtures, British Report AEEW-R-163, March 1962.
3. L. W. Nordheim, A New Calculation of Resonance Integrals, *Nucl. Sci. Eng.*, 12(2): 293 (February 1962).
4. S. K. Pattenden and C. R. Patterson, Measurement of the Fission Ratio for Several Configurations of Uranium Oxide Rod Clusters, British Report AEEW-R-166, Feb. 14, 1962.
5. C. E. Branyan, Core A Critical Studies for the Enrico Fermi Atomic Power Plant on ZPR-III, USAEC Report ANL-6629, Argonne National Laboratory, October 1962.
6. The Babcock & Wilcox Co., Spectral Shift Control Reactor — Basic Physics Program. Quarterly Technical Report No. 8, July-September 1962, USAEC Report BAW-1262.
7. J. Miller, R. L. Brehm, and W. J. Roberts, Temperature Coefficients and Spectra in the Hydride Moderated SNAP Reactors, USAEC Report NAA-SR-7140, Atomics International, Dec. 30, 1962.
8. N. P. Baumann, Exponential Measurements on 19-Rod Clusters of UO_2 Rods in D_2O, USAEC Report DP-758, Savannah River Laboratory, August 1962.
9. P. Meyer and W. C. Ballowe, An Experimental Parametric Study of the Effects of Control Rods on the Prompt Neutron Decay Constant in Multiplying Media, USAEC Report GEAP-4019, Vallecitos Atomic Laboratory, April 1962.
10. L. Welshans, An Experimental Program on Water-Moderated Arrays of Uranium and Stainless Steel, USAEC Report MND-C-2502, Martin Co., May 1962.
11. A. F. Avery, The Prediction of Neutron Attenuation in Iron-Water Shields, British Report AEEW-R-125, April 1962.
12. A. F. Avery, United Kingdom Atomic Energy Authority, October 1959. (Unpublished)
13. E. G. Peterson, MAC — A Bulk Shielding Code, USAEC Report HW-73381, Hanford Atomic Products Operation, April 1962.
14. R. J. Holl and D. W. Stephen, Pathfinder Atomic Power Plant Shielding Analysis, USAEC Report ACNP-62016, Allis-Chalmers Mfg. Co., July 15, 1962.
15. E. P. Blizard, T. V. Blosser, R. M. Freestone, Jr., The Radiation Leakage Survey of the Shield of the Nuclear Ship *Savannah*, USAEC Report ORNL-3336, Oak Ridge National Laboratory, Aug. 29, 1962.
16. W. R. Smith and M. A. Turner, Nuclear Merchant Ship Reactor Shield Design Summary Report, USAEC Report BAW-1144-1, The Babcock & Wilcox Co., Aug. 1, 1959.
17. M. Grotenhuis, A. E. McArthy, and A. D. Rossin, Experimental Breeder Reactor-II (EBR-II) Shield Design, USAEC Report ANL-6614, Argonne National Laboratory, September 1962.
18. D. C. Piercey and D. E. Bendall, The Transmission of Fast Neutrons Along Air Filled Ducts in Water, British Report AEEW-R-69, June 1962.
19. D. C. Piercey, The Transmission of Thermal Neutrons Along Air Filled Ducts in Water, British Report AEEW-R-70, June 1962.
20. A. D. Krumbein, Summary of NDA Unclassified Results of Moments Calculations for the Penetration of Neutrons Through Various Materials, USAEC Report NDA-92-2(Rev.), Nuclear Development Corp. of America, Aug. 30, 1957.

LEGAL NOTICE

This document was prepared under the sponsorship of the U. S. Atomic Energy Commission. Neither the United States, nor the Commission, nor any person acting on behalf of the Commission:

A. Makes any warranty or representation, expressed or implied, with respect to the accuracy, completeness, or usefulness of the information contained in this report, or that the use of any information, apparatus, method, or process disclosed in this report may not infringe privately owned rights; or

B. Assumes any liabilities with respect to the use of, or for damages resulting from the use of any information, apparatus, method, or process disclosed in this report.

As used in the above, "person acting on behalf of the Commission" includes any employee or contractor of the Commission, or employee of such contractor, to the extent that such employee or contractor of the Commission, or employee of such contractor prepares, disseminates, or provides access to, any information pursuant to his employment or contract with the Commission, or his employment with such contractor.

NUCLEAR SCIENCE ABSTRACTS

The U. S. Atomic Energy Commission, Division of Technical Information, publishes *Nuclear Science Abstracts (NSA)*, a semimonthly journal containing abstracts of the literature of nuclear science and engineering.

NSA covers (1) research reports of the U. S. Atomic Energy Commission and its contractors; (2) research reports of government agencies, universities, and industrial research organizations on a world-wide basis; and (3) translations, patents, books, and articles appearing in technical and scientific journals.

Complete indexes covering subject, author, source, and report number are included in each issue. These are cumulated quarterly, semiannually, and annually providing a detailed and convenient key to the literature.

Availability of *NSA*

SALE *NSA* is available on subscription from the Superintendent of Documents, U. S. Government Printing Office, Washington 25, D. C., at $22.00 per year for the semimonthly abstract issues and $15.00 per year for the four cumulated-index issues. Subscriptions are postpaid within the United States, Canada, Mexico, and all Central and South American countries, except Argentina, Brazil, British and French Guiana, Surinam, and British Honduras. Subscribers in these Central and South American countries, and in all other countries throughout the world, should remit $27.50 per year for subscriptions to semimonthly abstract issues and $17.50 per year for the four cumulated-index issues.

EXCHANGE *NSA* is also available on an exchange basis to universities, research institutions, industrial firms, and publishers of scientific information. Inquiries should be directed to the Division of Technical Information Extension, U. S. Atomic Energy Commission, P. O. Box 62, Oak Ridge, Tennessee.

TECHNICAL PROGRESS REVIEWS may be purchased from Superintendent of Documents, U. S. Government Printing Office, Washington 25, D. C. for $2.00 per year for each subscription or for $0.55 per issue. The use of the coupon below will facilitate the handling of your order.

POSTAGE AND REMITTANCE: Postpaid within the United States, Canada, Mexico, and all Central and South American countries except as hereinafter noted. Add $0.50 per year, or $0.15 per single issue, for postage to all other countries, including Argentina, Brazil, British and French Guiana, Surinam, and British Honduras. Payment should be by check, money order, or document coupons, and MUST accompany order. Remittances from foreign countries should be made by international money order, or draft on an American bank, payable to the Superintendent of Documents, or by UNESCO book coupons.

order form

SUPERINTENDENT OF DOCUMENTS
U. S. GOVERNMENT PRINTING OFFICE
WASHINGTON 25, D. C.

Enclosed:
document coupons ☐ check ☐ money order ☐

Charge to Superintendent of Documents No._____

Please send a one-year subscription to

☐ REACTOR MATERIALS
☐ POWER REACTOR TECHNOLOGY
☐ NUCLEAR SAFETY
☐ REACTOR FUEL PROCESSING

(Each subscription $2.00 a year; $0.55 per issue.)

SUPERINTENDENT OF DOCUMENTS
U. S. GOVERNMENT PRINTING OFFICE
WASHINGTON 25, D. C.

(Print clearly)

Name_____

Street_____

City_____ Zone____ State_____